# TEMPO-OXIDIZED NANOCELLULOSES: SURFACE MODIFICATION AND USE AS ADDITIVES IN CELLULOSIC NANOCOMPOSITES

**Richard K. Johnson**

A Dissertation Submitted to the faculty of the
Virginia Polytechnic Institute & State University
in partial fulfillment of the requirements for the degree of

**Doctor of Philosophy**

**in**

**Macromolecular Science and Engineering**

Audrey Zink-Sharp, Chair
Wolfgang G. Glasser
Scott H. Renneckar
Charles E. Frazier
Alan R. Esker
Maren Roman

August 18, 2010
Blacksburg, Virginia

Keywords: TEMPO-oxidized, nanocellulose, nanocomposite, surface modification, octadecylamine, amidation, ionic complexation, thermal decomposition

# TEMPO-OXIDIZED NANOCELLULOSES: SURFACE MODIFICATION AND USE AS ADDITIVES IN CELLULOSIC NANOCOMPOSITES

Richard K. Johnson

## Abstract

The process of TEMPO-mediated oxidation has gained broad usage towards the preparation of highly charged, carboxyl-functionalized polysaccharides. TEMPO-oxidized nanocelluloses (TONc) of high surface charge and measuring 3 to 5 nm in width have been recently prepared from TEMPO-oxidized pulp. This study examines as-produced and surface-hydrophobized TONc as reinforcing additives in cellulosic polymer matrices. In the first part of the work, covalent (amidation) and non-covalent (ionic complexation) coupling were compared as treatment techniques for the hydrophobization of TONc surfaces with octadecylamine (ODA). Subsequently, TONc and its covalently coupled derivative were evaluated as nanofiber reinforcements in a cellulose acetate butyrate (CAB) matrix. The properties of the resulting nanocomposites were compared with those of similarly prepared ones reinforced with conventional microfibrillated cellulose (MFC).

It was found that both ionic complexation and amidation resulted in complete conversion of carboxylate groups on TONc surfaces. As a result of surface modification, the net crystallinity of TONc was lowered by 15 to 25% but its thermal decomposition properties were not significantly altered. With respect to nanocomposite performance, the maximum TONc reinforcement of 5 vol % produced negligible changes to the optical transmittance

behavior and a 22-fold increase in tensile storage modulus in the glass transition region of CAB. In contrast, hydrophobized TONc and MFC deteriorated the optical transmittance of CAB by *ca* 20% and increased its tensile storage modulus in the glass transition region by only 3.5 and 7 times respectively. These differences in nanocomposite properties were attributed to homogeneous dispersion of TONc compared to aggregation of both the hydrophobized derivative and the MFC reference in CAB matrix. A related study comparing TONc with MFC and cellulose nanocrystals (CNC) as reinforcements in hydroxypropylcellulose (HPC), showed TONc reinforcements as producing the most significant changes to HPC properties. The results of dynamic mechanical analysis and creep compliance measurements could be interpreted based on similar arguments as those made for the CAB-based nanocomposites.

Overall, this work revealed that the use of TONc (without the need for surface hydrophobization) as additives in cellulosic polymer matrices leads to superior reinforcing capacity and preservation of matrix transparency compared to the use of conventional nanocelluloses.

## Acknowledgements

It has been a great privilege for me to work under the guidance and counsel of my advisor, Dr Audrey Zink-Sharp and my chief mentor, Dr Wolfgang Glasser. Throughout my time as a graduate student, not only have they been consistent in providing guidance to me academically, they have also taken keen interest in my personal success and have never failed to provide support whenever possible. I especially thank them both for their patience and endurance during the rather slow start of my PhD research.

I am indeed grateful to Drs. Charles Frazier, Maren Roman, Alan Esker, and Scott Renneckar, members of my academic committee, for their advice and suggestions that really helped to sharpen the focus of my research. I will be remiss without saying a special thank you to Dr. Scott Renneckar for his invaluable friendship and mentorship to me over our many years of acquaintance. I also wish to thank Dean Paul Winistorfer for his warm personality and his admirable leadership (both as former head of Wood Science Department and current Dean of the College of Natural Resources and Environment).

My sincere thanks go to Rick Caudill, David Jones, and Kenny Albert (currently retired) for the variety of ways they have assisted me. These gentlemen have been good friends to me and whenever I am around them, there is no shortage of humor and laughter. Steve McCartney and John McIntosh of NCFL, thank you both for your time spent training and assisting me with SEM and TEM work. I wish to make special mention of Debbie Garnand, Senior Administrative Assistant in the Wood Science Department, and express my sincerest appreciation to her. Debbie is truly devoted, caring, and she does everything in her power to help bring a problem to closure. I am greatly indebted to her for the innumerable ways she has assisted me over the years. I also thank Angie Riegel, Secretary, and Linda Caudill, Managing Director of WBC and SEMI, for their help and friendship over the years. I have been fortunate to work in the same lab with graduate students from the Frazier, Renneckar, and Roman groups, with whom sharing ideas, jokes, and personal experiences have been both enlightening and entertaining. Their names are too many to mention individually. Dr. Gi Young Jeong and Angela (Yu Zhou) have been truly wonderful colleagues in our shared office space.

To my family: parents, Abraham and Margaret Johnson; siblings Theresa, Bennette, David, and Bernard, there are not enough words to describe how fortunate I consider myself to be a son and a brother to you all. Your prayers, encouragement, and support have helped bring me this far and I will continue to need them for the rest of life's journey. To my dearest wife Mary, I dedicate this work to you because you have travelled this road alongside me, and have done so with love, patience, and devotion. Thank you for enduring the long hours I have spent away from home and all the tough times we've been through. God richly bless you.

Ultimately, I thank my Lord and Savior Jesus Christ for His divine intervention in my life and promised guidance in all of my life's endeavors, past, present, and future!

## Table of Contents

## List of Figures

## List of Tables

# Chapter 1. Introduction

Nanoscale celluloses (nanocelluloses) are cellulosic elements having unit sizes of less than 100 nm in at least one dimension. A survey of recent and current literature reveals that nanoscale celluloses are being studied intensively for potential utilization in a range of applications such as biomedicine,[1-2] biomaterials engineering,[3-7] membranes,[8-12] and polymer nanocomposites. [13-23] A polymer nanocomposite was defined by Schadler *et al.*[24] as a polymer matrix composite in which the fillers are less than 100 nm in at least one dimension. When the fillers or reinforcements are nanocelluloses, the resulting nanocomposites are referred to as cellulose nanocomposites or nanocellulose composites. Extensive studies[13-23] have been conducted on utilization of bacterial cellulose,[25-26] nanocrystalline celluloses from acid hydrolysis,[27-29] and micro or nanofibrillated celluloses from mechanical disintegration[20,30-31] as reinforcements in polymer nanocomposites. Efficiency of nanofiller dispersion in the matrix and adequacy of nanofiller-matrix interfacial interactions are widely known to critically affect nanocomposite physical and mechanical properties. For example, fibril entanglements lead to self-aggregation of carbon nanotubes in polymer matrices, which results in adverse effects on nanocomposite performance.[32-33] To prevent self-aggregation and promote efficient nanotube dispersion and nanotube-matrix interaction, researchers modify the surfaces of carbon nanotubes with hydrophobic compounds using covalent[33-35] and non-covalent[36-38] coupling techniques. With respect to cellulose nanocomposites, it is difficult to achieve dispersion of nanocellulose reinforcements in water-insoluble or non-water dispersible polymer matrices. This limitation stems primarily from the high affinity of nanocelluloses for water and their inability to disperse readily in organic solvents. To promote nanocellulose dispersion in non-aqueous media, a wide variety of chemical modification techniques including coupling hydrophobic small molecules,[39-41] grafting polymers and oligomers,[42-43] and adsorbing hydrophobic compounds[44-45] to surface hydroxyl groups of nanocelluloses are employed. Besides the problem of incompatibility with matrix polymers, most conventional nanocelluloses are characterized by hydrogen bonding-induced aggregation of their nanosized rod-like and fibrillar structures. Cellulose nanocrystals (CNCs) from acid hydrolysis do naturally occur as bundles of rod-like crystallites although intense mechanical agitation[46] and further surface derivatization[47] promote some nanocrystal individualization. Microfibrillated celluloses (MFCs) on the other hand, continue to exist as

interconnected nanofibrillar structures even after intense attrition from multiple passes through high intensity homogenizers[19] and grinders.[48]

In recently published articles by Saito *et al.*,[49-50] it was reported that 2,2,6,6-tetramethylpiperidine-1-oxyl **(TEMPO, structure 1.I)**-mediated oxidation of cellulose fibers, allowed for low energy mechanical disintegration of the oxidized fibers in aqueous suspensions. TEMPO is a highly stable nitroxyl radical which is used extensively in the selective oxidation of primary alcohols to corresponding aldehydes and carboxylic acids. In aqueous environments, TEMPO catalyzes the conversion of carbohydrate primary alcohols to carboxylate ($COO^-$) functionalities in the presence of a primary oxidizing agent e.g. sodium hypochlorite (NaOCl).[51] When applied to polysaccharides, the carboxylate-functionalized (oxidized) products are sodium

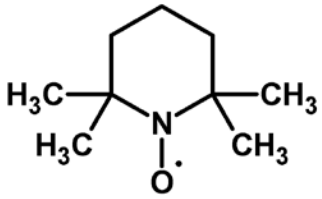

**2,2,6,6-tetramethylpiperidine-1-oxyl (TEMPO)**

**(1.I)**

salts of the corresponding polyglucuronic acids. In the studies by Saito *et al.*,[49-50] three to four nanometer-wide and several hundred nanometers to a few microns-long nanofibrils were obtained without any loss to the nanocellulose degree of crystallinity. The oxidized nanocellulose suspensions were also observed to be transparent, which was attributed to aqueous medium repulsion and individualization of nanofibrils due to their high surface charge densities. In contrast to conventional CNCs and MFCs, these TEMPO-oxidized nanocelluloses (TONc) represent a different form of highly individualized and multi-functionalized nanocelluloses, for which proposed and demonstrated potential applications include additives for paper wet strength [52] additives in food,[53] substitutes for cellulose ethers,[51] and coatings for oxygen barrier properties.[54]

So far, application of TONc as additives in nanocomposite applications has yet to be explored. Given that TONc possess multiple surface functionalities, preserve the structural integrity of cellulose, and form transparent aqueous suspensions, we perceived potential advantages in the utilization of TONc as nanocomposite reinforcements. In this work, we first prepared hydrophobic derivatives of TONc, and evaluated TONc and its hydrophobized forms as reinforcements in polymer nanocomposites.

## 1.1. Research Goals

The first goal of this research was to convert the carboxyl groups on TONc surfaces into hydrophobic groups for the promotion of TONc dispersion in organic media. TONc surfaces were derivatized with octadecylamine (ODA) as a model hydrophobic compound. Two main pathways to attach ODA to TONc surfaces were evaluated: (1) Ionic complexation of TONc and ODA through physical blending in a water-DMF co-solvent system, and (2) covalent coupling through amidation reactions. Our second goal was to utilize TONc and their surface-modified derivatives as reinforcements in cellulosic polymer nanocomposites.

The following specific objectives were set to accomplish the research goals:

1. Evaluate the efficiency of (1) ionic complexation and (2) carbodiimide-mediated amidation as treatment methods for the coupling of ODA molecules to TONc surfaces.
2. Evaluate the effects of ionic complexation and amidation on the surface polarity, crystallinity, and thermal degradation behavior of TONc.
3. Evaluate and compare the dynamic mechanical, optical, and thermal decomposition properties of nanocomposites reinforced with TONc (as-prepared and surface-modified) and conventional microfibrillated cellulose (MFC).

## 1.2. Outline of Dissertation

A literature review, in which we address multiple aspects of nanocelluloses and their nanocomposite applications, TEMPO-mediated oxidation and its use in the oxidation of cellulose, and derivation of nanocelluloses from the TEMPO-oxidized celluloses, is presented in Chapter 2.

In Chapter 3, ionic complexation and amidation are compared as techniques for the coupling of ODA to TONc surface carboxyl groups. The degrees of carboxyl substitution by ODA molecules are determined and used as the metric for efficiency of the treatment technique. Effects of surface modification on selected physical characteristics of TONc are also evaluated and discussed.

Preparation and characterization of native and surface hydrophobized TONc-reinforced nanocomposites based on a cellulose acetate butyrate (CAB) matrix are the subjects of Chapter 4. Optical, dynamic mechanical, and thermal decomposition properties of the nanocomposites are characterized and compared with one another, and with unfilled CAB.

In Chapter 5, nanocomposites based on hydroxypropylcellulose (HPC) matrix reinforced with TONc are described. Ultrasonication time was used as the factor to control degree of fibrillation of the oxidized pulp. Effects of fibrillation degree on the morphological and thermal decomposition properties of the nanocelluloses are reported. Dynamic mechanical properties of the TONc-reinforced nanocomposites are examined and compared with those of conventional CNC and MFC reinforced counterparts. Overall conclusions regarding TONc surface modification and performance as nanocomposite reinforcements are given in Chapter 6.

## 1.3. References


(1) Dong, S. P.; Roman, M. *Journal of the American Chemical Society* **2007**, *129*, 13810.

(2) Song, Y. B.; Zhou, J. P.; Li, Q.; Guo, Y.; Zhang, L. N. *Macromol. Biosci.* **2009**, *9*, 857.

(3) Backdahl, H.; Helenius, G.; Bodin, A.; Nannmark, U.; Johansson, B. R.; Risberg, B.; Gatenholm, P. *Biomaterials* **2006**, *27*, 2141.

(4) Helenius, G.; Backdahl, H.; Bodin, A.; Nannmark, U.; Gatenholm, P.; Risberg, B. *Journal of Biomedical Materials Research Part A* **2006**, *76A*, 431.

(5) Svensson, A.; Nicklasson, E.; Harrah, T.; Panilaitis, B.; Kaplan, D. L.; Brittberg, M.; Gatenholm, P. *Biomaterials* **2005**, *26*, 419.

(6) Cai, Z.; Kim, J. *Cellulose* **2010**, *17*, 83.

(7) Xing, Q.; Zhao, F.; Chen, S.; McNamara, J.; DeCoster, M. A.; Lvov, Y. M. *Acta Biomaterialia* **2010**, *6*, 2132.

(8) Lu, P.; Hsieh, Y. L. *Nanotechnology* **2009**, *20*.

(9) Paralikara, S. A.; Simonsen, J.; Lombardi, J. *J Membrane Sci* **2008**, *320*, 248.

(10) Xiang, C. H.; Joo, Y. L.; Frey, M. W. *Journal of Biobased Materials and Bioenergy* **2009**, *3*, 147.

(11) Ma, Z. W.; Kotaki, M.; Ramakrishna, S. *J Membrane Sci* **2005**, *265*, 115.

(12) Thielemans, W.; Warbey, C. R.; Walsh, D. A. *Green Chemistry* **2009**, *11*, 531.

(13) Ayuk, J. E.; Mathew, A. P.; Oksman, K. *Journal of Applied Polymer Science* **2009**, *114*, 2723.

(14) Capadona, J. R.; Van Den Berg, O.; Capadona, L. A.; Schroeter, M.; Rowan, S. J.; Tyler, D. J.; Weder, C. *Nat Nanotechnol* **2007**, *2*, 765.

(15) Dufresne, A.; Vignon, M. R. *Macromolecules* **1998**, *31*, 2693.

(16) Favier, V.; Chanzy, H.; Cavaille, J. Y. *Macromolecules* **1995**, *28*, 6365.

(17) Grunert, M.; Winter, W. T. *Journal of Polymers and the Environment* **2002**, *10*, 27.

(18) Ljungberg, N.; Bonini, C.; Bortolussi, F.; Boisson, C.; Heux, L.; Cavaille, J. Y. *Biomacromolecules* **2005**, *6*, 2732.

(19) Nakagaito, A. N.; Yano, H. *Applied Physics a-Materials Science & Processing* **2004**, *78*, 547.

(20) Nakagaito, A. N.; Yano, H. *Applied Physics a-Materials Science & Processing* **2005**, *80*, 155.

(21) Oksman, K.; Mathew, A. P.; Bondeson, D.; Kvien, I. *Composites Science and Technology* **2006**, *66*, 2776.

(22) Ruiz, M. M.; Cavaille, J. Y.; Dufresne, A.; Graillat, C.; Gerard, J. F. Lyon, France, 1999, p 211.

(23) Siqueira, G.; Bras, J.; Dufresne, A. *Biomacromolecules* **2009**, *10*, 425.

(24) Schandler, L. S.; Brinson, L. C.; Sawyer, W. G. *Jom-Us* **2007**, *59*, 53.

(25) Klemm, D.; Schumann, D.; Kramer, F.; Hessler, N.; Hornung, M.; Schmauder, H. P.; Marsch, S. *Adv Polym Sci* **2006**, *205*, 49.

(26) Klemm, D.; Schumann, D.; Kramer, F.; Hessler, N.; Koth, D.; Sultanova, B. *Macromol Symp* **2009**, *280*, 60.

(27) Battista, O. A. *Microcrystal Polymer Science*; McGraw Hill Book Company: New York, 1975.

(28) Ranby, B. G. *Discussions of the Faraday Society* **1951**, 158.

(29) Revol, J. F.; Bradford, H.; Giasson, J.; Marchessault, R. H.; Gray, D. G. *International Journal of Biological Macromolecules* **1992**, *14*, 170.

(30) Herrick, F. W.; Casebier, R. L.; Hamilton, J. K.; Sandberg, K. R. *Microfibrillated Cellulose: Morphology and Accessibility*, 1983; Vol. 37.

(31) Turbak, A. F.; Snyder, F. W.; Sandberg, K. R. *Journal of Applied Polymer Science: Applied Polymer Symposium* **1983**, *37*, 815.

(32) Moniruzzaman, M.; Winey, K. I. *Macromolecules* **2006**, *39*, 5194.

(33) Thostenson, E. T.; Ren, Z. F.; Chou, T. W. *Composites Science and Technology* **2001**, *61*, 1899.

(34) Hill, D. E.; Lin, Y.; Rao, A. M.; Allard, L. F.; Sun, Y. P. *Macromolecules* **2002**, *35*, 9466.

(35) Ramanathan, T.; Liu, H.; Brinson, L. C. *Journal of Polymer Science Part B-Polymer Physics* **2005**, *43*, 2269.

(36) Chen, R. J.; Zhang, Y. G.; Wang, D. W.; Dai, H. J. *Journal of the American Chemical Society* **2001**, *123*, 3838.

(37) O'Connell, M. J.; Boul, P.; Ericson, L. M.; Huffman, C.; Wang, Y. H.; Haroz, E.; Kuper, C.; Tour, J.; Ausman, K. D.; Smalley, R. E. *Chem Phys Lett* **2001**, *342*, 265.

(38) Star, A.; Stoddart, J. F.; Steuerman, D.; Diehl, M.; Boukai, A.; Wong, E. W.; Yang, X.; Chung, S. W.; Choi, H.; Heath, J. R. *Angew Chem Int Edit* **2001**, *40*, 1721.

(39) Andresen, M.; Johansson, L. S.; Tanem, B. S.; Stenius, P. *Cellulose* **2006**, *13*, 665.

(40) Gousse, C.; Chanzy, H.; Excoffier, G.; Soubeyrand, L.; Fleury, E. *Polymer* **2002**, *43*, 2645.

(41) Yuan, H. H.; Nishiyama, Y.; Wada, M.; Kuga, S. *Biomacromolecules* **2006**, *7*, 696.

(42) Araki, J.; Wada, M.; Kuga, S. *Langmuir* **2001**, *17*, 21.

(43) Lonnberg, H.; Fogelstrom, L.; Berglund, M.; Malmstrom, E.; Hult, A. *European Polymer Journal* **2008**, *44*, 2991.

(44) Heux, L.; Chauve, G.; Bonini, C. *Langmuir* **2000**, *16*, 8210.

(45) Zhou, Q.; Brumer, H.; Teeri, T. T. *Macromolecules* **2009**, *42*, 5430.

(46) Dong, X. M.; Revol, J. F.; Gray, D. G. *Cellulose* **1998**, *5*, 19.

(47) Araki, J.; Wada, M.; Kuga, S.; Okano, T. *Langmuir* **2000**, *16*, 2413.

(48) Iwamoto, S.; Nakagaito, A. N.; Yano, H. *Applied Physics a-Materials Science & Processing* **2007**, *89*, 461.

(49) Saito, T.; Kimura, S.; Nishiyama, Y.; Isogai, A. *Biomacromolecules* **2007**, *8*, 2485.

(50) Saito, T.; Nishiyama, Y.; Putaux, J. L.; Vignon, M.; Isogai, A. *Biomacromolecules* **2006**, *7*, 1687.

(51) Bragd, P. L.; van Bekkum, H.; Besemer, A. C. *Topics in Catalysis* **2004**, *27*, 49.

(52) Saito, T.; Isogai, A. *Ind Eng Chem Res* **2007**, *46*, 773.

(53) Suh, D. S.; Lee, K. S.; Chang, P. S.; Kim, K. O. *Journal of Food Science* **2007**, *72*, C235.

(54) Fukuzumi, H.; Saito, T.; Wata, T.; Kumamoto, Y.; Isogai, A. *Biomacromolecules* **2009**, *10*, 162.

# Chapter 2. Literature Review

## 2.1. Nanocelluloses

### 2.1.1. Origins

Nanoscale rod-like or fibrillar elements composed primarily of cellulose and measuring 100 nm or less in one dimension are referred to as nanocelluloses. Due to the diversity of cellulose, nanocelluloses can, in principle, be derived from a wide variety of sources. However, with respect to their research and development towards practical applications, the most significant sources have been wood, cotton, bacteria (*Acetobacter strains*), [1-2] and tunicin (cellulose extracted from the mantle of the sea animal, tunicate).[3]

### 2.1.2. Nanocelluloses from the Disintegration of Wood Pulp

Wood-based nanocellulose is extracted from wood pulp, which is produced in much larger quantities around the globe than the other sources of nanocellulose. From a utilization perspective, cellulose disintegration refers to reduction of fibrous celluloses from the micron scale into widths on the order of $\leq$ 100 nm and lengths on the order of > 100 nm to a few microns. The term "fibrillation" is sometimes used interchangeably with disintegration. However, fibrillation is also used to describe a partial form of mechanical degradation in which the fibrillated strands remain attached to the parent fiber. The goal is to create additional surface area for fiber-fiber or fiber-resin bonding. An example is the beating[4] of pulp to improve interfiber bonding during papermaking. Fiber disintegration can be achieved chemically and or mechanically. Mechanical disintegration in its strictest sense would refer to the breakdown of cellulose fibers into micro- and or nanofibrillar entities without chemical or enzymatic pretreatment. However, significant energy inputs are needed to disintegrate the pulped wood cells into cellulose microfibrils because the latter are bound together by interfibrillar hydrogen bonds into both crystalline and amorphous domains. Extraction of nanocellulose from the direct mechanical disintegration of wood pulp was first demonstrated by Herrick *et al*.[5] and Turbak *et al*.[6] in the early 1980s. Their approach which involved refining of the pulp followed by several passes of the refined pulp through a high pressure homogenizer, resulted in gel-like suspensions of highly fibrillated cellulose named microfibrillated cellulose (MFC). This approach also

involved high energy usage and the MFCs, imaged under the electron microscope, existed as highly networked fibrils 25 to 100 nm in diameter.[5-6]

Mechanical disintegration can also be performed on chemically or enzymatically pretreated fibers whereby the pretreatment serves to lower cohesive interactions between microfibrils. In a recent report by Paakko *et al.*,[7] the MFC disintegration process was preceded by enzymatic treatment of cellulose, resulting in improved product homogeneity and reduced energy consumption. A chemical pretreatment approach involving chlorite bleaching (delignification) and potassium hydroxide treatment (hemicelluloses removal) of wood powder generated uniform (15 nm-wide) fibrils after a single pass through a grinder.[8] SEM images revealed that the chemical treatments extracted encrusted material from the surfaces of and the spaces between cell wall microfibrils thereby easing the disintegration process. Other chemical pretreatment methods that need mentioning are carboxymethylation[9] and TEMPO-mediated oxidation.[10-12] TEMPO-mediated oxidation is the pretreatment used in preparing nanocellulose for the current study, and is described comprehensively in section 2.2 of this chapter.

Chemical pretreatment, mainly sulfuric acid hydrolysis, converts wood pulp into nanoscale rod-like crystallites or whiskers commonly referred to as cellulose nanocrystals (CNCs) or nanocrystalline cellulose.[13-15] Acid hydrolysis products occur as short rod-like whiskers that naturally aggregate into bundles. The common practice employed for mechanical disintegration of these whisker bundles is ultrasonic agitation from a few to several minutes. Ranby, obtained well dispersed nanocrystals (down to a few whiskers per bundle) after subjecting sulfuric acid hydrolyzed cellulose to ~90 min. of ultrasonication.[14] Sulfuric acid CNC suspensions are well known for their formation of anisotropic liquid crystalline (chiral nematic) structures at relatively low solids concentrations (~4 wt %).[16]

## 2.2. TEMPO-mediated Oxidation of Primary Alcohols

2,2,6,6-tetramethylpiperidine-1-oxyl (TEMPO) belongs to the highly stable nitroxyl or nitroxide radical class of compounds. The use of TEMPO for the selective oxidation of primary alcohols in the presence of secondary ones was first demonstrated by Semmelhack *et al.*[17-18] Primary alcohols of several organic compounds were electrochemically oxidized in organic media to aldehydes without further oxidation to carboxylic acids. A significant finding from their work was the *in situ* regeneration of the TEMPO radical, which excluded the need to use stoichiometric amounts, instead requiring the use of catalytic amounts. Several papers on the

application of TEMPO-mediated oxidation to carbohydrates (including cellulose) have since appeared[19-23] including an extensive review by Bragd *et al.*[18] Carbohydrate based studies have largely been performed under mildly alkaline conditions with the oxidation products being predominantly uronic acids. A primary oxidant is required in amounts commensurate with the desired degree of oxidation. The proposed mechanism of TEMPO-mediated oxidation (Figure 2.1) assumes that the actual oxidation of the substrate is effected by a nitrosonium ion, which is derived from the TEMPO radical by the primary oxidant.[18] During the reaction, the nitrosonium ion is reduced to a hydroxylamine molecule, which subsequently reacts with one molecule of nitrosonium ion (in alkaline medium) to regenerate 2 molecules of TEMPO radical and water.[21] TEMPO-mediated oxidation in alkaline media is commonly performed with NaOCl and sodium bromide (NaBr) as primary oxidant and co-oxidant, respectively. The addition of NaBr generates the more reactive hypobromite (OBr-) molecule, which has been shown to accelerate the reaction.[20] Under the TEMPO/NaOCl/NaBr system, de Nooy *et al.*[22] found a linear relationship between NaBr concentration and the oxidation rate of a methyl α-glucopyranoside substrate. When NaBr was eliminated from the reaction system, the reaction rate decreased significantly.

### 2.2.1. TEMPO-mediated Oxidation of Cellulose Primary Alcohols

#### 2.2.1.1. Reaction Process and Proposed Mechanisms

Most TEMPO-mediated oxidation of cellulose is carried out in aqueous media at alkaline pH (9 – 11). A TEMPO/NaOCl/NaBr system is often used whereby the degree of cellulose oxidation is determined by the amount of NaOCl added. The proposed reaction mechanism[24] (Figure 2.2) shows that two molar equivalents of hypochlorite, the primary oxidant, are required to transform a single anhydroglucose primary alcohol to its carboxylate derivative. Because TEMPO and NaBr are regenerated in the course of the reaction, only catalytic amounts are sufficient for the reaction to go to completion. It is necessary to maintain pH by adding dilute alkali solution, which is continuously being consumed by the protons released during the reaction. The effects of three reaction parameters, namely temperature, amount of TEMPO, and amount of NaBr, were studied by Suh et al.[25] Yields of 6-carboxycellulose decreased with increasing temperature and increased with increasing NaBr concentration. Primary alcohol selectivity was favored by increasing temperature but was significantly reduced with increasing amounts of TEMPO and NaBr. All three parameters were found to increase the reaction rate.

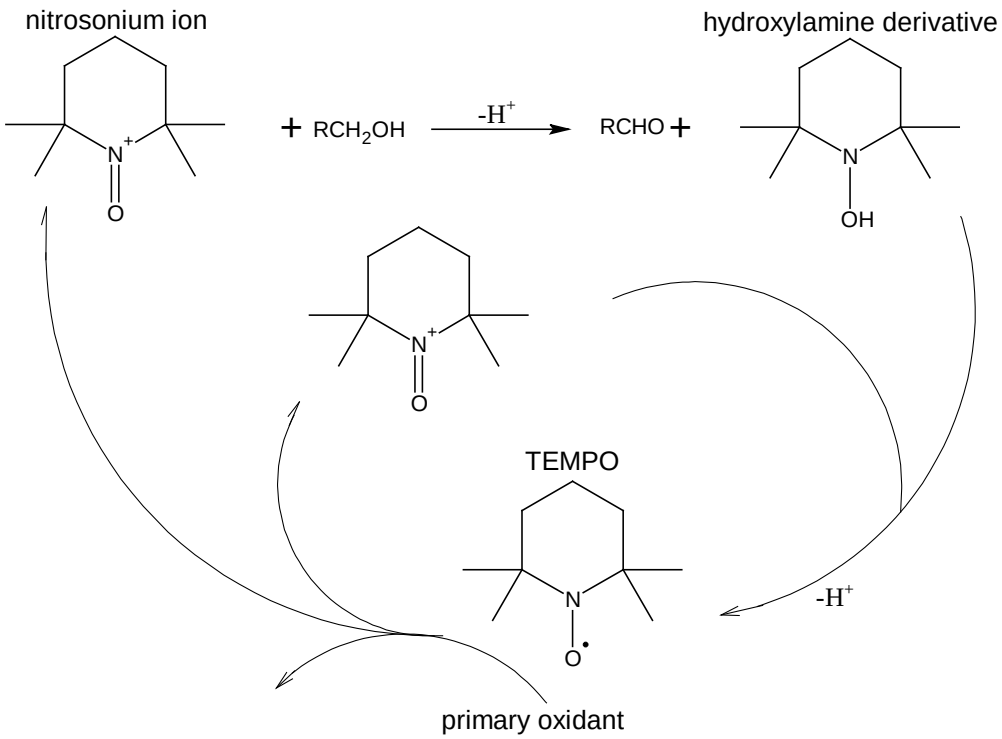


**Figure 2.1** Schematic of TEMPO-mediated oxidation mechanism of primary alcohols in a mildly alkaline environment. A primary oxidant generates nitrosonium ion from TEMPO, which is regenerated cyclically by a reaction between nitrosonium ion and hydroxylamine. (Adapted from ref. 18; fair use; Copyright 2004 Springer)

#### 2.2.1.2. Characteristics of TEMPO-oxidized Celluloses

The unique molecular and supramolecular architecture of cellulose allows significant flexibility in its chemical and morphological derivatization. This has been found to apply in the TEMPO-mediated oxidation of cellulose as well. Not surprisingly, the crystalline morphology of cellulose was reported to significantly influence its degree of oxidation by TEMPO.[18] Native cellulose resists high levels of conversion because of its high crystallinity index compared to mercerized/regenerated celluloses.[23, 26] The partial oxidation of native celluloses was reported to produce only superficial modification of microfibril surfaces without altering their core

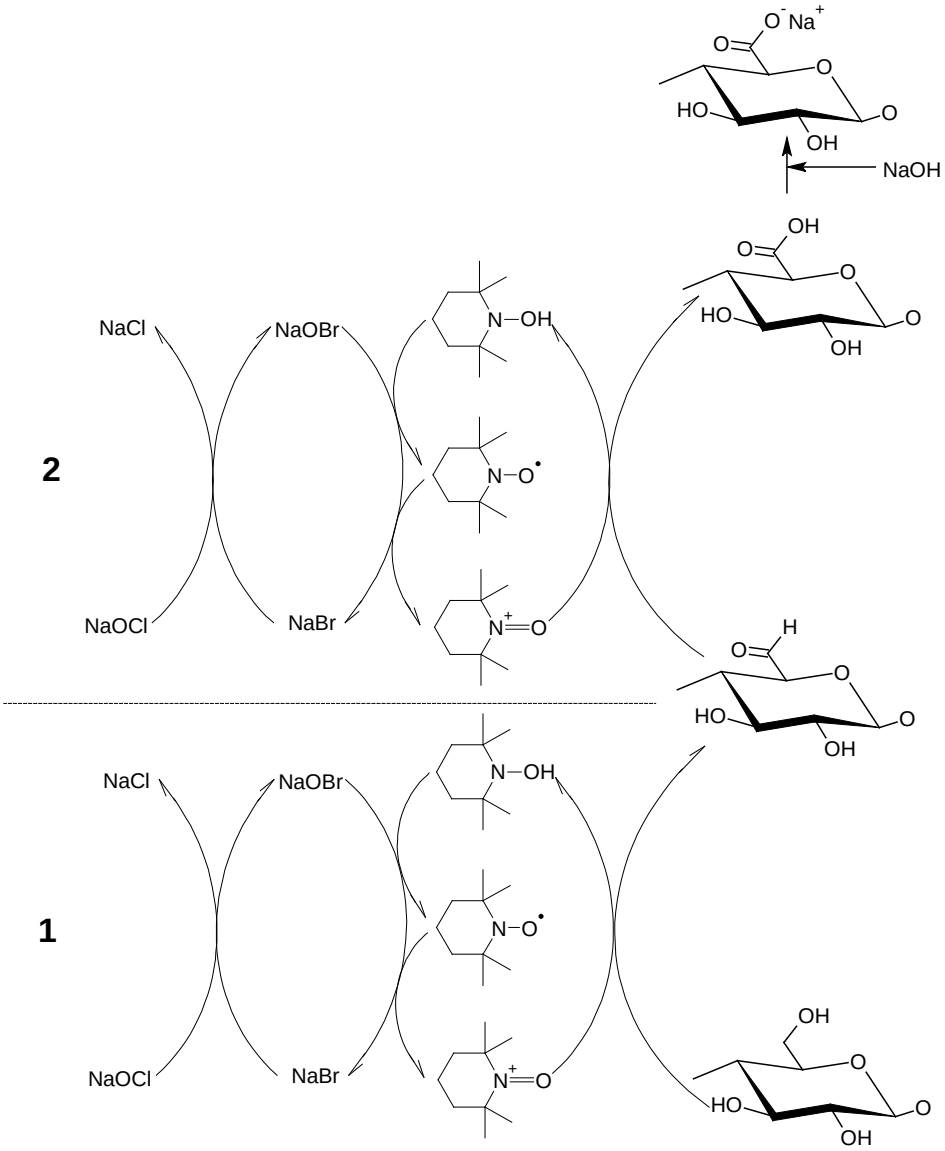


**Figure 2.2** Proposed mechanism for the oxidation of anhydroglucose to 6-carboxycellulose moieties via TEMPO/NaOCl/NaBr system in alkaline media. Numbers represent two levels of oxidation: (1) -$CH_2OH$→-CHO and (2) -CHO→-$CO_2H$. (Adapted from ref. 24; fair use; Copyright 2003 Springer)

crystalline characteristics.[23, 26-29] In contrast, mercerized/regenerated celluloses underwent quantitative oxidation of available primary hydroxyl groups to form the water soluble 6-carboxycellulose derivative.[23, 30] Reports on a wide range of TEMPO-oxidized cellulose properties (molecular weight,[23-24, 30-31] moisture retention,[26, 32] ion exchange,[33] biodegradation,[34] thermal degradation,[35] mechanical degradation,[11-12, 36] microscopic,[28] rheological,[37]

topochemical,[29, 36] optical,[38] etc.) have also appeared in the literature. A number of these characteristics have been explored, as discussed in the next section, towards developing potential applications for TEMPO-oxidized celluloses.

#### 2.2.1.3. Potential Applications of TEMPO-oxidized Celluloses

It is suggested that fully functionalized, water-soluble 6-carboxycelluloses have the potential to perform similar functions as cellulose ethers.[18] So far however, it is the presence of multiple chemical functionalities and the capacity for heterogeneous derivatization of the fiber surfaces that has attracted novel applications for TEMPO-oxidized celluloses. Saito and Isogai[39-41] investigated TEMPO-mediated oxidation as pretreatment for improvement of paper wet strength. Wet strength is an important performance parameter for certain paper products e.g. tissue paper, paper towel, paperboard (for packaging), printing and writing papers that are designed for interaction with wet environments.[41] Using bleached hardwood kraft pulps as starting materials, they reported that aldehyde, and not carboxylic groups formed at the fiber surfaces, contributed to wet strength improvement (Figure 2.3).[40] The authors cited inter-fiber cross-linking, specifically hemiacetal linkages between the formed aldehydes and hydroxyl groups of cellulose as the main source of the improved wet strength.

Araki *et al.*[42] employed TEMPO-mediated oxidation to prepare carboxyl functionalized microcrystalline celluloses for subsequent conversion to sterically stabilized colloidal suspensions. Steric stabilization was readily accomplished by grafting amine-terminated polyethylene glycol chains (PEG) onto carboxylic sites of the TEMPO-oxidized microcrystals. The grafted samples produced stable suspensions in the presence of high concentration electrolyte (2M NaCl) compared to a maximum 0.5 M NaCl concentration for ungrafted microcrystals. Additional benefits included ability of the grafted microcrystals to form (1) stable birefringent suspensions and (2) liquid crystalline chiral nematic structures in organic solvents. Successful grafting of non-polar groups onto TEMPO-oxidized celluloses has also been reported by Lasseuguette[43] and Follain *et al.*[44]

Alila *et al.*[45] used carboxyl functionalized celluloses (synthesized via TEMPO-mediated oxidation) as substrates in the co-adsorption of cationic surfactants and some organic hydrophobic compounds.[45-46] Surfactant aggregation onto charged solid substrates finds applications in a variety of fields including soil remediation,[47] chemical sensors,[48] synthetic membranes,[49] cosmetic formulation,[50] and immobilization of organic pollutants.[51-54] Results

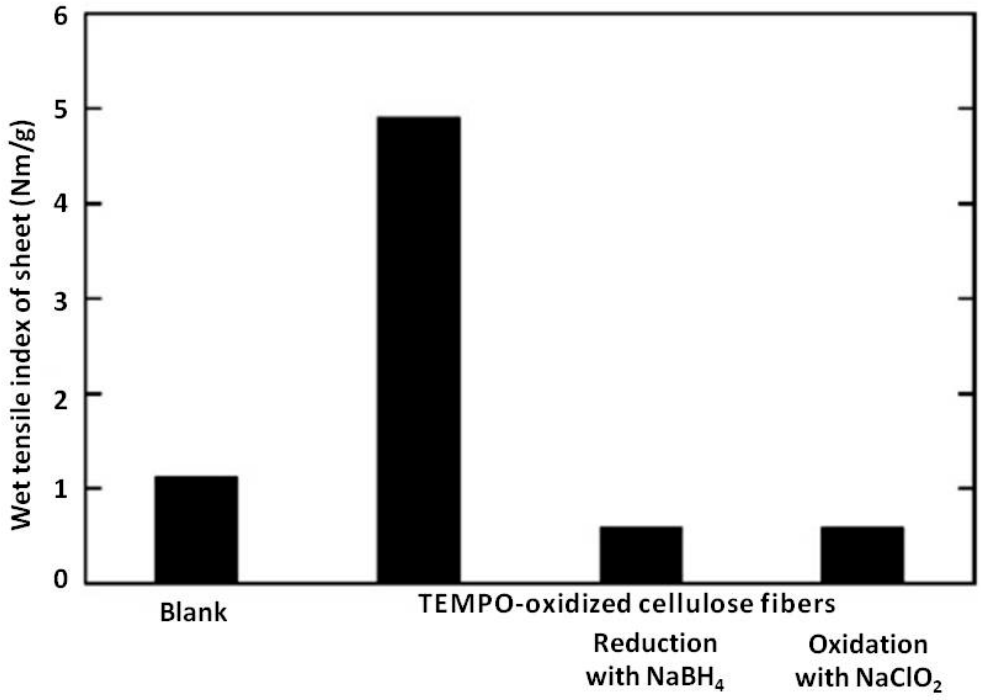


**Figure 2.3** Wet tensile strength as a function of fiber surface functionality. Reduced ($NaBH_4$ treated) and fully oxidized ($NaClO_2$ treated) versions of TEMPO-oxidized fibers are devoid of aldehyde groups. (Adapted from ref. 40; fair use; Copyright 2006 Elsevier B. V.)

from their studies showed that the adsorbed amounts of both surfactants and organic solutes strongly depended on the degree of TEMPO-oxidation i.e. the concentration of carboxylate groups on the oxidized fiber surfaces. Concentrations of adsorbed cationic surfactants varied linearly with surface carboxylate concentration of TEMPO-oxidized cellulose fibers. For most organic solutes, adsorbed amounts increased 4 to 6 fold when cellulose fibers were pre-oxidized with TEMPO.

### 2.3. Mechanical Disintegration of TEMPO-oxidized Cellulose

Saito *et al.*[12] recently reported successful disintegration of celluloses from various sources following TEMPO-mediated oxidation. A mild TEMPO/NaOCl/NaBr system was used at room temperature with NaOCl concentrations ranging from 2.5 to 3.8 mmol/g AGU[a]. These

[a] Anhydroglucose unit.

conditions allowed for disintegration of more than 90% of the oxidized pulp in an ordinary lab blender. The TEMPO-oxidized nanofibrils ranged from 3 – 5 nm in width and several hundred nanometers to a few microns in length as measured from TEM images. The researchers attributed the ease of disintegration to interfibrillar repulsive forces generated by carboxylate groups formed on microfibril surfaces. TEM micrographs of the oxidized nanofibrils also revealed the absence of interfibrillar networking and fibril aggregation typically observed in conventional MFCs [5-6] and CNCs.[13-15, 55] Figure 2.4 is a sample TEM micrograph of TEMPO-oxidized nanocelluloses which was prepared in the course of the current research by ultrasonication of TEMPO-oxidized pulp. Saito *et al.*[12] also reported preservation of nanocellulose crystallinity based on the appearance of birefringence when the nanofibril suspensions were examined between crossed polarizers. A later study[11] was performed with the goal of testing the limits of possibilities for low energy mechanical disintegration. In this second study, magnetic stirrers, instead of a lab blender, were used to agitate wood pulp suspensions (0.1% w/v) treated to various degrees of TEMPO-oxidation. It was discovered that when the degree of oxidation reached 1.5 mmol carboxylate content per gram AGU, 97% of the fibers disintegrated into nanofibrils by the tenth day of stirring.

## 2.4. Cellulose Nanocomposites

A composite is defined by the International Union of Pure and Applied Chemistry (IUPAC) as a multicomponent material comprising multiple different (non-gaseous) phase domains in which at least one type of phase domain is a continuous phase; it is a nanocomposite if at least one of the phases has at least one dimension on the order of nanometers.[56] Schadler *et al.*[57] define polymer nanocomposites as polymer matrix composite in which the fillers are less than 100 nm in at least one dimension. When the fillers or reinforcements are nanocelluloses, the resulting nanocomposites are referred to as cellulose nanocomposites or nanocellulose composites[58] Thus far, nanocelluloses from a range of sources such as wood,[59-60] cotton,[61] bacterial cellulose,[62] tunicin,[63] sugar beet,[64] and wheat straw[65] have been prepared and used in nanocomposite applications. Their use in a range of bio-based and petroleum-based matrix materials including cellulose derivatives,[60, 62, 66] polyvinyl alcohol,[67-68] polylactic acid,[69] thermoplastic starch,[70-71] polyhydroxyalkanoates,[72-73] polyolefins,[74-75] synthetic polyesters,[63, 76] epoxy,[77-78] and regenerated cellulose[79] have been reported. In general, justification for polymer nanocomposites research is founded on the dramatic improvements of important polymer

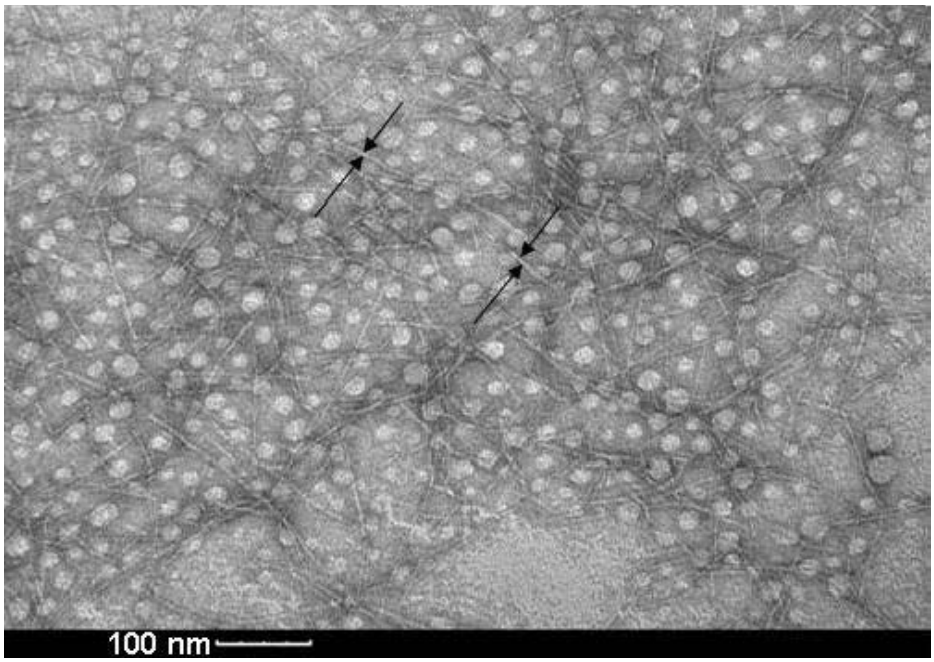


**Figure 2.4** TEM image of TEMPO-oxidized cellulose nanofibrils (shown with arrows) after ultrasonic treatment. Sample was extracted from supernatant after centrifugation of the sonicated suspension.

properties afforded by the presence of the nanofillers.[80] These typically include mechanical, thermal, electrical, optical, barrier, flame retardant, and biodegradable properties.[80] For the remainder of this section, a number of notable publications in the literature on cellulosic nanocomposites research are reviewed.

Favier *et al*.[63] reported dynamic mechanical thermal properties for tunicin whisker reinforced poly(styrene-*co*-butylacrylate) nanocomposites solvent-cast into 2 mm films. Dramatic differences, both in magnitude and shape, of shear storage moduli (G´) versus temperature plots were observed between the pristine polymer and the nanocomposites. Whisker reinforcements of 6 wt % and above were noted to generate the most significant transformations, undergoing only a single order of magnitude drop in G´ (1.0 to 0.1 GPa) during the glass to rubber transition. In contrast, the unfilled polymer underwent three orders of magnitude decline (1.0 to 0.001 GPa) in G´ over the same temperature range. No further decrease in G´ of the nanocomposite was observed up to about 500K, beyond which the nanowhiskers began to thermally degrade. By comparison, the unfilled polymer temperature-to-failure was only 350K. On account of micromechanical analyses, the authors attributed the extraordinary performance of the

nanocomposites to mechanical percolation of whiskers promoted by the strong inter-fibrillar hydrogen bonding capacity of the cellulose whiskers.

Advancing cellulosic nanocomposite performance through surface modification was the goal of Grunert and Winter.[62] Nanocomposites based on sulfuric acid hydrolyzed bacterial cellulose reinforcements in cellulose acetate butyrate (CAB) were studied. A post hydrolysis trimethylsilylation of bacterial cellulose was used as a surface modification approach against an unmodified control. With the aid of thermal analysis techniques, the authors concluded that at higher temperatures (post glass transition) trimethylsilylation induced stronger filler-matrix interaction than did conventional hydrolysis. Contrary to expectations in support of the above conclusion, the storage moduli of silylated crystal nanocomposites were lower than those of unmodified nanocrystals at equal filler loadings. A possible explanation for the observation given by the authors was that 18 wt % of the silylated nanocrystals belonged to silyl groups. Thus the effective filler content in these samples was less than that in the unsilylated crystal nanocomposites.

Researchers at Kyoto University in Japan reported on the mechanical, optical, and thermal expansion properties of nanocellulose reinforced polymer composites.[59, 81-83] Both MFC and bacterial cellulose were used as reinforcements in phenol formaldehyde (PF) and acrylic based resins. Degree of MFC fibrillation was examined as a factor in PF-based nanocomposite mechanical properties.[59] MFC fibrillation was controlled by varying the number of passes through (1) a refiner only and (2) a refiner followed by a homogenizer. A significant increase in bending strength of nanocomposites was found when MFCs underwent 30 passes through the refiner and subsequent passes through the homogenizer. Young's modulus on the other hand was only marginally influenced. Morphological studies on the MFCs revealed that fibrillation of the starting pulp fibers was only superficial when the number of refiner passes was fewer than 16. By 30 passes, the bulk of the pulp fibers had fibrillated into fine nanofibril networks, which provided the needed surface area for the observed strength enhancement. In another report,[82] a three-step (refiner-high pressure homogenizer-grinder) disintegration process was applied to wood pulp fibers to yield a highly disintegrated nanocellulose network. The nanocelluloses were formed into thin films (by filtration) and formulated into nanocomposites (of 70 wt % nanofibril loading) by impregnation with an acrylic resin. Reported film properties included a 70% light transmittance (about 20% short of that of unfilled acrylic resin at 600 nm), 7 GPa Young's

modulus, and $1.7 \times 10^{-5}$ $K^{-1}$ coefficient of thermal expansion (CTE) compared to a $8.6 \times 10^{-5}$ $K^{-1}$ CTE of unfilled resin. Comparable materials prepared with bacterial cellulose resulted in light transmittance, Young's modulus, and CTE of 80%, 21 GPa, and $0.6 \times 10^{-5}$ $K^{-1}$ respectively.[82, 84]

An interesting approach to cellulosic nanocomposites development has involved heterogeneous derivatization of native cellulose fibers in non-swelling media. The technique tends to derivatize the easily accessible regions in the native cellulose fibers leaving the highly crystalline domains intact. Subsequently, a moldable composite material whereby the derivatized component serves as a matrix and the non-derivatized crystalline domain as reinforcement is created.[60, 79] This kind of approach was originally reported by Matsumura *et al*. who partially derivatized dissolving grade hardwood pulps into cellulose hexanoates.[60] Thermally deformable products whose properties depended on the degree of substitution (DS) of hexanoate were obtained. Modulus and strength properties of compression molded sheets peaked at intermediate DS (0.5 – 1.0) but declined beyond these levels. Pronounced fiber-matrix delamination was evident in SEM images of the high DS samples, which affirmed the observed mechanical properties. Enzymatic degradation studies, using cellulases, also resulted in higher biodegradability (~50 %) of these partially derivatized materials (DS 0.5) compared to 20 % in homogeneously synthesized cellulose hexanoates of similar DS. XRD spectra revealed decreasing cellulose I crystal size with increasing DS, from which the authors concluded that hexanoylation proceeded at the microfibril surfaces rather than the bulk fiber surfaces (i.e. skin-core morphology). A subsequent AFM study revealed distinctive phase dimensions on the order of tens of nanometers in the compression molded sheets.[85] Findings from the XRD and AFM data supported the characterization of the pressed products as having nanoscale reinforcements in a thermoplastic matrix. Gindl and Keckes used a similar concept to later produce nanocomposites of native cellulose crystallites embedded in a regenerated cellulose matrix.[79]

## 2.5. Techniques for Modification of Nanocellulose Surfaces Towards Nanocomposite Applications

Cellulose fibers can be classified as hydrophilic because of the high hydroxyl content of cellulose (3 per anhydroglucose unit, AGU). Therefore when used as reinforcing fibers in non-polar polymer matrices, the durability and mechanical performance of the resulting composites are limited by poor fiber-matrix adhesion. Scientists devote substantial time and resources

towards solving these compatibility problems because among other factors, cellulosic fibers are abundant, biodegradable, and are characterized by favorable mechanical properties. A major part of the scientific work involves chemical reactions that modify cellulose fiber surfaces with appropriate functional groups leading to intermolecular and/or covalent bonding with polymer matrix molecules. Owing to their identical chemical compositions, practically the same surface modification techniques used on native cellulose fibers are also applicable to nanocelluloses. As is the case for essentially all cellulose derivatizations, hydroxyl groups are the primary reactive sites for cellulose surface modification. A significant fraction of the literature involves coupling with isocyanates and organosilanes, grafting of oligomeric and polymeric groups, acetylation, and mercerization. A comprehensive review of these major techniques with numerous references was published in 1999 by Bledzki and Gassan.[86] Gandini, Belgacem and co-workers[87-93] have also published a series of papers on reactions of isocyanates, organosilanes, and organometallic compounds with cellulose fiber surfaces. Coupling with organosilanes involves hydrolysis and condensation mechanisms, some of which are analogous to those encountered in glass fiber surface modifications.[87-88] Graft copolymerization entails the preformation (on cellulose fiber surfaces) of polymer chains compatible with the matrix polymer. Different approaches to graft copolymerization have been reported. For example, grafting of cellulosic fiber surfaces with maleic anhydride functionalized polypropylene (MA-PP) for subsequent reinforcement in polypropylene (PP) matrices has been extensively studied. In other grafting processes, the cellulose surface is first coupled to one end of a bifunctional compound making available the unreacted active end for copolymerization with suitable monomers.[89] Physical methods such as plasma and corona discharge treatments have also been effective for surface modification of cellulosic fibers.[94-98]

### 2.5.1. Amidation Reactions Involving Polysaccharides

Chemical modification of amine or carboxyl functionalized polysaccharides has been accomplished, respectively, through amidation reactions with carboxylic acids and amines. These reactions have been performed both homogeneously and heterogeneously on polysaccharides such as hyaluronic acid,[99] chitosan,[100-106] and carboxyl functionalized celluloses including fully and partially derivatized products from TEMPO-mediated oxidation.[43-44, 107] Proposed applications include drug delivery,[107] biocompatible hydrogels,[99] cross-linked biodegradable coatings/materials,[100-106] and stabilization of colloidal suspensions.[42]

Most of the published work involves the use of carbodiimides as coupling agents. Bulpitt and Aeschlimann[99] used this approach to functionalize hyaluronic acid with several homobifunctional amines towards development of cross-linked biocompatible hydrogels. A significant feature of their work was their use of N-hydroxysulfosuccinimide (sulfo-NHS) to obtain stable (active ester) intermediates in the amidation reaction. Addition of sulfo-NHS led to improved conversion efficiencies through the avoidance of hydrolysis sensitive *O*-acylisourea intermediates. The method has subsequently been adapted for the successful coupling of carboxycelluloses (homogeneous phase reactions)[44, 107] and carboxyl functionalized nanocelluloses (heterogeneous phase reactions).[42-43]

Using physical interventions (mixing and heating) only, Glasser and co-workers regenerated chitin from solutions of chitosan in dilute acetic acid.[100-106] Dissolving chitosan with acetic acid (1 – 10 % solutions) led to the formation of chitosonium acetate complexes which could be subsequently converted into chitin via heat-induced amidation. Water removal at temperatures ranging from 100 to 130 °C led to chitosonium salt condensation into chitin. In ensuing patents,[101-104] the authors suggested that the method could be extended to include a variety of mono-, di-, and tribasic ($C_{1-30}$) organic acids. The resultant products would be *N*-acylglucosamines derived from the process of polyanionic condensation. It was also suggested that the chitosonium salt solutions could be preformed into films, fibers, filaments, and injection molded materials (by adequate control of viscosity) prior to their heat-induced amidation into *N*-acylglucosamines.

## 2.6. References


(1) Klemm, D.; Schumann, D.; Kramer, F.; Hessler, N.; Hornung, M.; Schmauder, H. P.; Marsch, S., Nanocelluloses as innovative polymers in research and application. *Adv Polym Sci* **2006,** *205*, 49-96.

(2) Klemm, D.; Schumann, D.; Kramer, F.; Hessler, N.; Koth, D.; Sultanova, B., Nanocellulose Materials - Different Cellulose, Different Functionality. *Macromol Symp* **2009,** *280*, 60-71 150.

(3) Kamel, S., Nanotechnology and its applications in lignocellulosic composites, a mini review. *Express Polym Lett* **2007,** *1* (9), 546-575.

(4) Bowyer, J. L.; Shmulsky, R.; Haygreen, J. G., *Forest Products and Wood Science An Introduction*. Fourth ed.; Blackwell Publishing: Ames, 2003; p 554.

(5) Herrick, F. W.; Casebier, R. L.; Hamilton, J. K.; Sandberg, K. R., *Microfibrillated Cellulose: Morphology and Accessibility*. 1983; Vol. 37, p 797 - 813.

(6) Turbak, A. F.; Snyder, F. W.; Sandberg, K. R., Microfibrillated Cellulose, a new Cellulose Product: Properties, Uses, and Commercial Potential. *Journal of Applied Polymer Science: Applied Polymer Symposium* **1983,** *37*, 815.

(7) Paakko, M.; Ankerfors, M.; Kosonen, H.; Nykanen, A.; Ahola, S.; Osterberg, M.; Ruokolainen, J.; Laine, J.; Larsson, P. T.; Ikkala, O.; Lindstrom, T., Enzymatic hydrolysis combined with mechanical shearing and high-pressure homogenization for nanoscale cellulose fibrils and strong gels. *Biomacromolecules* **2007,** *8* (6), 1934-1941.

(8) Abe, K.; Iwamoto, S.; Yano, H., Obtaining cellulose nanofibers with a uniform width of 15 nm from wood. *Biomacromolecules* **2007,** *8* (10), 3276-3278.

(9) Wagberg, L.; Decher, G.; Norgren, M.; Lindstrom, T.; Ankerfors, M.; Axnas, K., The build-up of polyelectrolyte multilayers of microfibrillated cellulose and cationic polyelectrolytes. *Langmuir* **2008,** *24* (3), 784-795.

(10) Saito, T.; Hirota, M.; Tamura, N.; Kimura, S.; Fukuzumi, H.; Heux, L.; Isogai, A., Individualization of Nano-Sized Plant Cellulose Fibrils by Direct Surface Carboxylation Using TEMPO Catalyst under Neutral Conditions. *Biomacromolecules* **2009,** *10* (7), 1992-1996.

(11) Saito, T.; Kimura, S.; Nishiyama, Y.; Isogai, A., Cellulose nanofibers prepared by TEMPO-mediated oxidation of native cellulose. *Biomacromolecules* **2007,** *8* (8), 2485-2491.

(12) Saito, T.; Nishiyama, Y.; Putaux, J. L.; Vignon, M.; Isogai, A., Homogeneous suspensions of individualized microfibrils from TEMPO-catalyzed oxidation of native cellulose. *Biomacromolecules* **2006,** *7* (6), 1687-1691.

(13) Battista, O. A., *Microcrystal Polymer Science*. McGraw Hill Book Company: New York, 1975; p 208.

(14) Ranby, B. G., The Colloidal Properties of Cellulose Micelles. *Discussions of the Faraday Society* **1951,** (11), 158-164.

(15) Revol, J. F.; Bradford, H.; Giasson, J.; Marchessault, R. H.; Gray, D. G., Helicoidal self-ordering of celluulose microfibrils in aqueous suspension. *International Journal of Biological Macromolecules* **1992,** *14* (3), 170-172.

(16) Revol, J. F.; Godbout, L.; Dong, X. M.; Gray, D. G.; Chanzy, H.; Maret, G., Chiral nematic suspensions of cellulose crystallites - phase-separation and magnetic-field orientation *Liquid Crystals* **1994,** *16* (1), 127-134.

(17) Semmelhack, M. F.; Chou, C. S.; Cortes, D. A., Nitroxyl-mediated electrooxidation of alcohols to aldehydes and ketones. *Journal of the American Chemical Society* **1983,** *105* (13), 4492-4494.

(18) Bragd, P. L.; van Bekkum, H.; Besemer, A. C., TEMPO-mediated oxidation of polysaccharides: survey of methods and applications. *Topics in Catalysis* **2004,** *27* (1-4), 49-66.

(19) Davis, N. J.; Flitsch, S. L., Selective Oxidation of Monosaccharide Derivatives to Uronic-Acids. *Tetrahedron Letters* **1993,** *34* (7), 1181-1184.

(20) de Nooy, A. E. J.; Besemer, A. C.; van Bekkum, H., Highly Selective Tempo Mediated Oxidation of Primary Alcohol Groups in Polysaccharides. *Recueil Des Travaux Chimiques Des Pays-Bas-Journal of the Royal Netherlands Chemical Society* **1994,** *113* (3), 165-166.

(21) de Nooy, A. E. J.; Besemer, A. C.; van Bekkum, H., Selective Oxidation of Primary Alcohols Mediated by Nitroxyl Radical in Aqueous-Solution - Kinetics and Mechanism. *Tetrahedron* **1995,** *51* (29), 8023-8032.

(22) de Nooy, A. E. J.; Besemer, A. C.; van Bekkum, H., Highly Selective Nitroxyl Radical-Mediated Oxidation of Primary Alcohol Groups in Water-Soluble Glucans. *Carbohydrate Research* **1995,** *269* (1), 89-98.

(23) Isogai, A.; Kato, Y., Preparation of polyuronic acid from cellulose by TEMPO-mediated oxidation. *Cellulose* **1998,** *5* (3), 153-164.

(24) Shibata, I.; Isogai, A., Depolymerization of cellouronic acid during TEMPO-mediated oxidation. *Cellulose* **2003,** *10* (2), 151-158.

(25) Suh, D. S.; Lee, K. S.; Chang, P. S.; Kim, K. O., Physicochemical properties of cellulose selectively oxidized with the 2.2,6,6-tetramethyl-1-piperidinyl oxoammonium ion. *Journal of Food Science* **2007,** *72* (5), C235-C242.

(26) Saito, T.; Isogai, A., TEMPO-mediated oxidation of native cellulose. The effect of oxidation conditions on chemical and crystal structures of the water-insoluble fractions. *Biomacromolecules* **2004,** *5* (5), 1983-1989.

(27) Habibi, Y.; Chanzy, H.; Vignon, M. R., TEMPO-mediated surface oxidation of cellulose whiskers. *Cellulose* **2006,** *13* (6), 679-687.

(28) Saito, T.; Okita, Y.; Nge, T. T.; Sugiyama, J.; Isogai, A., TEMPO-mediated oxidation of native cellulose: Microscopic analysis of fibrous fractions in the oxidized products. *Carbohydr. Polym.* **2006,** *65* (4), 435-440.

(29) Saito, T.; Shibata, I.; Isogai, A.; Suguri, N.; Sumikawa, N., Distribution of carboxylate groups introduced into cotton linters by the TEMPO-mediated oxidation. *Carbohydr. Polym.* **2005,** *61* (4), 414-419.

(30) Tahiri, C.; Vignon, M. R., TEMPO-oxidation of cellulose: Synthesis and characterisation of polyglucuronans. *Cellulose* **2000,** *7* (2), 177-188.

(31) Isogai, T.; Yanagisawa, M.; Isogai, A., Degrees of polymerization (DP) and DP distribution of cellouronic acids prepared from alkali-treated celluloses and ball-milled native celluloses by TEMPO-mediated oxidation. *Cellulose* **2009,** *16* (1), 117-127.

(32) Dang, Z.; Zhang, J. G.; Ragauskas, A. J., Characterizing TEMPO-mediated oxidation of ECF bleached softwood kraft pulps. *Carbohydr. Polym.* **2007,** *70* (3), 310-317.

(33) Saito, T.; Isogai, A., Ion-exchange behavior of carboxylate groups in fibrous cellulose oxidized by the TEMPO-mediated system. *Carbohydr. Polym.* **2005,** *61* (2), 183-190.

(34) Kato, Y.; Habu, N.; Yamaguchi, J.; Kobayashi, Y.; Shibata, I.; Isogai, A.; Samejima, M., Biodegradation of beta-1,4-linked polyglucuronic acid (cellouronic acid). *Cellulose* **2002,** *9* (1), 75-81.

(35) Fukuzumi, H.; Saito, T.; Wata, T.; Kumamoto, Y.; Isogai, A., Transparent and High Gas Barrier Films of Cellulose Nanofibers Prepared by TEMPO-Mediated Oxidation. *Biomacromolecules* **2009,** *10* (1), 162-165.

(36) Montanari, S.; Rountani, M.; Heux, L.; Vignon, M. R., Topochemistry of carboxylated cellulose nanocrystals resulting from TEMPO-mediated oxidation. *Macromolecules* **2005,** *38* (5), 1665-1671.

(37) Lasseuguette, E.; Roux, D.; Nishiyama, Y., Rheological properties of microfibrillar suspension of TEMPO-oxidized pulp. *Cellulose* **2008,** *15* (3), 425-433.

(38) Habibi, Y.; Goffin, A. L.; Schiltz, N.; Duquesne, E.; Dubois, P.; Dufresne, A., Bionanocomposites based on poly(epsilon-caprolactone)-grafted cellulose nanocrystals by ring-opening polymerization. *J. Mater. Chem.* **2008,** *18* (41), 5002-5010.

(39) Saito, T.; Isogai, A., A novel method to improve wet strength of paper. *Tappi Journal* **2005,** *4* (3), 3-8.

(40) Saito, T.; Isogai, A., Introduction of aldehyde groups on surfaces of native cellulose fibers by TEMPO-mediated oxidation. *Colloid Surface A* **2006,** *289* (1-3), 219-225.

(41) Saito, T.; Isogai, A., Wet strength improvement of TEMPO-oxidized cellulose sheets prepared with cationic polymers. *Ind Eng Chem Res* **2007,** *46* (3), 773-780.

(42) Araki, J.; Wada, M.; Kuga, S., Steric stabilization of a cellulose microcrystal suspension by poly(ethylene glycol) grafting. *Langmuir* **2001,** *17* (1), 21-27.

(43) Lasseuguette, E., Grafting onto microfibrils of native cellulose. *Cellulose* **2008,** *15* (4), 571-580.

(44) Follain, N.; Montanari, S.; Jeacomine, I.; Gambarelli, S.; Vignon, M. R., Coupling of amines with polyglucuronic acid: Evidence for amide bond formation. *Carbohydr. Polym.* **2008,** *74* (3), 333-343.

(45) Alila, S.; Aloulou, F.; Beneventi, D.; Boufi, S., Self-aggregation of cationic surfactants onto oxidized cellulose fibers and coadsorption of organic compounds. *Langmuir* **2007,** *23* (7), 3723-3731.

(46) Alila, S.; Boufi, S.; Belgacem, M. N.; Beneventi, D., Adsorption of a cationic surfactant onto cellulosic fibers - I. Surface charge effects. *Langmuir* **2005,** *21* (18), 8106-8113.

(47) Christian, S. D.; Scamehorn, J. F., Solubilization in Surfactant Aggregates. In *Surfactant Science Series*, Marcel Dekker: New York, 1995; Vol. 38.

(48) Yan, Y. G.; Bein, T., Molecular recognition through intercalation chemistry - immobilization of organoclays on piezoelectric devices. *Chemistry of Materials* **1993,** *5* (7), 905-907.

(49) Okahata, Y.; Shimizu, A., Preparation of bilayer-intercalated clay films and permeation control responding to temperature, electric-field, and ambient pH changes permeability controllable membranes 10. *Langmuir* **1989,** *5* (4), 954-959.

(50) Aloulou, F.; Boufi, S.; Belgacem, N.; Gandini, A., Adsorption of cationic surfactants and subsequent adsolubilization of organic compounds onto cellulose fibers. *Colloid and Polymer Science* **2004,** *283* (3), 344-350.

(51) Boyd, S. A.; Lee, J. F.; Mortland, M. M., Attenuating organic contaminant mobility by soil modification. *Nature* **1988,** *333* (6171), 345-347.

(52) Lee, J. F.; Crum, J. R.; Boyd, S. A., Enhanced retention of organic contaminants by soils exchanged with organic cations. *Environmental Science & Technology* **1989,** *23* (11), 1365-1372.

(53) Nayyar, S. P.; Sabatini, D. A.; Harwell, J. H., Surfactant adsolubilization and modified admicellar sorption of nonpolar, polar, and ionizable organic contaminants. *Environmental Science & Technology* **1994,** *28* (11), 1874-1881.

(54) Wang, Y. L.; Banziger, J.; Dubin, P. L.; Filippelli, G.; Nuraje, N., Adsorptive partitioning of an organic compound onto polyelectrolyte-immobilized micelles on porous glass and sand. *Environmental Science & Technology* **2001,** *35* (12), 2608-2611.

(55) Marchessault, R. H.; Morehead, F. F.; Walter, N. M., Liquid Crystalline Systems from Fibrillar Polysaccharides. *Nature* **1959,** *184*, 632.

(56) Work, W. J.; Horie, K.; Hess, M.; Stepto, R. F. T., Definitions of terms related to polymer blends, composites, and multiphase polymeric materials - (IUPAC recommendations 2004). *Pure and Applied Chemistry* **2004,** *76* (11), 1985-2007.

(57) Schandler, L. S.; Brinson, L. C.; Sawyer, W. G., Polymer nanocomposites: A small part of the story. *Jom-Us* **2007,** *59* (3), 53-60.

(58) Samir, M. A. S. A.; Alloin, F.; Dufresne, A., Review of recent research into cellulosic whiskers, their properties and their application in nanocomposite field. *Biomacromolecules* **2005,** *6* (2), 612-626.

(59) Nakagaito, A. N.; Yano, H., The effect of morphological changes from pulp fiber towards nano-scale fibrillated cellulose on the mechanical properties of high-strength plant fiber based composites. *Applied Physics a-Materials Science & Processing* **2004,** *78* (4), 547-552.

(60) Matsumura, H.; Sugiyama, J.; Glasser, W. G., Cellulosic nanocomposites. I. Thermally deformable cellulose hexanoates from heterogeneous reaction. *Journal of Applied Polymer Science* **2000,** *78* (13), 2242-2253.

(61) Wang, Y. X.; Cao, X. D.; Zhang, L. N., Effects of cellulose whiskers on properties of soy protein thermoplastics. *Macromol. Biosci.* **2006,** *6* (7), 524-531.

(62) Grunert, M.; Winter, W. T., Nanocomposites of cellulose acetate butyrate reinforced with cellulose nanocrystals. *Journal of Polymers and the Environment* **2002,** *10* (1-2), 27-30.

(63) Favier, V.; Chanzy, H.; Cavaille, J. Y., Polymer Nanocomposites Reinforced by Cellulose Whiskers. *Macromolecules* **1995,** *28* (18), 6365-6367.

(64) Samir, M.; Alloin, F.; Paillet, M.; Dufresne, A., Tangling effect in fibrillated cellulose reinforced nanocomposites. *Macromolecules* **2004,** *37* (11), 4313-4316.

(65) Helbert, W.; Cavaille, J. Y.; Dufresne, A., Thermoplastic nanocomposites filled with wheat straw cellulose whiskers .1. Processing and mechanical behavior. *Polymer Composites* **1996,** *17* (4), 604-611.

(66) Gindl, W.; Keckes, J., Tensile properties of cellulose acetate butyrate composites reinforced with bacterial cellulose. *Composites Science and Technology* **2004,** *64* (15), 2407-2413.

(67) Bhatnagar, A.; Sain, M., Processing of cellulose nanofiber-reinforced composites. *Journal of Reinforced Plastics and Composites* **2005,** *24* (12), 1259-1268.

(68) Chakraborty, A.; Sain, M.; Kortschot, M., Reinforcing potential of wood pulp-derived microfibres in a PVA matrix. *Holzforschung* **2006,** *60* (1), 53-58.

(69) Oksman, K.; Mathew, A. P.; Bondeson, D.; Kvien, I., Manufacturing process of cellulose whiskers/polylactic acid nanocomposites. *Composites Science and Technology* **2006,** *66* (15), 2776-2784.

(70) Angles, M. N.; Dufresne, A., Plasticized starch/tunicin whiskers nanocomposites. 1. Structural analysis. *Macromolecules* **2000,** *33* (22), 8344-8353.

(71) Angles, M. N.; Dufresne, A., Plasticized starch/tunicin whiskers nanocomposite materials. 2. Mechanical behavior. *Macromolecules* **2001,** *34* (9), 2921-2931.

(72) Dubief, D.; Samain, E.; Dufresne, A., Polysaccharide microcrystals reinforced amorphous poly(beta-hydroxyoctanoate) nanocomposite materials. *Macromolecules* **1999,** *32* (18), 5765-5771.

(73) Dufresne, A.; Kellerhals, M. B.; Witholt, B., Transcrystallization in Mcl-PHAs/cellulose whiskers composites. *Macromolecules* **1999,** *32* (22), 7396-7401.

(74) Chazeau, L.; Cavaille, J. Y.; Canova, G.; Dendievel, R.; Boutherin, B., Viscoelastic properties of plasticized PVC reinforced with cellulose whiskers. *Journal of Applied Polymer Science* **1999,** *71* (11), 1797-1808.

(75) Ljungberg, N.; Bonini, C.; Bortolussi, F.; Boisson, C.; Heux, L.; Cavaille, J. Y., New nanocomposite materials reinforced with cellulose whiskers in atactic polypropylene: Effect of surface and dispersion characteristics. *Biomacromolecules* **2005,** *6* (5), 2732-2739.

(76) Favier, V.; Canova, G. R.; Cavaille, J. Y.; Chanzy, H.; Dufresne, A.; Gauthier, C., Nanocomposite Materials from Latex and Cellulose Whiskers. *Polymers for Advanced Technologies* **1995,** *6* (5), 351-355.

(77) Ruiz, M. M.; Cavaille, J. Y.; Dufresne, A.; Gerard, J. F.; Graillat, C., Processing and characterization of new thermoset nanocomposites based on cellulose whiskers. *Composite Interfaces* **2000,** *7* (2), 117-131.

(78) Ruiz, M. M.; Cavaille, J. Y.; Dufresne, A.; Graillat, C.; Gerard, J. F. In *New waterborne epoxy coatings based on cellulose nanofillers*, Lyon, France, Sep 06-09; Lyon, France, 1999; pp 211-222.

(79) Gindl, W.; Keckes, J., All-cellulose nanocomposite. *Polymer* **2005,** *46* (23), 10221-10225.

(80) Chen, B.; Evans, J. R. G.; Greenwell, H. C.; Boulet, P.; Coveney, P. V.; Bowden, A. A.; Whiting, A., A critical appraisal of polymer-clay nanocomposites. *Chemical Society Reviews* **2008,** *37* (3), 568-594.

(81) Iwamoto, S.; Nakagaito, A. N.; Yano, H., Nano-fibrillation of pulp fibers for the processing of transparent nanocomposites. *Applied Physics a-Materials Science & Processing* **2007,** *89* (2), 461-466.

(82) Iwamoto, S.; Nakagaito, A. N.; Yano, H.; Nogi, M., Optically transparent composites reinforced with plant fiber-based nanofibers. *Applied Physics a-Materials Science & Processing* **2005,** *81* (6), Cp8-1112.

(83) Nakagaito, A. N.; Yano, H., Novel high-strength biocomposites based on microfibrillated cellulose having nano-order-unit web-like network structure. *Applied Physics a-Materials Science & Processing* **2005,** *80* (1), 155-159.

(84) Yano, H.; Sugiyama, J.; Nakagaito, A. N.; Nogi, M.; Matsuura, T.; Hikita, M.; Handa, K., Optically transparent composites reinforced with networks of bacterial nanofibers. *Adv. Mater.* **2005,** *17* (2), 153-+.

(85) Matsumura, H.; Glasser, W. G., Cellulosic nanocomposites. II. Studies by atomic force microscopy. *Journal of Applied Polymer Science* **2000,** *78* (13), 2254-2261.

(86) Bledzki, A. K.; Gassan, J., Composites reinforced with cellulose based fibres. *Progress in Polymer Science* **1999,** *24* (2), 221-274.

(87) Abdelmouleh, M.; Boufi, S.; Belgacem, M. N.; Duarte, A. P.; Ben Salah, A.; Gandini, A., Modification of cellulosic fibres with functionalised silanes: development of surface properties. *International Journal of Adhesion and Adhesives* **2004,** *24* (1), 43-54.

(88) Abdelmouleh, M.; Boufi, S.; ben Salah, A.; Belgacem, M. N.; Gandini, A., Interaction of silane coupling agents with cellulose. *Langmuir* **2002,** *18* (8), 3203-3208.

(89) Botaro, V. R.; Gandini, A., Chemical modification of the surface of cellulosic fibres. 2. Introduction of alkenyl moieties via condensation reactions involving isocyanate functions. *Cellulose* **1998,** *5* (2), 65-78.

(90) Botaro, V. R.; Gandini, A.; Belgacem, M. N., Heterogeneous chemical modification of cellulose for composite materials. *Journal of Thermoplastic Composite Materials* **2005,** *18* (2), 107-117.

(91) Castellano, M.; Gandini, A.; Fabbri, P.; Belgacem, M. N., Modification of cellulose fibres with organosilanes: Under what conditions does coupling occur? *Journal of Colloid and Interface Science* **2004,** *273* (2), 505-511.

(92) Gandini, A.; Belgacem, M. N., Recent contributions to the preparation of polymers derived from renewable resources. *Journal of Polymers and the Environment* **2002,** *10* (3), 105-114.

(93) Gandini, A.; Belgacem, M. N. In *Modified cellulose fibers as reinforcing fillers for macromolecular matrices*, Alicante, Spain, Sep 08-11; Alicante, Spain, 2003; pp 257-270.

(94) Couto, E.; Tan, I. H.; Demarquette, N.; Caraschi, J. C.; Leao, A., Oxygen plasma treatment of sisal fibers and polypropylene: Effects on mechanical properties of composites. *Polymer Engineering and Science* **2002,** *42* (4), 790-797.

(95) Felix, J.; Gatenholm, P.; Schreiber, H. P., Plasma modification of cellulose fibers - Effects on some polymer composite properties. *Journal of Applied Polymer Science* **1994,** *51* (2), 285-295.

(96) Gassan, J.; Gutowski, V. S., Effects of corona discharge and UV treatment on the properties of jute-fibre epoxy composites. *Composites Science and Technology* **2000,** *60* (15), 2857-2863.

(97) Martin, A. R.; Manolache, S.; Denes, F. S.; Mattoso, L. H. C., Functionalization of sisal fibers and high-density polyethylene by cold plasma treatment. *Journal of Applied Polymer Science* **2002,** *85* (10), 2145-2154.

(98) Yuan, X. W.; Jayaraman, K.; Bhattacharyya, D., Mechanical properties of plasma-treated sisal fibre-reinforced polypropylene composites. *Journal of Adhesion Science and Technology* **2004,** *18* (9), 1027-1045.

(99) Bulpitt, P.; Aeschlimann, D., New strategy for chemical modification of hyaluronic acid: Preparation of functionalized derivatives and their use in the formation of novel biocompatible hydrogels. *Journal of Biomedical Materials Research* **1999,** *47* (2), 152-169.

(100) Toffey, A.; Samaranayake, G.; Frazier, C. E.; Glasser, W. G., Chitin derivatives .1. Kinetics of the heat-induced conversion of chitosan to chitin. *Journal of Applied Polymer Science* **1996,** *60* (1), 75-85.

(101) Roy, S. K.; Todd, J. G.; Glasser, W. G. Manufacture of crosslinked hydrogel beads from chitosan. 5,770,712, March 14., 1998.

(102) Glasser, W. G.; Jain, R. K. Method of Making Ester-Crosslinked Chitosan Support Materials and Products Thereof. 5,874,551, Feb 23, 1999.

(103) Glasser, W. G.; Jain, R. K. Method of making magnetic, crosslinked chitosan support materials and products thereof. 5,864,025, June 23., 1999.

(104) Glasser, W. G.; Samaranayake, G.; Toffey, A. Preparation of N-acyl glucosamine polymer from chitosan for chitin films and filaments. 5,900,479, March 20., 1999.

(105) Toffey, A.; Glasser, W. G., Chitin derivatives. II. Time-temperature-transformation cure diagrams of the chitosan amidization process. *Journal of Applied Polymer Science* **1999,** *73* (10), 1879-1889.

(106) Toffey, A.; Glasser, W. G., Chitin derivatives III formation of amidized homologs of chitosan. *Cellulose* **2001,** *8* (1), 35-47.

(107) Zhu, L. H.; Kumar, V.; Banker, G. S., Examination of oxidized cellulose as a macromolecular prodrug carrier: preparation and characterization of an oxidized cellulose-phenylpropanolamine conjugate. *International Journal of Pharmaceutics* **2001,** *223* (1-2), 35-47.

# Chapter 3. Surface Modification and Characterization of TEMPO-oxidized Nanocelluloses (TONc) Towards Nanocomposite Applications

## 3.1. Abstract

TONc surface carboxyls were derivatized into hydrophobic groups using octadecylamine (ODA), a hydrophobic aliphatic amine. Two approaches were proposed to evaluate their effectiveness in coupling ODA to TONc surfaces. These were physical mixing of TONc and ODA to yield ODA-TONc ionic complexes and carbodiimide-mediated amidation using a water-soluble carbodiimide. Both treatment methods were successful in generating ODA-TONc ionic complexes and amides, and both methods resulted in the total consumption of available TONc carboxyl groups. Effects of the two surface modification methods on the properties of TONc were investigated through a variety of techniques including x-ray diffraction (XRD), contact angle (CA), and thermogravimetric analysis (TGA) studies. Based on results of XRD experiments, it was found that the crystallinity index of TONc decreased, respectively, by *ca.* 25% and 15% in response to ionic complexation and amidation treatments. The modified nanocelluloses from both treatments formed birefringent dispersions in organic solvents of varying polarities and exhibited water contact angles significantly higher than that of TONc control. However, the formed suspensions were unstable over time and their flocculation was complete in a matter of hours. It was determined from TGA investigations that the main decomposition reactions of TONc and its surface-modified derivatives occurred at lower temperatures and were associated with lower activation energies than that of natural cellulose. Furthermore, activation energies associated with thermal decomposition revealed that thermal stabilities of the amidation and ionic complexation products increased and decreased, respectively, relative to that of TONc control.

## 3.2. Introduction

Saito *et al.*[1, 2] recently discovered TEMPO-oxidized nanocelluloses (TONc) from the low energy mechanical disintegration of TEMPO-oxidized pulp. Proposed and demonstrated applications for TONc, which rely on their predominantly hydrophilic character, include additives in paper and food,[3, 4] substitutes for cellulose ethers,[5] and coatings for oxygen barrier

properties.[6] To date, TONc have also been employed as components in a variety of patented applications namely oxygen barrier,[7] gel,[8] thickener,[9] papermaking,[10] composite[11] and cosmetic[12] preparations. As yet unexplored applications of TONc are their use in non-aqueous medium processes, such as reinforcing additives in water-insoluble polymer matrices. TONc possess favorable attributes for nanocomposite reinforcement such as multiple surface functionalities (-COOH and –OH), high fibril individualization, small (3 – 5 nm) fibril widths (large surface area to volume ratio), and degree of crystallinity similar to that of native cellulose fibers.[13-16] The hydrophilic character of TONc (reported in terms of water retention values as 400% for the salt form and 200% for the acid form[1]), is the most likely deterrent to its use in organic medium processes.

The goal of this study was to surface-modify TONc for dispersion in organic media and to further compare characteristics of unmodified TONc control and the surface-modified derivatives. TEMPO-oxidized celluloses have been shown to be amenable to aqueous medium modification through carbodiimide-mediated coupling of the oxidized cellulose carboxylate groups to primary amines.[17-20] A prime example is the work of Araki *et al.*,[17] which involved the coupling of amine-terminated polyethylene glycol (PEG) chains onto the surfaces of TEMPO-oxidized cellulose whiskers. Their use of 1-ethyl-3-(3-dimethylaminopropyl) carbodiimide hydrochloride (EDC) in combination with N-hydroxysuccinimide (NHS)[17, 21-23] (Figure 3.1 A and B) as coupling agents led to successful amide bonding of PEG chains to the whisker surfaces. The grafted nanocelluloses were reported to not flocculate in as high as a 2M sodium chloride solution and to form chiral nematic structures in chloroform. In related studies, EDC-mediated amidation was employed to couple fully and partially water-soluble amines to wood pulp TONc[20] and water-soluble TEMPO-oxidized cellulose (6-carboxy cellulose).[18] Surface modification of TONc has not only been limited to covalent coupling reactions but has also been accomplished by non-covalent adsorption of hydrophobic molecules onto TONc carboxyl sites. Fukuzumi *et al*. demonstrated this approach through the electrostatic adsorption of alkylketene dimer (AKD) onto the carboxylate sites of TONc films.[6] Exposure of the TONc films to an AKD solution (0.05%) for 10 s increased the water contact angle on the film surfaces from 47° to 94°.

To achieve the stated goals for this study, we employed octadecylamine (ODA, Figure 3.1 C), a hydrophobic aliphatic amine for the surface modification of TONc. Two treatment

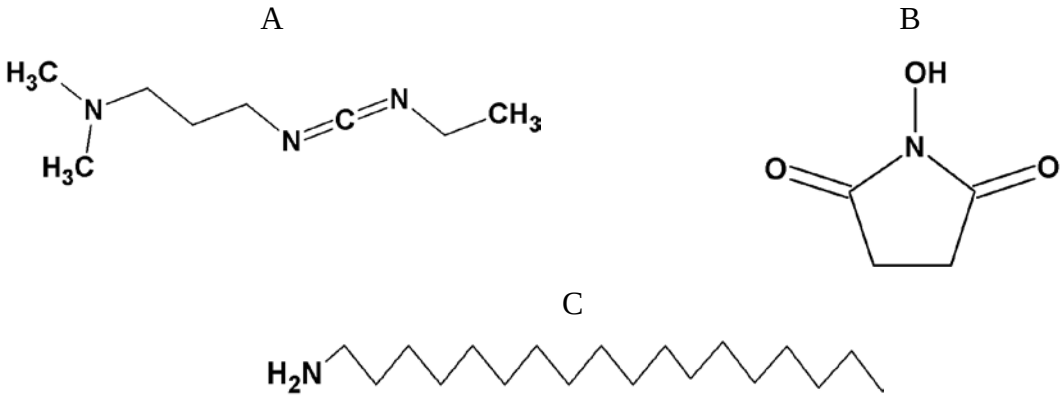


**Figure 3.1** Chemical structures of (A) EDC, (B) NHS, and (C) octadecylamine

methods to ODA coupling, namely physical mixing of ODA solutions with TONc suspensions to form ODA-TONc ionic complexes and EDC/NHS-mediated amidation between ODA and TONc surface carboxyl groups, were considered. The effectiveness of the treatment methods in achieving the desired coupling were evaluated by Fourier transform infrared (FTIR) spectroscopy and elemental analysis (EA). Dispersibilities of the treated samples in organic solvents were tested using flow birefringence examinations between crossed polarizers. In addition, treatment effects on the crystallinity, surface polarity, and thermal decomposition properties of the treated nanocelluloses were evaluated and compared with those of unmodified TONc control and conventional microfibrillated celluloses (MFC).

## 3.3. Experimental Section

### 3.3.1. Materials

Never-dried kraft pulp (Douglas fir) was kindly donated by Weyerhaeuser Company, Longview, WA and stored frozen until used. Microfibrillated cellulose (MFC) was a commercial product (Celish KY) supplied by Daicel Chemical Industries, Tokyo, Japan. Chemicals for TEMPO-mediated oxidation: TEMPO (99.8%), sodium hypochlorite (NaOCl) (reagent grade, 13.4% available chlorine) solution, sodium bromide (NaBr) (99.0%), NaOH (0.5 N) standard solution, HCl (0.1 and 1.0 N) standard solution, and ethanol (200 proof) were purchased from Sigma-Aldrich. Reagents and solvents for surface modification treatments were octadecylamine (ODA) (99.0%) and dimethylformamide (DMF), ACS reagent grade (99.8%)

purchased from Sigma-Aldrich, and EDC and NHS (both > 98.0% purity), purchased from Pierce Protein Research Products, Rockford, IL.

#### 3.3.1.1. TEMPO-Oxidized Pulp

The general procedure and reagent ratios used by Saito *et al.*[1] were followed for TEMPO-mediated oxidation of never-dried pulp. A typical oxidation reaction started with never-dried pulp (20 g dry weight, 123 mmol AGU) suspended in 800 mL ultrapure water (18 MΩ·cm at 25 °C) in a three-neck round bottom flask. The pulp suspension was stirred continuously at 400 – 500 rpm with an overhead stirrer. NaBr (2.5 g, 24.3 mmol) and TEMPO (0.25 g, 1.60 mmol pre-dissolved in 10 mL of ultrapure water) were added to the pulp suspension, and pH was adjusted to 10.0 ± 0.1 with NaOH (0.5 N). A pH probe (Mettler Toledo InLab® Expert Pro) attached to a pH/conductivity meter (Mettler Toledo Seven Multi™) was used for monitoring pH of the reaction. Next, NaOCl (46.1 mL, 5.0 mmol) was added drop-wise from a plastic syringe mounted on a syringe pump (Harvard Apparatus model 44), while maintaining the pH of the reaction system at 10.0 ± 0.1. The end of the reaction was reached when no further change in pH was observed and then the reaction was fully quenched with the addition of ethanol (30 mL). The oxidized pulp was recovered by vacuum filtration, washed several times with ultrapure water to neutral pH, and stored wet at 5 – 8 °C until used. The carboxyl content (1.62 ± 0.01 mmol / g AGU) was determined by conductometric titration as described in section 3.3.3.2.

#### 3.3.1.2. TONc

Fibrillation of TEMPO-oxidized pulp into TONc was accomplished by ultrasonication of oxidized pulp suspensions. TEMPO-oxidized pulp was suspended in ultrapure water at a solids concentration of 0.5 wt %. The suspensions were sonicated in batches of 150 mL with an ultrasonic processor (Sonics model GE 505) fitted with a half-inch probe. Sonication was performed in a specially designed double-walled beaker connected to a cooling bath to minimize overheating of suspensions. Twenty minutes of sonication was found sufficient to generate visually transparent suspensions similar to earlier reported examples.[2, 24] An average ultrasonication energy of 124 ± 0.72 kJ $g^{-1}$ solids was calculated using sonicator readings from individual batches. Generally, after ultrasonication, a small residue of unfibrillated fibers were observed floating in the sonicated suspensions that were removed by centrifugation (4500 rpm, 5

min) using an Eppendorf 5804 centrifuge. The resulting TONc suspensions were stored in a refrigerator at 5 – 8 °C until used.

#### 3.3.1.3. MFC Suspensions

The manufacturer-supplied MFC suspensions were further homogenized by blending (Waring Blender) for 12 min and subsequently by ultrasonication for 2 h. Blending was performed on 400 mL batches of 0.75 wt % while ultrasonication was performed on 150 mL batches at the same concentration as blending, using a similar setup as described under section 3.3.1.2.

### 3.3.2. Surface Modification of TONc

For both ionic complexation and amidation treatments, a carboxyl : amine mole ratio of 1 : 4 was used. Miscibility of ODA with aqueous TONc suspensions was achieved by dissolving ODA in DMF (at 4% w/v) prior to mixing with the TONc suspension. Control **(Ctrl)** samples were prepared by repeating the ionic complexation and amidation procedures (sections 3.3.2.1 and 3.3.2.2) on TONc without the use of ODA or coupling agent. Details of the individual surface modification procedures are presented next with their proposed reaction schemes displayed in Figure 3.2.

#### 3.3.2.1. Physical Mixing (Ionic Complexation)

TONc suspension (1000 mL of 0.5 wt %, 8.1 mmol COOH content) was transferred into a three-neck round bottom flask with overhead stirring (400-500 rpm) and the flask was equilibrated at 50 °C in an oil bath. The solution of ODA (8.7 g, 32.4 mmol) in DMF (250 mL) was added to the TONc suspension, which instantly changed in appearance from transparent to white. The pH of the mixture was subsequently adjusted to and maintained at 7.5 – 8.0 using HCl (1 N) and NaOH (0.5 N). Stirring was continued for 4 h, during which the suspension turned slightly yellow. The product **(ICmplx)** was then recovered as later described in section 3.3.2.3.

##### *3.3.2.1.a. Heat Treatment of ICmplx*

ICmplx was subjected to heat treatment with the purpose of generating amide bonds via condensation of the formed ionic bonds. This approach was motivated by the work of Toffey *et al.*,[25-27] in which chitin was generated from the controlled heating of the acetate salt of chitosan

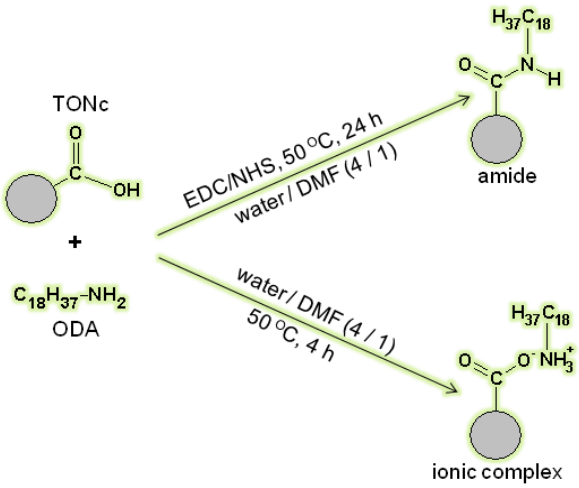


**Figure 3.2** Proposed simplified reaction schemes for modification of TONc surfaces.

(chitosonium acetate). Specifically, a concentrated suspension (*ca.* 2 wt %) of dialyzed ionic complex (see section 3.3.2.3 for description of the dialysis procedure) was placed in the platinum pan of a thermogravimetric analyzer (referenced in section 3.3.3.5) and heated rapidly (40 °C/min) to the desired condensation temperature (120 or 150 °C). The sample was held at this temperature for 4 h, cooled to room temperature and then recovered for FTIR analysis.

#### 3.3.2.2. Carbodiimide-Mediated Amidation

Our procedure for EDC/NHS-mediated amidation was similar to that of Araki *et al.*,[17] except for minor differences in the concentrations of coupling agents used and the order in which reagents were added. Adjustments in process conditions were found necessary to achieve satisfactory surface modification. A typical treatment process started with the same amount and preconditions of TONc suspension described for ionic complexation (section 3.3.2.1). Next EDC (7.76 g, 40.5 mmol) and NHS (5.59 g, 48.6 mmol) were dissolved in 20 mL of ultrapure water and added to the TONc suspension. The pH of the reaction mixture was adjusted to 5.5 – 6.0 and maintained for 30 min to complete the activation of TONc surface carboxyl groups. Finally, the ODA solution (identical to that described in the previous section) was added and the reaction was continued for an additional 12 h at pH 7.5 – 8.0. The amidation product **(Amd)** followed similar color changes and was similarly recovered as the ionic complexation product.

#### 3.3.2.3. Sample Recovery

Both Ctrl and ODA-treated TONc were recovered by centrifugation, dialysis, and freeze-drying. First, the suspensions were centrifuged to separate the nanocelluloses (residue) from the mixture of solvents and dissolved reagents (supernatant). The residues were twice dispersed and centrifuged in ultrapure water to remove traces of reagents remaining. Additional washes were performed with HCl (0.1 N) and ethanol respectively, to regenerate any residual carboxyl remaining after the treatments and to extract any remaining traces of unbound ODA. These steps were followed by multiple water washes until pH was neutral. The washed residues were re-suspended in ultrapure water and dialyzed using Spectra/Por (Spectrum Laboratories) regenerated cellulose membranes (cut-off molecular weight 12 – 14 kD). Dialysis was ended when the conductivity of the surrounding water remained constant.

#### 3.3.2.4. Storage

To obtain suitable specimens for the various characterization techniques, Ctrl, Amd, and ICmplx suspensions were processed and stored in different forms as follows: (1) Fractions of the dialyzed suspensions were stored at 5 – 8 °C for use in conductometric titration. (2) Fractions of dialyzed suspensions were freeze-dried, further dried in *vacuo* (1.33 mbar, 50 °C, 2 h), and kept dry by continuous storage in a desiccator under phosphorus pentoxide ($P_2O_5$). (3) The remaining dialyzed suspensions were dispersed by sonication in ethanol solution (80% v / v), transferred into polytetrafluoroethylene (PTFE) dishes, and solvent-cast into 200 ± 40 µm thick films by evaporation in a fume hood. The air-dried films were further vacuum-dried (1.33 mbar, 50 °C, 1 h) and transferred into desiccators under $P_2O_5$. To minimize surface contamination, the films were stored in sealable polyethylene bags inside the desiccator.

With the exception of centrifugation washing and dialysis, similar drying and storage steps as described above for TONc-based samples were used to obtain MFC samples.

### 3.3.3. Characterization

For certain characterization techniques, MFC was used as unoxidized nanocellulose reference for comparison with TONc-based samples.

#### 3.3.3.1. Surface Chemical Properties - FTIR

Effects of modification treatments on surface chemistry of TONc were examined by FTIR. Transmission FTIR was performed on freeze-dried samples (~2.5 mg) mounted in *ca.* 200 mg KBr (Spectrograde Powder, International Crystal Labs, Garfield, NJ). Spectra were obtained at room temperature on a Thermo Scientific Nicolet 8700 spectrometer under continuous purging with dry air. Each spectrum was acquired from 32 scans at a resolution of 4 $cm^{-1}$. A separate background spectrum was collected and automatically subtracted from the raw spectrum for each specimen.

#### 3.3.3.2. Degree of Surface Modification – Conductometric Titration (CT) and Elemental Analysis (EA)

Carboxyl concentrations in both the original and treated nanocelluloses were evaluated by conductometric titration (CT). CTs were carried out on freshly dialyzed suspensions using a conductivity probe (Mettler Toledo InLab® 730) attached to a pH/conductivity meter (Mettler Toledo Seven Multi™). NaOH (0.1 N standard solution) was dispensed from a microburette (Brinkmann Bottletop Buret 50) against 100 mL of sample suspension (0.5 wt % solids) under continuous nitrogen flow and stirring with a magnetic bar. The initial strong acid dissociation region[28] of the CT curve was obtained by addition of HCl (5mL of 0.1 N standard solution) to the sample suspension prior to addition of NaOH. Carboxyl concentration was expressed as degree of oxidation (DO) according to equation 3.1.[29]

$$DO = \frac{162 n_{COOH}}{w - 14 n_{COOH}} \qquad 3.1$$

where (162) refers to the molar mass of AGU, $n_{COOH}$ is the moles of carboxylic acid in the sample (calculated directly from CT data), w is the initial dry weight of the sample, and (14) represents the molecular weight difference between TONc (acid form) and unoxidized cellulose.

ODA content was quantified directly from nitrogen content data obtained through the Kjeldahl elemental analysis technique. Kjeldahl tests were conducted on freeze-dried samples (*ca.* 0.5 g) at Galbraith Laboratories Inc (GLI), Knoxville, TN using the GLI test protocol E7-1 (Appendix A). ODA content was expressed as degree of substitution (DS), which was

determined in accordance with the method developed by Vaca-Garcia et al.[30] Details of DS calculations are given in Appendix B.

#### 3.3.3.3. Film Surface Roughness and Surface Polarity – AFM and Contact Angle (CA) Measurements

The solvent-cast films were first examined by AFM to quantify their surface roughnesses prior to CA measurements. MFC films were included as an unoxidized nanocellulose reference. AFM images were acquired with an Asylum Research MFP-3D Bio AFM on vacuum dried films mounted on glass slides with the aid of double-sided tape. Measurements were performed in tapping mode using standard Si probes (Olympus AC-240TS, force constant (2 N $m^{-1}$), tip length and radius (240 µm and 9 ± 2 nm), resonance frequency (~70 kHz)).

Advancing contact angles of water sessile drops were used to represent changes in surface polarity as a result of TONc surface modification. The contact angle (CA) setup (First Ten Angstroms, FTA) consisted of a CCD[a] camera-microscope lens assembly and a movable samplestage. Water sessile drops (~20 µL) were deposited on film samples attached to glass slides by means of double-sided tape. MFC films were included as an unoxidized nanocellulose reference. Four hundred advancing contact angle images were acquired at a rate of 33 images per second, beginning at the instant the drop contacted the surface (0 s). Following image acquisition, contact angles were measured automatically with the instrument software (FTA 32) and subsequently plotted as a function of time.

#### 3.3.3.4. Crystallinity Properties – X-ray Diffraction (XRD) Analysis

Film samples were examined by XRD to evaluate treatment effects on the crystalline characteristics of TONc. MFC films were included as an unoxidized nanocellulose reference. Discs (7.5 mm diameter) were punched out of vacuum-dried films and stacked to ~800 µm thickness (4 layers). Film stacks were examined in a Bruker ASX D8 Discover wide angle x-ray diffractometer using Ni-filtered CuKα radiation (λ = 0.154 nm) operated at 40 kv and 40 mA. X-ray diffractograms were acquired at 0.01° $sec^{-1}$ over a 2θ (Bragg angle) scan range of 10–40°. Crystallinity index (C.I.) values for cellulose Iβ, the main form of cellulose in wood pulp, were calculated as

[a] Charged couple device

$$C.I. = \left[ \frac{I_{200} - I_{AM}}{I_{200}} \right] \times 100 \qquad 3.2$$

where $I_{200}$ is the intensity of the 200 reflection ($2\theta$ = ~22.5°) and $I_{AM}$ is the minimum value at $2\theta$ = ~18°, which represents the reflection intensity of the amorphous content.

#### 3.3.3.5. Thermal Decomposition Properties – Thermogravimetric Analysis (TGA) -

TGA experiments were carried out on a TA Instruments Q500 thermogravimetric analyzer. Thermal decomposition behavior and the kinetics of thermal decomposition were both studied. Freeze-dried samples (10 – 12 mg) were scanned from room temperature to 600 °C in dry air (flow rate 60 mL $min^{-1}$) at 10 °C $min^{-1}$. MFC was included as an unoxidized nanocellulose reference. To gain superior control over sample decomposition kinetics, TGA experiments were performed using the high-resolution (Hi-Res™) dynamic heating rate option[31] at resolution and sensitivity settings of 4 and 1. In high-resolution (Hi-Res™) dynamic rate experiments, the instrument heating rate responds to the rate of the thermal decomposition reaction by decreasing towards a fixed minimum[a31] as reaction rate increases and increasing towards the maximum (operator-set) ramp rate when there is no thermal event taking place. This method generates data in significantly less time than constant heating rate or isothermal experiments of comparable resolution. Use of high-resolution dynamic rate experiments are noted to be particularly useful for the characterization of multicomponent materials.

Additional scans were performed at resolutions 2, 3, 5, and 6 to obtain data for analysis of decomposition kinetics using the method developed by Salin and Seferis.[32] Their method, developed to specifically address the nonlinear and nonisothermal conditions associated with dynamic rate experiments is given by

$$\ln \frac{q}{T^2} = \frac{E_a}{R} \frac{1}{T} + \ln \left[ \frac{AR}{E_A} n(1-\alpha)^{n-1} \right] \qquad 3.3$$

where q is the heating rate observed at the maximum rate of weight loss (WL) (peak of derivative of weight loss (DWL) curve in a dynamic rate scan), T is the absolute temperature, $E_a$

[a] This non-zero minimum is determined automatically by resolution, sensitivity, and initial temperature ramp settings

is the activation energy, R is the molar gas constant, A is the pre-exponential (or frequency) factor, n is the order of the reaction, and α is the sample conversion given by

$$\alpha = \frac{M_o - M_t}{M_o - M_f} \qquad 3.4$$

where $M_o$, $M_t$, and $M_f$ represent original sample mass, sample mass at any time t, and final sample mass, respectively. From a plot of ln $(q/T^2)$ vs. (1/T), $E_a$ and A were calculated from the slope and intercept, respectively. Salin and Seferis derived the following equation for calculating n from experimental data:

$$n = \left(\frac{d\alpha}{dT}\right)^{-1} \frac{E_a B}{qR}(1-\alpha)\exp\left(\frac{-E_a}{RT}\right) \qquad 3.5$$

where B is the exponential of the intercept, I, from the ln $(q/T^2)$ vs. (1/T) plots and all other symbols retain their previously defined meanings.

To generate useful data for kinetic analysis, resolution rather than heating rate (as is normally done for constant heating rate experiments) was varied as recommended by Salin and Seferis.[32] Through preliminary investigations, a heating rate of 30 °C $min^{-1}$ was selected for generation of all kinetic analysis data because thermograms produced at 30 °C $min^{-1}$ showed the least disturbances at all resolutions compared to those produced at 10 or 20 °C $min^{-1}$.

## 3.4. Results and Discussion

### 3.4.1. Effects of Coupling Methods on Surface Chemical Properties of TONc

Previous studies have shown that during aqueous medium TEMPO-oxidation of cellulose nanofibrils and nanocrystals, only the surface hydroxyl groups of the cellulosic elements are oxidized leaving the inner crystalline domains intact.[1, 16] By using similar reactant concentrations as those used on kraft pulp by Saito *et al.*[1], we presumed that TONc in the present study were primarily surface-oxidized. In the FTIR spectrum originating from Ctrl (Figure 3.3 A and Figure 3.4 A), characteristic cellulose peaks are present in addition to a strong 1729 $cm^{-1}$ – carbonyl (C=O) stretching peak due to –COOH groups formed.[2, 16-18] Neat ODA (Figure 3.3 D

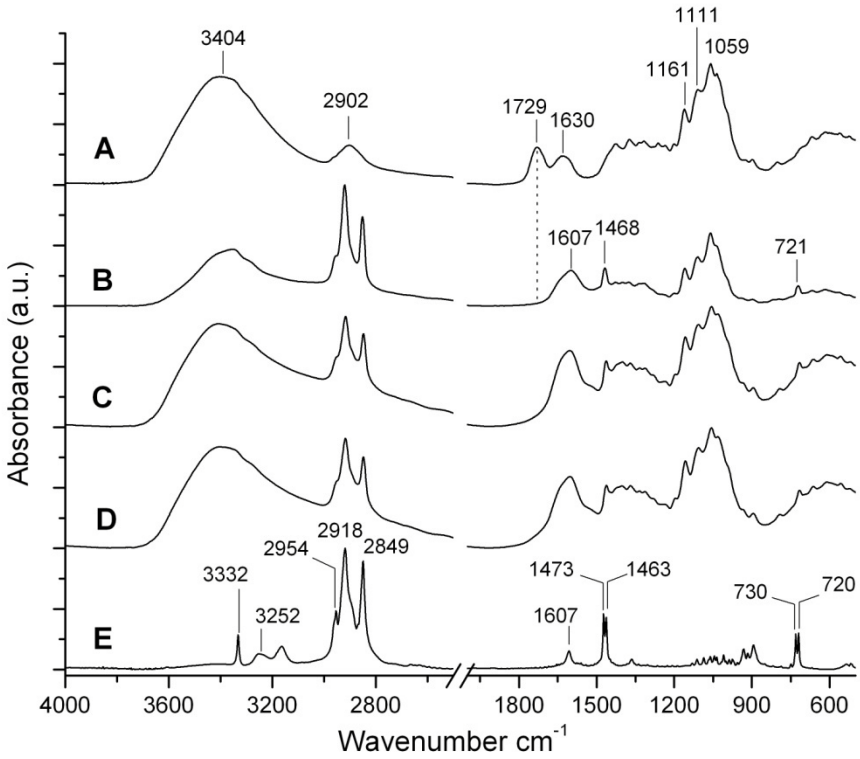


**Figure 3.3** FTIR absorbance spectra of (A) Ctrl, (B) ICmplx, (C) and (D) ICmplx heat-treated at 120 and 150 °C respectively, and (E) ODA. Absence of 1729 $cm^{-1}$ peak in spectrum B (guided by dotted line) indicates complete consumption of available –COOH groups. Peak at 1607 $cm^{-1}$ is believed to originate from combination of asymmetric $COO^-$ and $NH_3^+$ stretching vibrations of formed octadecylammonium carboxylate complex. Also present, symmetric and asymmetric –CH stretching (2954-2849 $cm^{-1}$) and deformation (1468 and 721 $cm^{-1}$) vibrations from ODA tails. Spectra C and D retain features of spectrum B and show no evidence of amidation in response to heat treatment.

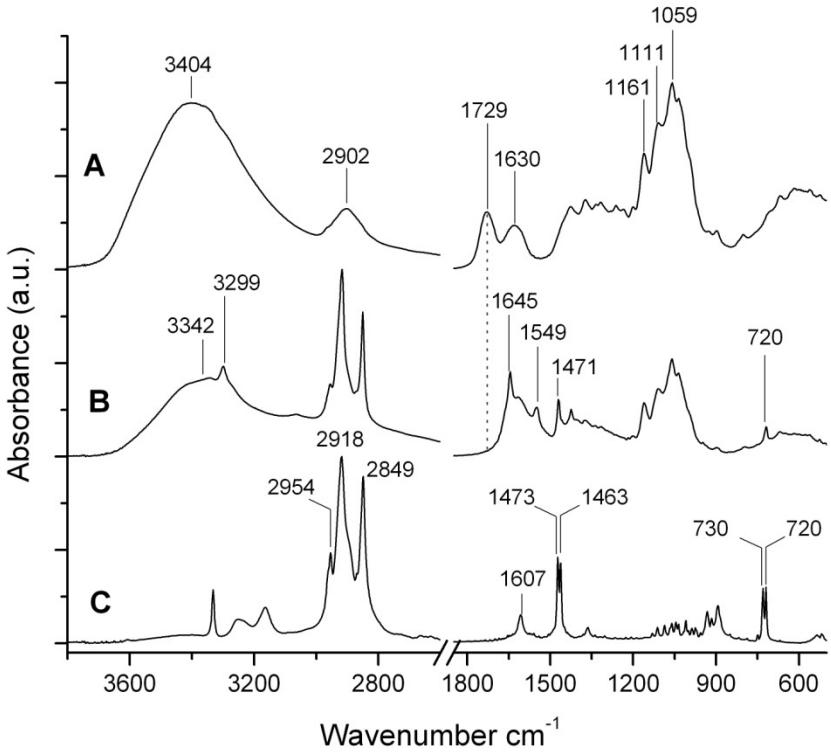


**Figure 3.4** FTIR absorbance spectra of (A) Ctrl, (B) Amd, and (C) ODA. Amidation evident (spectrum B) from presence of amide I (1645 $cm^{-1}$) and amide II (1549 $cm^{-1}$) bands. Also, disappearance of 1729 $cm^{-1}$ peak (guided by dotted line) indicates complete consumption of available –COOH groups during amidation. Peak at 3299 $cm^{-1}$ represents N-H stretching vibration of secondary amides.[33] Also present, peaks originating from native cellulose and ODA, identified in Figure 3.3 and in text.

and Figure 3.4 C) is characterized by –NH stretching (3332 and 3252 $cm^{-1}$) and deformation (1607 $cm^{-1}$) vibrations as well as –CH methyl and methylene stretching (2849 – 2954 $cm^{-1}$) and deformation (1463 $cm^{-1}$ / 720 $cm^{-1}$) bands of the octadecyl tail. Spectra from ICmplx (Figure 3.3) and Amd (Figure 3.4) reveal that both surface modification treatments succeeded in coupling ODA molecules with TONc carboxyl groups. Several of the bands originating from Ctrl and ODA spectra are shared by spectra of both ICmplx (Figure 3.3 B) and Amd (Figure 3.4

B) and indicates co-existence of the two starting materials in the modified products. However, the C=O peak (1729 $cm^{-1}$) from Ctrl (Figure 3.3 A and Figure 3.4 A) is clearly absent from both the ICmplx and Amd spectra, signifying complete conversion of available TONc carboxyl groups.

New bands present in the spectra of ICmplx and Amd provide evidence in support of the types of bonding expected from their respective treatment reactions. The appearance of a broad 1607 $cm^{-1}$ peak in ICmplx spectrum is attributed to the formed octadecylammonium carboxylate groups (see structure in reaction scheme, Figure 3.2). This peak appears very broad and its origin may be a combination of asymmetric $–COO^-$ stretching (1550 – 1610 $cm^{-1}$) from TONc carboxylates and asymmetric $NH_3^+$ deformation (1560 – 1625 $cm^{-1}$) from octadecylammonium groups.[33-35] A survey of the literature revealed that electrostatic adsorption of water-soluble amines and amine-functionalized polyelectrolytes, such as polyethyleneimine, onto charged cellulose surfaces has been fairly well studied.[3, 36-38] However, no references were found for electrostatic adsorption onto charged celluloses by distinctly hydrophobic amines such as the higher aliphatic amine used in this study.

Carbodiimide-mediation clearly resulted in the generation of ODA-TONc amide bonds as shown by the presence of amide I (C=O stretching at 1645 $cm^{-1}$), amide II (combination of N-H deformation and C-N stretching at 1549 $cm^{-1}$)[17-19, 21, 33], and the solid state N-H stretching (3299 $cm^{-1}$)[33] bands of Amd (Figure 3.4 B). Previous EDC/NHS-mediated amidation reactions between carboxylated celluloses and primary amines were characterized by only a partial conversion of the available –COOH groups. A fraction of the starting –COOH groups often remained unconverted or perhaps regenerated during acid washing of the reaction product.[17-20] In these studies, water was used as the only medium, and the coupling reactions involved primary amines of varying water solubilities. In the present work, the complete conversion of available –COOH groups clearly indicates adequate amine solubility in the water-DMF co-solvent medium even with the use of a strongly water-repelling amine like ODA. The co-solvent medium is evidently responsible for the feasibility of ionic complexation and demonstrates a simple and direct route to the surface modification of TONc. Clearly, the presence and the abundance of charged surface functionalities are advantages that can be further exploited towards utilization of TONc.

Another interesting observation is the resistance of ICmplx to regeneration of –COOH groups following exposure to acidic media. The nanocellulose recovery process following modification reactions included HCl washing at pH 1.3 – 1.4, which was expected to regenerate –COOH groups from the octadecylammonium carboxylate complexes. As FTIR results have shown, regeneration of –COOH did not occur. Saito and Isogai reported the metal ion-dependent stability of metal ion carboxylate salts prepared by ion exchange between the sodium salt of TEMPO-oxidized cellulose and a variety of metal ions ($Pb^{2+}$, $La^{3+}$, $Al^{3+}$, $Ca^{2+}$, $Ba^{2+}$, $Ni^{2+}$, $Co^{2+}$, $Cd^{2+}$, $Sr^{2+}$, $Mn^{2+}$, $Ca^{2+}$, and $Mg^{2+}$).[39] Resistance of the various metal carboxylate salts to dissociation was examined by exposing the ion-exchanged oxidized fibers to nitric acid ($HNO_3$) solution (pH 1.7) and sodium nitrate ($NaNO_3$) solution (pH 7.0). Approximately 20% of $Pb^{2+}$ and $La^{3+}$ ions remained in their respective $HNO_3$–treated fibers compared to a near complete generation of free carboxylic acids in the fibers exchanged to the other metal ions. Also, substantially higher residual $Pb^{2+}$ and $La^{3+}$ concentrations remained in the $NaNO_3$–treated fibers relative to the $HNO_3$–treated samples. In the present study, a hydrophobic shielding effect is hypothesized. It is speculated that the alkyl tails of the attached octadecylammonium groups create a strongly hydrophobic environment in the immediate vicinity of modified nanofibrils, which resists dissociation in the low pH environment.

### 3.4.2. Effects of Heat-Treatment on ICmplx

The approach used by Toffey et al.[25-27] to convert chitosan-alkanoic acid complexes into amidized derivatives was adapted with the goal of converting octadecylammonium carboxylate groups into amide bonds. After heat-treating a concentrated ICmplx suspension at 120 and 150 °C for 4 h, the resulting dry pelletized samples were recovered and examined under FTIR. The recorded spectra (Figure 3.3 C and D) were essentially identical to that of ICmplx (Figure 3.3 B) and showed no evidence of amide bonding. In the experiments of Toffey *et al.*, ionic complexes of chitosan with $C_1$ to $C_4$ homologs of alkanoic acids underwent variable degrees of conversion, under heat, to N-acyl derivatives. The authors explained that volatility of alkanoic acid homologs and the differences in equilibrium constants of the amine-alkanoic acid-N-acylate mixtures contributed to lower than expected degrees of substitution (ranging from 0.1 for formyl to 0.6 for acetyl). With respect to ICmplx (current study), plausible explanations for the lack of conversion are the heterogeneity of the reaction system compared to a homogeneous phase in the

chitosan–alkanoic acid studies and the relatively short treatment time (4 h versus 24 h in the chitosan-based study). In this study, heat treatment was limited to reduce the potential for heat-induced degradation of the nanocelluloses. It is, however, possible that the heat treatment time for the current study was insufficient to effect condensation of the ionic complex into amide bonds.

### 3.4.3. Quantitation of Degree of Surface Modification

Conductometric titration and nitrogen analysis were the two measurement methods chosen to quantify the ODA content of surface-modified TONc.

Conductometric titration was used to directly quantify the amount of residual –COOH in the untreated and ODA-modified samples. The amounts of –COOH consumed during surface modification were calculated as the differences between the experimentally determined moles of –COOH in the control and ODA-modified samples. Under the assumption that all converted –COOH moieties were substituted with ODA molecules, ODA content (in moles) of the modified samples was equated with the calculated moles of –COOH. Representative conductometric titration plots for the untreated and ODA-modified TONc are shown in Figure 3.5 for Ctrl, ICmplx, and Amd. Residual –COOH content for the two ODA-modified samples was determined to be zero (Table 3.1), which is consistent with the qualitative observations from FTIR. These results indicate that all available –COOH groups on TONc surfaces were consumed in the course of ODA coupling, without regard to the treatment method (Table 3.1).

Direct quantification of ODA content from N content data (Table 3.1) show a slightly higher DS in ICmplx than Amd. The origin of such a difference was not directly traceable although its effects are observed in the XRD, CA, and TGA results (discussed later). Table 3.1 also reveals that ODA contents from elemental analysis are nearly identical to the –COOH content of Ctrl, and independently supports the assertion that all available –COOH groups in the original TONc were substituted with ODA molecules.

### 3.4.4. Crystallinity

X-ray diffractogram profiles typical of cellulose Iβ[40, 41] were obtained for both Ctrl and MFC (Figure 3.6). The 110 and $1\bar{1}0$ peaks (2θ angles ~15° and 16.5° respectively) are better resolved in MFC than TONc and indicate greater crystalline order in the former. It has been reported

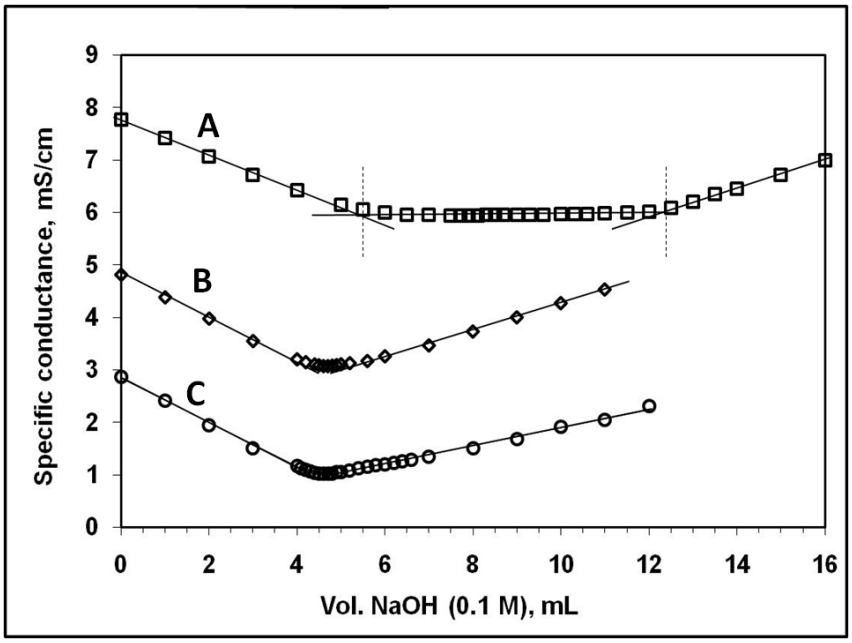


**Figure 3.5** Sample conductometric titration curves for (A) Ctrl, (B) ICmplx, and (C) Amd. The flat region of curve (A) (between two dotted lines) represents –COOH neutralization by NaOH, from which carboxyl content of Ctrl is determined. The absence of a flat region in curves (B) and (C) indicates complete consumption of available –COOH groups during the surface modification processes.

that TEMPO-mediated oxidation affects only the hydroxyl groups in the amorphous domains and at the surfaces of crystalline domains of cellulose I fibers.[14, 42-44] As a consequence, the crystallinity of native cellulose is not altered by TEMPO-mediated oxidation.

With respect to the ODA-modified TONc, the ICmplx diffractogram appears similar in shape to that of Ctrl but the profile of Amd around the 110 and $1\bar{1}0$ reflections is fairly broad and slightly distorted. Furthermore peak intensities of ICmplx and Amd are significantly reduced for the three (110, $1\bar{1}0$, and 200) main equatorial reflections displayed (Figure 3.6) but the intensity of the meridional 040 reflection (inset in Figure 3.6) is practically unaffected by the surface modification treatment. A similar pattern of intensity responses was observed when tunicate fibers were subjected to acetylation and the effect of acetylation time on crystallinity of tunicin microcrystals was monitored.[45] The authors observed decreasing intensities of the equatorial peaks but no change in intensity of the 040 reflection with increasing acetylation time. They

**Table 3.1** Carboxyl and ODA contents derived from conductometric titration and N content analysis. (Degree of oxidation (DO) computed from equation 3.1; degree of substitution (DS) computed from method of Vaca Garcia *et al.*,[30] Appendix B).

| Sample ID | N content, wt %[a] | Carboxyl | | ODA | |
|---|---|---|---|---|---|
| | | DO[b] | (mmol/g AGU) | DS | (mmol/g AGU) |
| Ctrl | 0.017 | 0.262 (0.001) | 1.62 (0.01) | - | - |
| Amd | 1.62 (0.02) | 0 | 0 | 0.267 (0.004) | 1.65 (0.02) |
| ICmplx | 1.67 (0.03) | 0 | 0 | 0.289 (0.007) | 1.78 (0.04) |

[a] Sample weight basis from Kjeldahl method

[b] Calculated on basis of total amount of AGU present in sample mass. Previous studies have determined that oxidation is confined to nanofibril surfaces. Therefore, values will be higher if only surface AGUs are considered.

Standard deviations are shown in parentheses for three replications

attributed the intensity decreases of the equatorial peaks to a progressive loss of lateral order in the cellulose Iβ crystallite while the retention of the 040 intensity indicated preservation of crystal spacings in the axis direction of crystallites. It was believed that acetylation of tunicin fibers proceeded, over time, in a skin-to-core fashion and was responsible for the progressive loss of lateral order. XRD peak intensity reductions and also peak broadening effects have been observed in other cellulose surface modification studies[40, 41, 45, 46] pertaining to aliphatic $C_6$ to $C_{22}$ esterification of cellulose I micro and nanoscale fibers. Reductions in peak intensities[40, 41, 46] and peak broadening[40, 41] were found to relate positively with lengths[40, 41] and degrees of substitution[40, 41, 46] of attached alkyl chains. The former was generally attributed to a relative increase in amorphous component and was typically observed to be accompanied by an increase in the intensity of amorphous scattering (2θ ~18°).[40, 41, 46] In this study, the lower intensities of ODA-modified TONc peaks imply a reduction in the fraction of crystalline cellulose as a result of ODA modification (Figure 3.6). ODA content of Amd and ICmplx (derived from N content data) (Table 3.1) were 35 and 40 vol % respectively. Crystallinity index values (Table 3.2) of Amd and ICmplx are 60.2 and 49.4 %, which represent reductions of 14.4 and 25.2 % respectively, from the C.I. of Ctrl. The slightly higher degree of ODA substitution in ICmpx

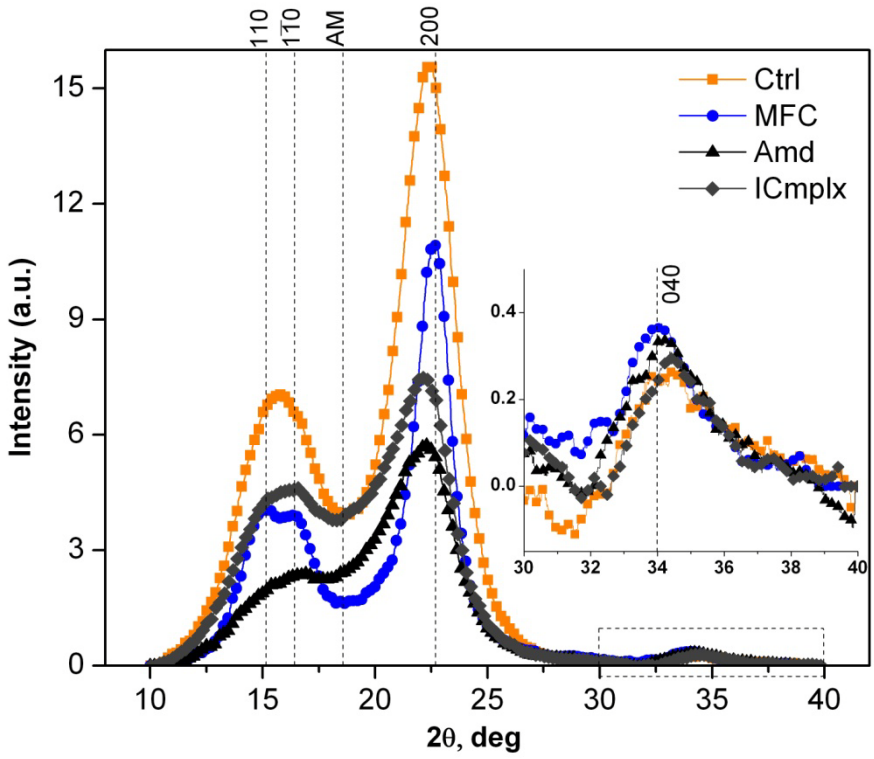


**Figure 3.6** XRD diffractograms of film samples (thicknesses ~800 µm) showing the main cellulose Iβ diffraction planes (labels at the top). AM represents the location of the amorphous scattering taken as the minimum point between the 1 0 and 200 peaks. The inset is an expansion of the 040 meridional reflection (boxed region on main plot). Plots shown are the results of baseline correction and a smoothing function applied to the original diffractograms.

than Amd may partially account for the lower crystallinity index of the former. Difficulty in identifying the exact maxima of the amorphous scattering intensities (at 2θ ~18°) among the different samples could also contribute to the disparity.

### 3.4.5. Dispersion and Stability in Organic Media

Appearance of flow birefringence is commonly used as a metric for efficient nanocellulose dispersion in aqueous suspensions.[47-49] More recently, observations of flow birefringence

**Table 3.2** Crystallinity indices of film samples calculated (according to equation 3.2) from XRD data.

| Sample ID | 2θ | $I_{200}$ | 2θ | $I_{AM}$ | C. I., % |
|---|---|---|---|---|---|
| Ctrl | 22.4 | 15.60 | 18.5 | 3.97 | 74.6 |
| MFC | 22.6 | 10.92 | 18.4 | 1.68 | 84.6 |
| ICmplx | 22.2 | 7.49 | 18.3 | 3.79 | 49.4 |
| Amd | 22.3 | 5.75 | 17.8 | 2.29 | 60.2 |

and chiral-nematic self ordering are routinely used as evidence for dispersion of surface-modified nanocelluloses in organic media.[17, 50-54] Dispersion behavior of Amd and ICmplx in organic solvents of varying polarities was assessed through flow birefringence observations of sample suspensions between crossed polarizers. First, the strongly hydrophilic character of TONc is shown by the strong presence of birefringence in an aqueous suspension of Ctrl sonicated for 5 min (Figure 3.7 A). Amd and ICmplx on the other hand, could not be re-dispersed in water after freeze-drying from their aqueous dialyzed suspensions. The freeze-dried samples merely floated on top of water or remained distinctly separated from water even after vigorous shaking. They could, however, be readily dispersed and did display birefringence in organic solvents of varying polarities, namely toluene (ε = 2.38), THF (ε = 7.52), isopropyl alcohol (IPA, ε = 20.18), and a solution of cellulose acetate butyrate (CAB) in THF (Figure 3.7 B to H). These observations confirm that following ODA modification, TONc surfaces were transformed from hydrophilic to hydrophobic character irrespective of the surface modification approach. They also confirm that both of the surface modification treatments drastically decreased the surface polarity of TONc leading to the appearance of birefringence in a substantially low-polarity solvent such as toluene. These findings complement the FTIR and elemental analysis results, both of which pointed to a complete substitution of available –COOH groups on TONc surfaces by ODA molecules.

Besides birefringence formation, the quality of nanocellulose dispersions is also judged by their stability or non-flocculation over time. Based on the observed dispersion behavior of the ODA-modified TONc, including birefringence in low polarity solvents, the hydrophobized TONc suspensions were expected to maintain stability over the long term. However, in contrast to this expectation, the nanofibrils began to settle within five minutes after agitation, and in

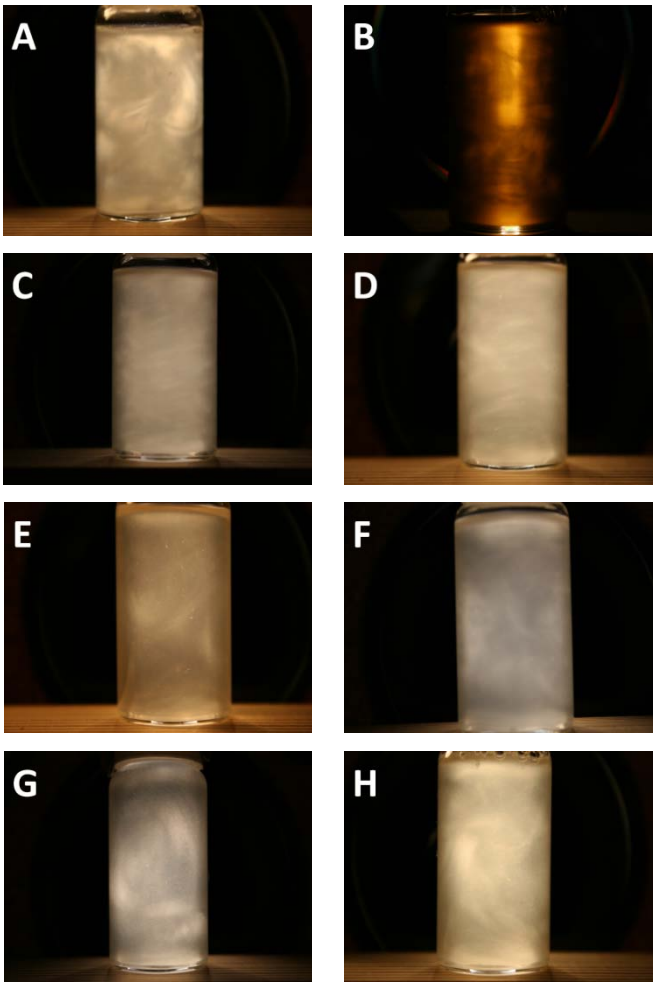


**Figure 3.7** Birefringent dispersions of nanocellulose samples in various solvents. Pictures were taken ~5 s after vigorous shaking of the vials. (A) Ctrl in water, (B) Amd in toluene, (C) Amd in THF, (D) ICmplx in THF, (E) Amd in IPA, (F) ICmplx in IPA, (G) Amd in CAB, and (H) ICmplx in CAB. CAB solutions were prepared in THF prior to nanocellulose dispersion. Suspension concentrations of (A) = 0.125 wt % and (B)-(H) = 0.5 wt %.

matter of several hours, phase separation appeared complete. Figure 3.8 shows side-by-side comparisons of three day-old suspensions of Amd-in-toluene and Ctrl-in-water. A similar pattern of flocculation as a function of time was observed for all the other Amd and ICmplx suspensions shown in Figure 3.7. Examples have been reported in the literature of surface-grafted nanocelluloses that flocculated in organic solvents[55-58] or formed aggregates when used as reinforcements in

**Figure 3.8** Ctrl in water (left) and Amd in toluene (right) three days after dispersion.

polymer matrices.[57, 59] In the case of octadecylisocyanate-grafted sisal nanowhiskers and MFC, the use of conventional solvent exchange resulted in non-dispersion of sisal MFC but complete dispersion of sisal nanowhiskers in dichloromethane.[58] However, when an in situ solvent exchange (boiling off acetone while simultaneously adding toluene to the reaction medium) approach was used, full dispersion was achieved for both modified nanowhiskers and MFC. According to the authors, accessibility to the hydroxyl sites on the highly networked MFC was poor when conventional solvent exchange was used. Dispersion properties of tunicin whiskers surface-modified with isopropyldimethylchlorosilane were also reported to depend on the degree of surface silylation, $\overline{DS_s}$.[56] $\overline{DS_s}$ values below 0.1 resulted in flocculation of silylated whiskers in THF at all whisker concentrations. Between $\overline{DS_s}$ of 0.1 and 0.4, flocculation was observed only when whisker concentrations exceeded 1% w/v. Additionally, the whiskers dispersed in low polarity solvents such as toluene and chloroform. With respect to Amd and ICmplx suspensions, excellent dispersion is achieved, as evidenced by the appearance of birefringence, when sufficient energy is supplied through agitation. However, at rest, fibril aggregation is favored that overwhelms fibril-solvent interactions and leads to flocculation. The origin of aggregation was not ascertained.

### 3.4.6. Film Surface Roughness and Water Contact Angles

Quantitative assessment of surface polarities resulting from the two surface modification treatments was made from contact angle measurements on the nanocellulose films. To account for the contribution of surface roughness to the measured contact angles, roughness

characteristics of the nanocellulose films were determined, first, through imagining of the film surfaces by AFM. Representative height images, roughness profiles, and roughness statistics from AFM are presented in Figure 3.9 and Table 3.3. A survey of the AFM height image cross-sections shows nanoscale roughness features that appear to be smallest on Ctrl and largest on the ODA-modified samples. Quantitative roughness parameters (Table 3.3) indicate that the root mean square (RMS) roughness, representative of overall surface roughness, and the mean maximum z-range values vary in the order: Ctrl < MFC < Amd < ICmplx. Ctrl films are roughly three times and more than four times smoother than MFC and the ODA-modified samples respectively. A close inspection of the AFM images of Amd and ICmplx shows no evidence of individual fibrils such as those clearly observed in the image of the Ctrl film. This effect is believed to originate from aggregation of the ODA-modified nanocelluloses having low surface polarities and dispersed on a relatively hydrophilic mica substrate. Another interesting film surface characteristic listed in Table 3.3 is the area percent (or area ratio), which represents the amount by which the surface area of the film sample exceeds a corresponding flat (featureless) x-y surface of the same area. Area percent of Amd and ICmplx, according to Table 3.3, are about twice that of Ctrl and nearly half that of MFC.

The shapes formed by deposited sessile drops on the various film samples (Figure 3.10) show Amd and ICmplx surfaces as hydrophobic (CAs > 90°) compared to the hydrophilic surfaces of Ctrl and MFC (CAs < 90°). A quantitative comparison of relative surface polarities is made in time-dependent advancing CA plots in which multiple images were acquired over approximately 12 s (Figure 3.11). From the 12s CA data, mean CAs of 36.3 ± 1.0, 29.8 ± 0.6, 108 ± 2.0, and 118 ± 3.0 were computed for Ctrl, MFC, Amd, and ICmplx, respectively. Due to the porous nature of nanocellulose films, water can be absorbed, over time, into the films by capillary action. This phenomenon is manifested as slight but noticeable decreases over time, in CAs of Ctrl and MFC films (Figure 3.11). With respect to Amd, an initial decline in CA is observed, which appears to level off over time. The most stable CA is seen on ICmplx, which also happens to be characterized by the most water-repellent surface. Fukuzumi *et al.*[6] have previously reported an advancing water CA of 47° on nanocellulose films prepared from the Na form of

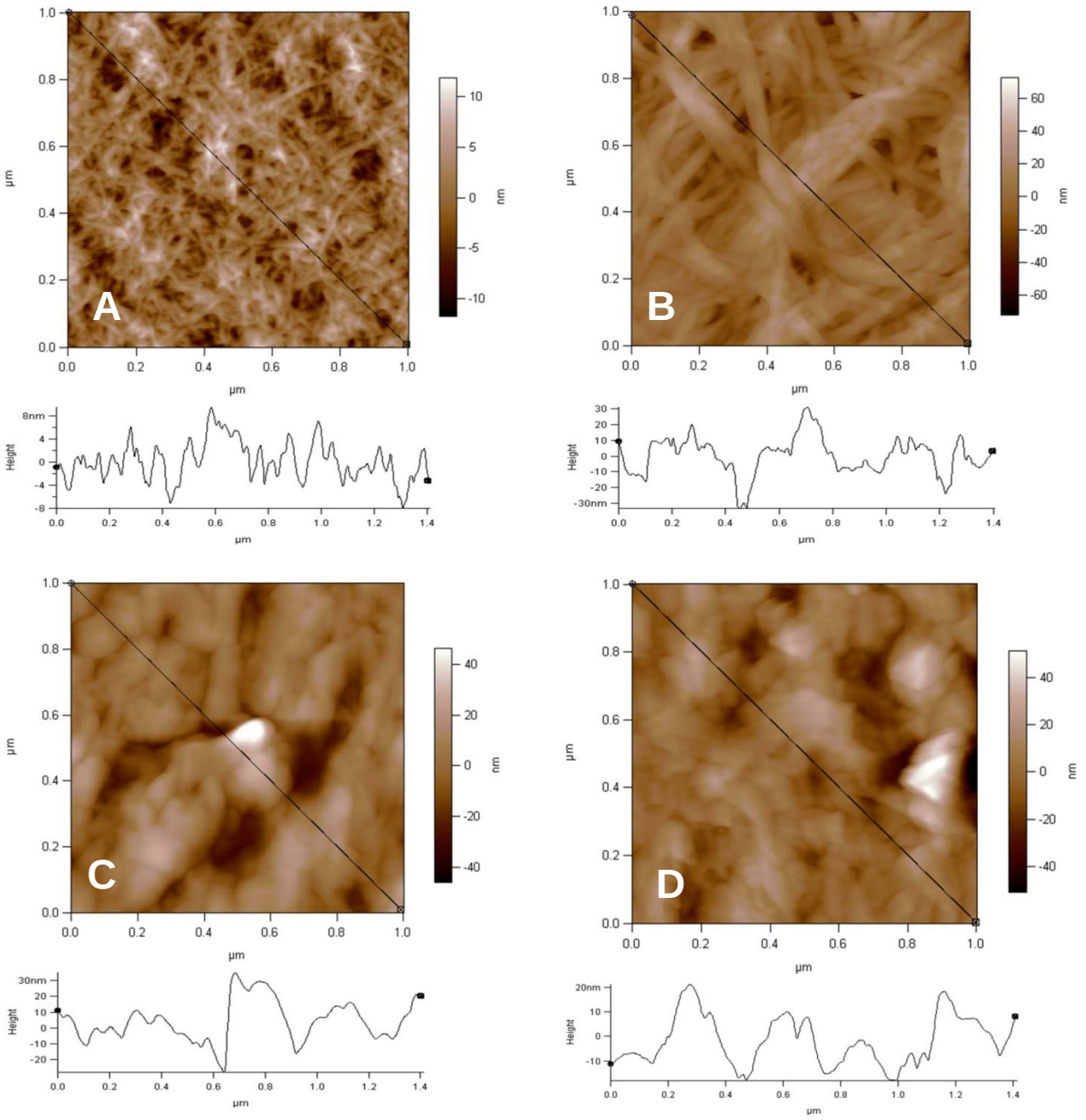


**Figure 3.9** AFM height images of (A) Ctrl, (B) MFC, (C) Amd, and (D) ICmplx films. Sections of film surface roughness profiles (along the diagonal lines) are shown below the images.

TONc. Their measurements were performed with 2 µL water droplets, which is an order of magnitude less in size than those used in the present study. However, no surface roughness data was provided for their films. In Figure 3.11, reasons for the 10° difference in CA between Amd

**Table 3.3** Film surface roughness statistics computed from height images of (1 μm × 1 μm) AFM scans.

| Film ID | RMS[a] roughness, nm | Maximum z-range, nm | Area percent[b], % |
|---|---|---|---|
| Ctrl | 3.20 (0.115) | 25.5 (2.61) | 4.46 (0.40) |
| MFC | 10.9 (1.61) | 84.8 (14.9) | 16.5 (2.38) |
| Amd | 12.6 (2.94) | 104 (36.7) | 9.24 (1.71) |
| ICmplx | 14.3 (2.09) | 123 (26.5) | 7.87 (2.62) |

[a]Root mean square = $\sqrt{\left(1/N\sum Y_i^2\right)}$ where N = number of data points and $Y_i$ = $i^{th}$ data point

[b]Surface area in excess of the geometric XY plan area

Standard deviations are shown in parentheses for three replications

and ICmplx are not fully apparent but the slightly higher DS of ODA (Table 3.1) in ICmplx is a relevant factor to consider.

#### 3.4.6.1. Effect of Surface Roughness on CAs

The effect of surface roughness on CAs was accounted for using Wenzel's[60] equation:

$$\cos\theta_W = \bar{r}\cos\theta_Y \qquad 3.6$$

where $\theta_W$ is the apparent or Wenzel contact angle, which is the same as the measured CAs, $\bar{r}$ is the average area ratio (previously defined) (Table 3.3), and $\theta_Y$ is the Young's contact angle or the contact angle on a flat, rigid, non-swelling, and chemically homogeneous surface. Wenzel's equation has been shown to produce correct estimates of $\theta_Y$ when the sessile drop is axisymmetric, its size (base diameter) is significantly larger (≥ 3 orders of magnitude) than the roughness scale of the solid surface, and it fully penetrates the roughness grooves of the solid surface (homogeneous wetting).[61-63] Our experimental drop size of 20 μL produced drop diameters ranging from 3.9 to 6.8 mm in comparison to the mean roughness scale of 3.2 to 14.3 nm shown in Table 3.3. Also based on the observed spherical shapes of sessile drops, axisymmetry was assumed, and complete penetration of the surface roughness grooves by water was a most likely occurrence considering the nanoscale roughness of the surfaces.

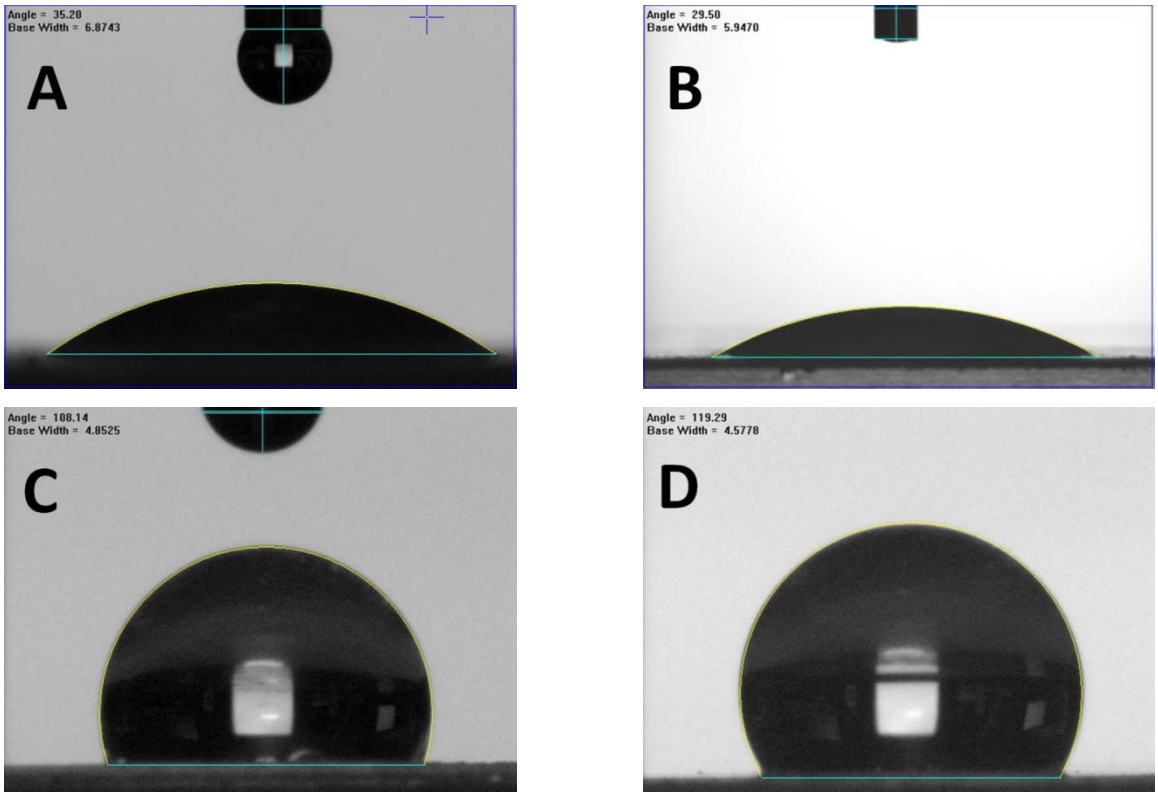


**Figure 3.10** Profiles of advancing water CAs on nanocellulose films five seconds after drop depostion. (A) Ctrl, (B) MFC, (C) Amd, and (D) ICmplx

Application of equation 3.6 to the experimental data thus resulted in $\theta_Y$ values of 39.5, 41.9, 107, and 116° for Ctrl, MFC, Amd, and ICmplx respectively. These values represent the CAs of roughness-free nanocellulose films, which were deviated from by the experimental $\theta_W$ values of 36.3 ± 1.0, 29.8 ± 0.6, 108 ± 2.0, and 118 ± 3.0 for Ctrl, MFC, Amd, and ICmplx respectively. For a more rigorous interpretation of $\theta_Y$, it would be necessary to distinguish the effects of swelling and surface chemical inhomogeneities from the effects of surface roughness. However, estimation of these quantities is not straightforward and they were therefore not considered in the present analysis.

### 3.4.7. Thermal Decomposition Properties

Weight loss and DWL plots for all samples are presented in Figure 3.12 A to C. The thermal decomposition behavior of MFC (Figure 3.12 B) resembles those reported for cellulose in an air atmosphere.[64-66] The first dominant transition (peak at 304 °C on Figure 3.12 B, see also Table 3.4) represents oxidation of flammable and volatile degradation products generated from

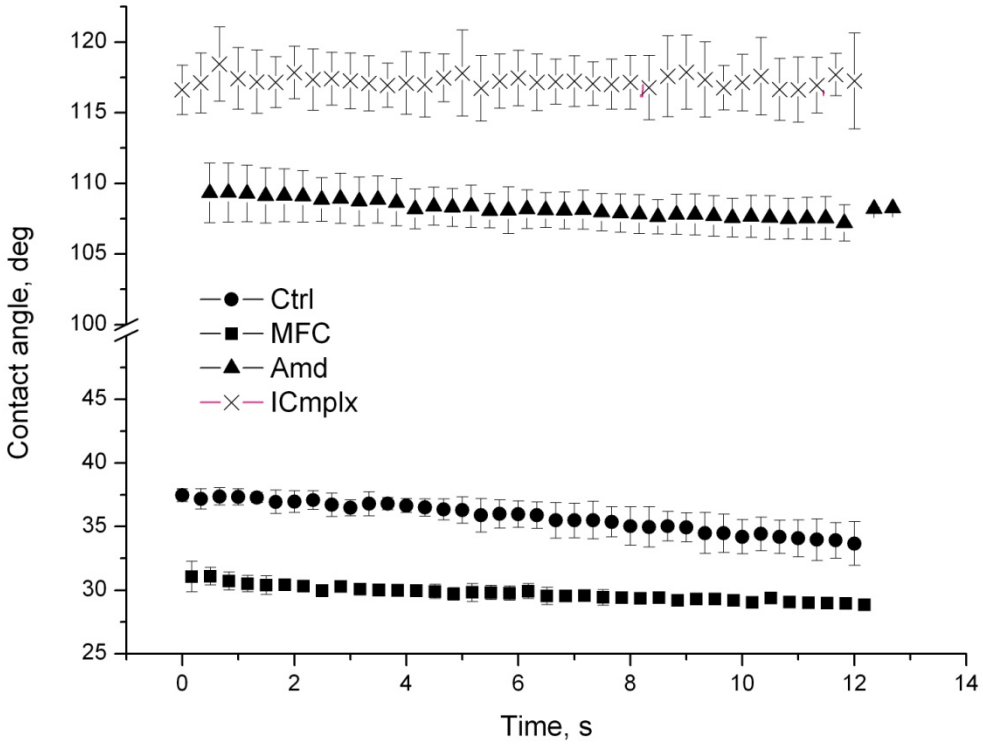


**Figure 3.11** Time dependence of advancing contact angles on film samples. Four hundred contact angle profiles were automatically acquired and analyzed over 12 s. The number of data points has been significantly reduced to aid presentation. Error bars represent ±1 standard deviations from three replications.

dehydration and depolymerization of cellulose, while the second transition represents oxidation of charred residues.[64, 65] The decomposition pattern of Ctrl (Figure 3.12 A) is consistent with previously reported thermal decomposition behavior of TEMPO-oxidized pulp and nanofibrils.[6, 67] A shift in the main decomposition event to lower temperatures is attributed to decarbonation of the anhydroglucuronic acid groups formed as a result of TEMPO-mediated oxidation.[67] Generally, lower thermal stabilities have been reported for chemically modified celluloses, including 2,3-dialdehydecellulose (DAC), 2,3-dicarboxycellulose (DCC), esterified (tosylated, tritylated, acetylated tosyl/trityl cellulose, benzoylated tosyl/trityl cellulose), and cyanoethylated cellulose.[64-66, 68-70] Stated causes for the lowering in cellulose degradation temperature include molecular weight degradation of chemically treated cellulose resulting in lowered thermal

degradation energies[66, 70] and increased surface reactivity of the cellulose by the attached, highly reactive functional groups.[64] With respect to Ctrl, the main decomposition event is resolved into two overlapping peaks: 248 and 270 °C. Char decomposition (peak at 433 °C in Figure 3.12 A) of Ctrl is larger and more intense than that of MFC (463 °C in Figure 3.12 B). It is reported[64] that during char decomposition of celluloses, the char residue ignites and undergoes a self-sustained exothermic process termed the region of glowing combustion.[65] In Figure 3.12, it appears to be more intense for the modified celluloses because larger amount of char residues are involved. For example, in Table 3.4, the fraction of sample remaining at the peak of Ctrl char decomposition (1.02 %) is more than twice that for MFC (0.37 %).

Decomposition processes for ICmplx and Amd are characterized by multiple degradation events (Figure 3.12 C) with identical peak shapes and locations. The behavior of ODA-modified TONc is clearly consistent with the patterns already described for modified celluloses. A relatively weak transition, which is absent from Ctrl thermograms, is observed at 185 °C for both materials followed by a second, slightly stronger transition at 222 °C (ICmplx) and 224 °C (Amd). The main decomposition processes attain a maximum temperature of 282 °C for Amd and occurs with greater intensity at 285 °C for ICmplx. Differences in peak decomposition intensities may be related to the fact that ICmplx is characterized by relatively weak ionic bonds, which are less resistant to thermal decomposition than the covalently coupled system in Amd. The ultimate decomposition event shows the char residue from ICmplx to be more thermally stable and decomposes at a temperature 10 °C higher than that of Amd.

Thermal decomposition studies on predominantly primary substituted cellulose (tosylate and tritylate) esters showed multiple peaks, including low temperature peaks at 144 °C (tosylate esters) and 140 °C (tritylate esters).[65] These transitions were attributed, by the authors, to scission of the attached ester groups. In this study, it was of interest to us to investigate which of the transitions in Figure 3.12 C were responsible for the loss of attached ODA groups. Our working hypothesis was that the ODA groups debond and evolve at one of the transitions preceding the main event. To investigate these effects, additional TGA runs were conducted to the upper temperature limit (determined to be 250 °C) of the second transition and the upper temperature limit (320 °C) of the main decomposition process. The test samples were held constant at these temperatures for at least one hour to ensure completion of the thermal transition. A similar run was performed to the upper temperature limit of the main

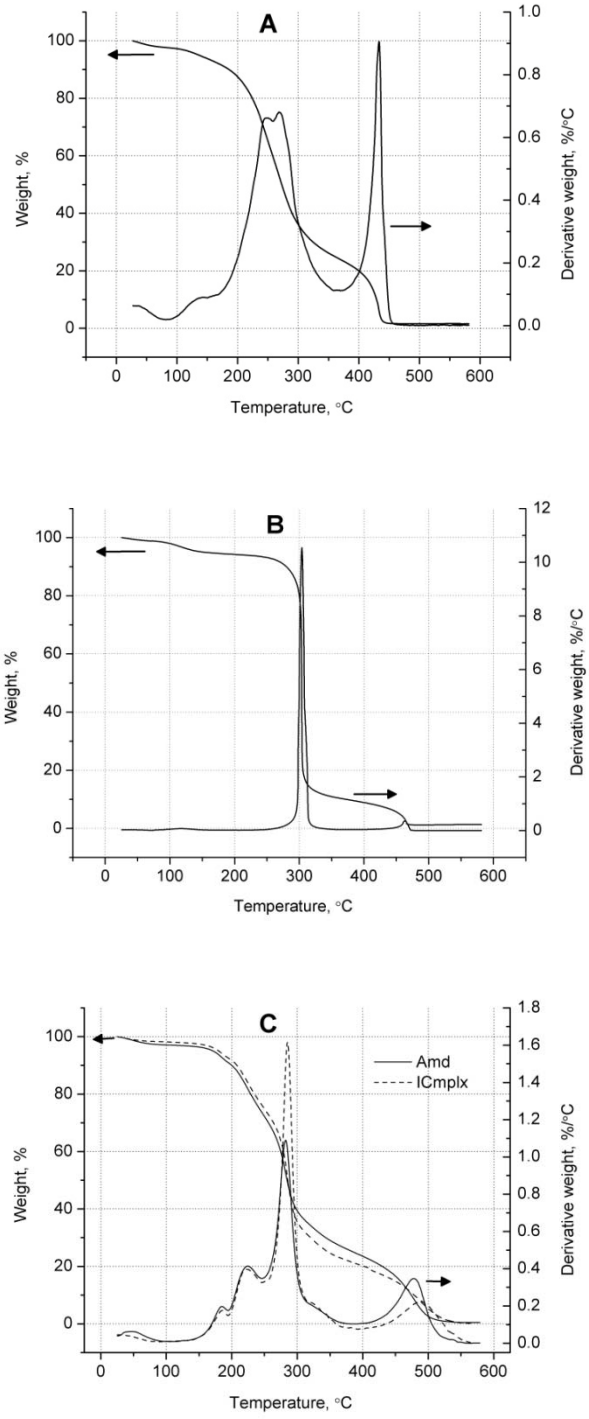


**Figure 3.12** High resolution TGA plots of (A) Ctrl, (B) MFC, and (C) Amd and ICmplx performed on 10 – 15 mg film samples in air at 10 °C/min.

**Table 3.4** TGA sample decomposition parameters at the peak of DWL (dW/dT).

| Sample ID | Temperature, °C | Residual weight,[a] % | (dW/dT), %/°C |
|---|---|---|---|
| Ctrl | 248 | 66.5 (0.65) | 0.662 |
| | 270 | 51.6 (0.91) | 0.679 |
| | 433 | 6.37 (2.42) | 1.02 |
| MFC | 304 | 41.7 (4.78) | 10.3 |
| | 463 | 3.13 (0.32) | 0.368 |
| Amd | 185 | 92.8 (0.39) | 0.197 |
| | 224 | 81.9 (0.25) | 0.414 |
| | 282 | 52.8 (0.13) | 1.09 |
| | 478 | 8.71 (0.33) | 0.347 |
| ICmplx | 185 | 94.3 (0.26) | 0.176 |
| | 222 | 84.9 (0.43) | 0.398 |
| | 285 | 51.0 (0.74) | 1.61 |
| | 488 | 7.80 (0.64) | 0.227 |

[a]Fraction of original weight remaining

Standard deviations are shown in parentheses for three replications

decomposition of Ctrl, for comparison with the ODA-modified samples. Sample residues from these experiments were ultimately recovered and examined with FTIR. Spectra of the samples treated at 250 °C (Figure 3.13 A and B) differ significantly from the original spectra of the respective nanocelluloses (Figure 3.13 Cand D). Interestingly, peaks attributable to ODA remain in the samples after treatment at 250 °C (Figure 3.13 A and B) whereas those originating from the C-O and ring vibrations (1000 – 1200 $cm^{-1}$) of cellulose are significantly altered. The severity of these distortions appears to be greater in the ICmplx spectrum, which may indicate a lower resistance of same to thermal degradation compared to Amd. When heated to the upper limit (350 °C) of the main decomposition event, both ODA and the major fingerprint vibrations of cellulose disappear from all spectra (Figure 3.14). In fact, the spectra from both control and ODA-modified samples are practically indistinguishable at this stage of the thermal decomposition process. Jain et al.[65] made similar observations from FTIR examination of TGA char residues recovered from cellulose and its esterified derivatives. They attributed the

appearance of dominant 1720 and 1630 $cm^{-1}$ peaks (analogous to ~1715–1730 and ~1600–1615 $cm^{-1}$ in Figure 3.14) to skeletal rearrangement of the cellulose backbone and the evolution of volatile products at these temperatures.

#### 3.4.7.1. Kinetics of Thermal Decomposition

Kinetic constants: $E_a$, A, and n of the study samples were determined for both the main and char degradation events. Thermal decomposition processes of the ODA-modified celluloses, MFC, and the main decomposition process of Ctrl were analyzed successfully and their data plotted (Figure 3.15). However, for Ctrl, highly unstable decomposition behavior of the char decomposition event was encountered at higher resolutions[a], making it impossible to obtain data for q (the heating rate at maximum decomposition rate (section 3.3.3.5 and equation 3.3)). Presumably, the instrument was unable to rapidly adjust the dynamic heating rate to match the rather explosive nature of the char decomposition reaction (see Figure 3.12 A). Figure 3.15 shows the expected linear dependencies of peak decomposition reaction rates on temperature. $E_a$, A, and n values (Table 3.5) were derived from these plots according to the Salin and Seferis[32] approach. According to Table 3.5, activation energies of all the derivatized nanocelluloses are lower than those of MFC, which here represents an unoxidized nanocellulose reference. In their TGA studies of cellulose and esterified celluloses, Jain et al.[65] reported significantly higher $E_a$ values for cellulose due to the high energies associated with dehydration of cellulose compared to deacylation of the esterified products. A similar reasoning is advanced to explain the differences observed between MFC and the modified celluloses in the current study. Relative to Ctrl, Amd and ICmplx possess higher and lower $E_a$ values respectively under the main decomposition process. It can be reasoned that the presence of relatively stronger amide bonds in Amd compared to ionic bonds in ICmpx is reflected by their respective $E_a$ values relative to that of Ctrl.

[a] Data unstable at resolutions 5 and 6.

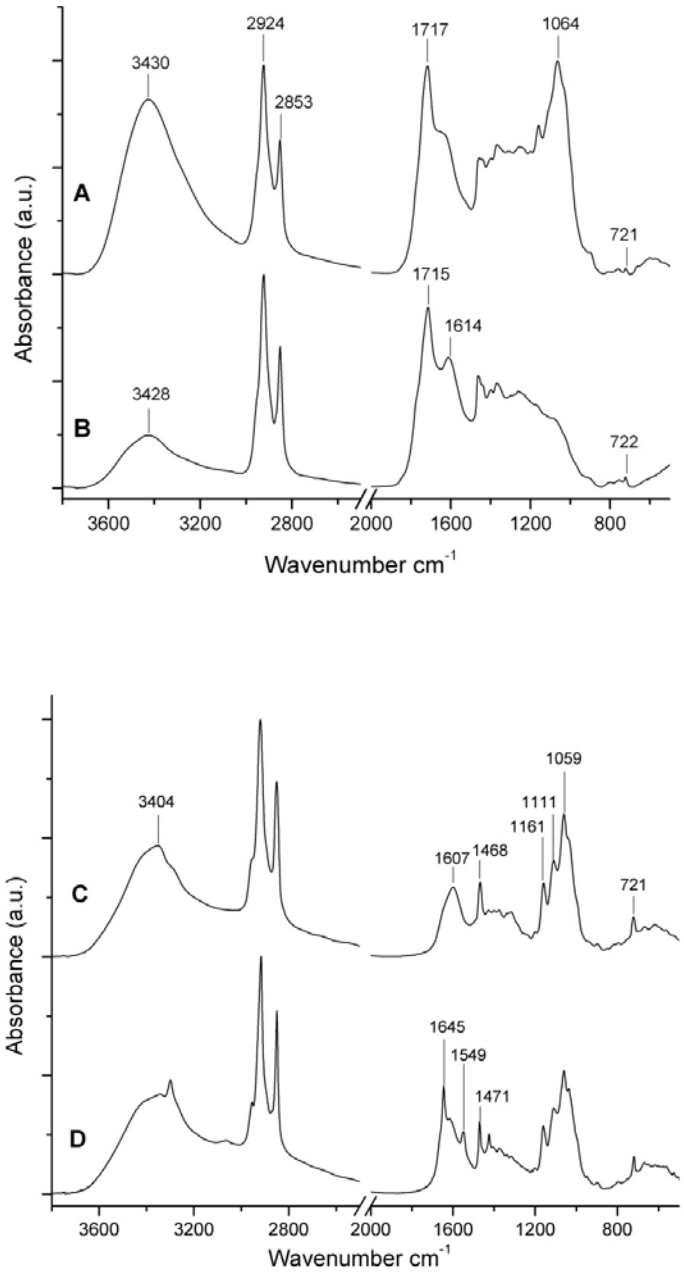


**Figure 3.13** FTIR spectra of (A) Amd and (B) ICmplx films heated in air at 250 °C for 1 h. (C) and (D) Spectra of ICmplx and Amd respectively for comparison with heat-treated samples. ODA peaks (C-H stretching, 2924 and 2853 $cm^{-1}$, and deformation, 720 $cm^{-1}$) remain whereas peaks originating from cellulose C-O and ring vibrations (1000 – 1200 $cm^{-1}$) are affected in the heat-treated samples.

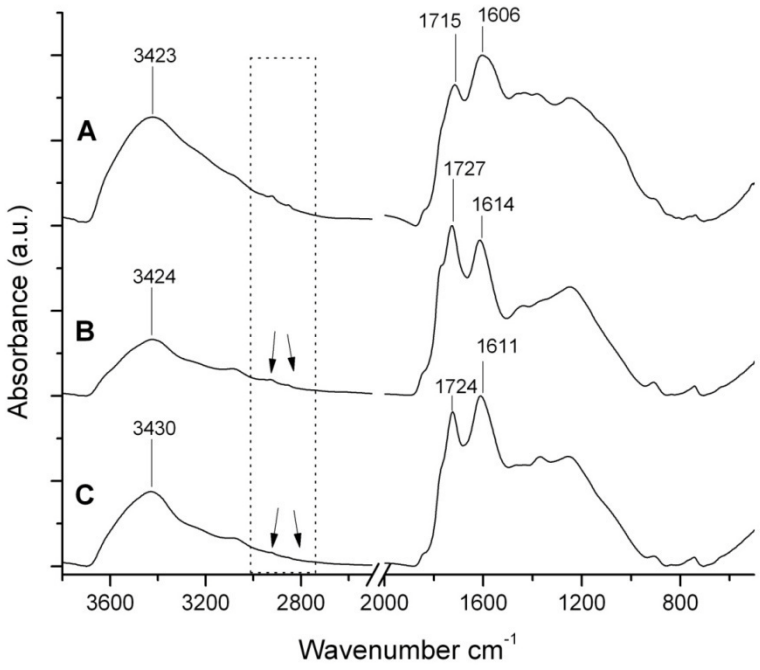


**Figure 3.14** FTIR spectra of (A) Ctrl, (B) Amd, and (C) ICmplx film samples heated in air at 320 °C for 1 h. ODA peaks (present in Figure 3.13) are no longer seen in the Amd and ICmplx spectra. Arrows indicate the expected positions of ODA peaks. The identical nature of the spectra suggests complete loss of all attached groups leaving only char residues of similar identity.

## 3.5. Conclusions

Coupling of ODA to TONc surfaces is readily achieved with the use of both ionic complexation and carbodiimide-mediated amidation. Available TONc carboxyl groups are shown to be completely substituted by ODA molecules leading to remarkably low surface polarities and excellent dispersions of the modified TONc in organic solvents. Contrary to expectation, the organic solvent dispersions of ODA-modified TONc are unstable over time, resulting in flocculation in a matter of hours.

Subjection of ICmplx to prolonged heating (up to 150 °C for 4 h) fails to generate amide

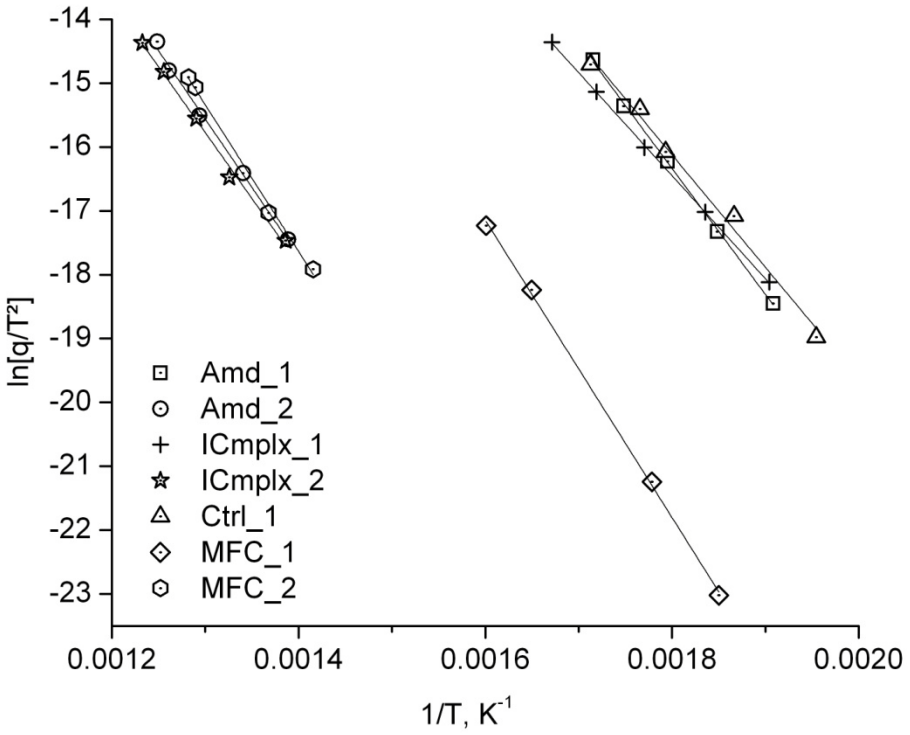


**Figure 3.15** Plots of $\ln[q/T^2]$ as a function of 1/T using the equation of Salin and Seferis. Numbers in legend refer to main (1) and char (2) decomposition steps respectively.

bonds via heat-induced condensation of ionic bonds. The heterogeneous nature of the reaction system and the relatively short heat-treatment time are suspected to be responsible for the failure to achieve condensation.

Coupling to ODA does not appear to alter, in any appreciable way, the cellulose I crystalline structure of TONc. In the modified TONc, however, the high ODA volume fraction necessarily implies a decrease in cellulose volume fraction and results in lower crystallinity indices compared to neat TONc.

ODA groups present in both the ionic complexation and amidation products exhibit identical resistances to thermal decomposition as the substrate cellulose. Between the two coupling methods, amidation induces a slightly higher thermal stability to TONc as evidenced by the magnitudes of experimentally derived activation energies.

**Table 3.5** Kinetic parameters at maximum decomposition rate for study materials obtained from applying the Salin and Seferis[32] approach (Eq. 3.3 – 3.5).

| Sample ID | Resolution | Main decomposition | | | Char decomposition | | |
|---|---|---|---|---|---|---|---|
| | | Ea, kJ $mol^{-1}$ | n | log A | $E_a$, kJ $mol^{-1}$ | n | log A |
| Ctrl | 2 | 146.3 | 1.07 | 11.00 | | - | - |
| | 3 | | 1.12 | 10.99 | | - | - |
| | 4 | | 1.93 | 11.05 | | - | - |
| | 5 | | 1.66 | 10.99 | | - | - |
| | 6 | | 1.27 | 10.96 | | - | - |
| MFC | 2 | 193.6 | 0.27 | 12.77 | 191.0 | 0.01 | 10.04 |
| | 3 | | 0.66 | 12.77 | | 0.02 | 9.51 |
| | 4 | | | | | - | - |
| | 5 | | 0.49 | 12.77 | | 0.01 | 10.32 |
| | 6 | | | | | - | - |
| Amd | 2 | 163.9 | 1.45 | 12.58 | 177.0 | 1.16 | 9.77 |
| | 3 | | 1.79 | 12.57 | | 1.50 | 10.00 |
| | 4 | | 1.88 | 12.56 | | 1.59 | 10.06 |
| | 5 | | 1.94 | 12.57 | | 1.53 | 10.01 |
| | 6 | | 1.72 | 12.56 | | 1.21 | 9.80 |
| ICmplx | 2 | 134.0 | 1.89 | 9.68 | 170.4 | 1.16 | 9.23 |
| | 3 | | 1.91 | 9.66 | | 1.47 | 9.42 |
| | 4 | | 2.24 | 9.68 | | 1.54 | 9.46 |
| | 5 | | 2.33 | 9.66 | | 1.56 | 9.52 |
| | 6 | | 2.39 | 9.66 | | 1.39 | 9.37 |

## 3.6. References


(1) Saito, T.; Kimura, S.; Nishiyama, Y.; Isogai, A., Cellulose nanofibers prepared by TEMPO-mediated oxidation of native cellulose. *Biomacromolecules* **2007,** *8* (8), 2485-2491.

(2) Saito, T.; Nishiyama, Y.; Putaux, J. L.; Vignon, M.; Isogai, A., Homogeneous suspensions of individualized microfibrils from TEMPO-catalyzed oxidation of native cellulose. *Biomacromolecules* **2006,** *7* (6), 1687-1691.

(3) Saito, T.; Isogai, A., Wet strength improvement of TEMPO-oxidized cellulose sheets prepared with cationic polymers. *Ind Eng Chem Res* **2007,** *46* (3), 773-780.

(4) Suh, D. S.; Lee, K. S.; Chang, P. S.; Kim, K. O., Physicochemical properties of cellulose selectively oxidized with the 2.2,6,6-tetramethyl-1-piperidinyl oxoammonium ion. *Journal of Food Science* **2007,** *72* (5), C235-C242.

(5) Bragd, P. L.; van Bekkum, H.; Besemer, A. C., TEMPO-mediated oxidation of polysaccharides: survey of methods and applications. *Topics in Catalysis* **2004,** *27* (1-4), 49-66.

(6) Fukuzumi, H.; Saito, T.; Wata, T.; Kumamoto, Y.; Isogai, A., Transparent and High Gas Barrier Films of Cellulose Nanofibers Prepared by TEMPO-Mediated Oxidation. *Biomacromolecules* **2009,** *10* (1), 162-165.

(7) Mukai, K.; Kumamoto, Y.; Isogai, A.; Meiwa, Z.; Maezawa, T.; Ugajin, T. Gas-barrier material, gas-barrier molded article, and method for producing the gas-barrier molded article. 2009-JP71889 2010074340, 20091225., 2010.

(8) Isogai, A.; Kado, H.; Goi, Y. Gel compositions containing oxidized cellulose fibers with good resistance to salts and ionic surfactants. 2008-197847 2010037348, 20080731., 2010.

(9) Isogai, A.; Kado, H.; Goi, Y. Spray compositions containing oxidized cellulose fibers as thickeners, and sprayers therefor. 2008-197849 2010037200, 20080731., 2010.

(10) Suzuki, A.; Miyawaki, S.; Katsukawa, S.; Abe, H.; Iijima, Y.; Isogai, A. Cellulose nanofiber-containing base paper for processing paper. 2008-93496 2009243010, 20080331., 2009.

(11) Kato, T.; Isogai, A.; Saito, T.; Oaki, Y.; Nishimura, T. Composite material, functional material, process for producing composite material, and process for producing composite-material thin film. 2008-206488 2010043144, 20080810., 2010.

(12) Isogai, A.; Kado, H.; Goi, Y. Cosmetics compositions containing oxidized cellulose fibers and functional components. 2008-197848 2010037199, 20080731., 2010.

(13) Saito, T.; Shibata, I.; Isogai, A.; Suguri, N.; Sumikawa, N., Distribution of carboxylate groups introduced into cotton linters by the TEMPO-mediated oxidation. *Carbohydr. Polym.* **2005,** *61* (4), 414-419.

(14) Saito, T.; Isogai, A., TEMPO-mediated oxidation of native cellulose. The effect of oxidation conditions on chemical and crystal structures of the water-insoluble fractions. *Biomacromolecules* **2004,** *5* (5), 1983-1989.

(15) Saito, T.; Okita, Y.; Nge, T. T.; Sugiyama, J.; Isogai, A., TEMPO-mediated oxidation of native cellulose: Microscopic analysis of fibrous fractions in the oxidized products. *Carbohydr. Polym.* **2006,** *65* (4), 435-440.

(16) Habibi, Y.; Chanzy, H.; Vignon, M. R., TEMPO-mediated surface oxidation of cellulose whiskers. *Cellulose* **2006,** *13* (6), 679-687.

(17) Araki, J.; Wada, M.; Kuga, S., Steric stabilization of a cellulose microcrystal suspension by poly(ethylene glycol) grafting. *Langmuir* **2001,** *17* (1), 21-27.

(18) Follain, N.; Montanari, S.; Jeacomine, I.; Gambarelli, S.; Vignon, M. R., Coupling of amines with polyglucuronic acid: Evidence for amide bond formation. *Carbohydr. Polym.* **2008,** *74* (3), 333-343.

(19) Zhu, L. H.; Kumar, V.; Banker, G. S., Examination of oxidized cellulose as a macromolecular prodrug carrier: preparation and characterization of an oxidized cellulose-phenylpropanolamine conjugate. *International Journal of Pharmaceutics* **2001,** *223* (1-2), 35-47.

(20) Lasseuguette, E., Grafting onto microfibrils of native cellulose. *Cellulose* **2008,** *15* (4), 571-580.

(21) Bulpitt, P.; Aeschlimann, D., New strategy for chemical modification of hyaluronic acid: Preparation of functionalized derivatives and their use in the formation of novel biocompatible hydrogels. *Journal of Biomedical Materials Research* **1999,** *47* (2), 152-169.

(22) Sehgal, D.; Vijay, I. K., A Method for the High-Efficiency of Water-Soluble Carbodiimide-Mediated Amidation. *Anal Biochem* **1994,** *218* (1), 87-91.

(23) Staros, J. V., N-Hydroxysulfosuccinimide Active Esters - Bis(N-Hydroxysulfosuccinimide) Esters of 2 Dicarboxylic-Acids Are Hydrophilic, Membrane-Impermeant, Protein Cross-Linkers. *Biochemistry-Us* **1982,** *21* (17), 3950-3955.

(24) Johnson, R. K.; Zink-Sharp, A.; Renneckar, S. H.; Glasser, W. G., A new bio-based nanocomposite: Fibrillated TEMPO-oxidized celluloses in hydroxypropyl cellulose matrix. *Cellulose* **2009,** *16* (2), 227-238.

(25) Toffey, A.; Glasser, W. G., Chitin derivatives III formation of amidized homologs of chitosan. *Cellulose* **2001,** *8* (1), 35-47.

(26) Toffey, A.; Samaranayake, G.; Frazier, C. E.; Glasser, W. G., Chitin derivatives .1. Kinetics of the heat-induced conversion of chitosan to chitin. *Journal of Applied Polymer Science* **1996,** *60* (1), 75-85.

(27) Toffey, A.; Glasser, W. G., Chitin derivatives. II. Time-temperature-transformation cure diagrams of the chitosan amidization process. *Journal of Applied Polymer Science* **1999,** *73* (10), 1879-1889.

(28) Katz, S.; Beatson, R. P.; Scallan, A. M., The Determination of Strong and Weak Acidic Groups in Sulfite Pulps. *Svensk Papperstidning* **1984,** *87* (6), R48 - R53.

(29) Perez, D. D.; Montanari, S.; Vignon, M. R., TEMPO-mediated oxidation of cellulose III. *Biomacromolecules* **2003,** *4* (5), 1417-1425.

(30) Vaca-Garcia, C.; Borredon, M. E.; Gaseta, A., Determination of the degree of substitution (DS) of mixed cellulose esters by elemental analysis. *Cellulose* **2001,** *8* (3), 225-231.

(31) TGA Hi-Res Operator's Guide, TA Instruments-Waters LLC: 2004; p 46.

(32) Salin, I. M.; Seferis, J. C., Kinetic-Analysis of High-Resolution TGA Variable Heating Rate Data. *Journal of Applied Polymer Science* **1993,** *47* (5), 847-856.

(33) Clothup, N. B.; Daly, L. H.; Wiberley, S. E., *Introduction to Infrared and Raman Sepectroscopy*. 3rd ed.; Academic Press, Inc: San Diego, 1990; p 547.

(34) Socrates, G., *Infrared and Raman Characteristic Group Frequencies*. 3 ed.; John Wiley and Sons, Ltd: Chichester, 2001; p 347.

(35) Williams, D. H.; Fleming, I., *Spectroscopic Methods in Organic Chemistr*. McGraw-Hill Book Company (UK) Ltd.: London, 1980; p 251.

(36) Wagberg, L.; Decher, G.; Norgren, M.; Lindstrom, T.; Ankerfors, M.; Axnas, K., The build-up of polyelectrolyte multilayers of microfibrillated cellulose and cationic polyelectrolytes. *Langmuir* **2008,** *24* (3), 784-795.

(37) Da Roz, A. L.; Leite, F. L.; Pereiro, L. V.; Nascente, P. A. P.; Zucolotto, V.; Oliveira, O. N.; Carvalho, A. J. F., Adsorption of chitosan on spin-coated cellulose films. *Carbohydr. Polym.* **2010,** *80* (1), 65-70.

(38) Yurkshtovich, T. L.; Alinovskaya, V. A., Sorption of aliphatic amines by monocarboxycellulose from aqueous and water-ethanol solutions. *Colloid J+* **2008,** *70* (3), 377-383.

(39) Saito, T.; Isogai, A., Ion-exchange behavior of carboxylate groups in fibrous cellulose oxidized by the TEMPO-mediated system. *Carbohydr. Polym.* **2005,** *61* (2), 183-190.

(40) Freire, C. S. R.; Silvestre, A. J. D.; Neto, C. P.; Belgacem, M. N.; Gandini, A., Controlled heterogeneous modification of cellulose fibers with fatty acids: Effect of reaction conditions on the extent of esterification and fiber properties. *Journal of Applied Polymer Science* **2006,** *100* (2), 1093-1102.

(41) Jandura, P.; Kokta, B. V.; Riedl, B., Fibrous long-chain organic acid cellulose esters and their characterization by diffuse reflectance FTIR spectroscopy, solid-state CP/MAS C-13-NMR, and X-ray diffraction. *Journal of Applied Polymer Science* **2000,** *78* (7), 1354-1365.

(42) Habibi, Y.; Goffin, A. L.; Schiltz, N.; Duquesne, E.; Dubois, P.; Dufresne, A., Bionanocomposites based on poly(epsilon-caprolactone)-grafted cellulose nanocrystals by ring-opening polymerization. *J. Mater. Chem.* **2008,** *18* (41), 5002-5010.

(43) Okita, Y.; Saito, T.; Isogai, A., TEMPO-mediated oxidation of softwood thermomechanical pulp. *Holzforschung* **2009,** *63* (5), 529-535.

(44) Saito, T.; Hirota, M.; Tamura, N.; Kimura, S.; Fukuzumi, H.; Heux, L.; Isogai, A., Individualization of Nano-Sized Plant Cellulose Fibrils by Direct Surface Carboxylation Using TEMPO Catalyst under Neutral Conditions. *Biomacromolecules* **2009,** *10* (7), 1992-1996.

(45) Sassi, J. F.; Chanzy, H., Ultrastructural Aspects of the Acetylation of Cellulose. *Cellulose* **1995,** *2* (2), 111-127.

(46) Berlioz, S.; Molina-Boisseau, S.; Nishiyama, Y.; Heux, L., Gas-Phase Surface Esterification of Cellulose Microfibrils and Whiskers. *Biomacromolecules* **2009,** *10* (8), 2144-2151.

(47) Lima, M. M. D.; Borsali, R., Rodlike cellulose microcrystals: Structure, properties, and applications. *Macromolecular Rapid Communications* **2004,** *25* (7), 771-787.

(48) Araki, J.; Wada, M.; Kuga, S.; Okano, T., Birefringent glassy phase of a cellulose microcrystal suspension. *Langmuir* **2000,** *16* (6), 2413-2415.

(49) Ranby, B. G., The Colloidal Properties of Cellulose Micelles. *Discussions of the Faraday Society* **1951,** (11), 158-164.

(50) Gousse, C.; Chanzy, H.; Excoffier, G.; Soubeyrand, L.; Fleury, E., Stable suspensions of partially silylated cellulose whiskers dispersed in organic solvents. *Polymer* **2002,** *43* (9), 2645-2651.

(51) Heux, L.; Chauve, G.; Bonini, C., Nonflocculating and chiral-nematic self-ordering of cellulose microcrystals suspensions in nonpolar solvents. *Langmuir* **2000,** *16* (21), 8210-8212.

(52) Petersson, L.; Mathew, A. P.; Oksman, K., Dispersion and Properties of Cellulose Nanowhiskers and Layered Silicates in Cellulose Acetate Butyrate Nanocomposites. *Journal of Applied Polymer Science* **2009,** *112* (4), 2001-2009.

(53) Yuan, H. H.; Nishiyama, Y.; Wada, M.; Kuga, S., Surface acylation of cellulose whiskers by drying aqueous emulsion. *Biomacromolecules* **2006,** *7* (3), 696-700.

(54) Zhou, Q.; Brumer, H.; Teeri, T. T., Self-Organization of Cellulose Nanocrystals Adsorbed with Xyloglucan Oligosaccharide-Poly(ethylene glycol)-Polystyrene Triblock Copolymer. *Macromolecules* **2009,** *42* (15), 5430-5432.

(55) Braun, B.; Dorgan, J. R., Single-Step Method for the Isolation and Surface Functionalization of Cellulosic Nanowhiskers. *Biomacromolecules* **2009,** *10* (2), 334-341.

(56) Gousse, C.; Chanzy, H.; Cerrada, M. L.; Fleury, E., Surface silylation of cellulose microfibrils: preparation and rheological properties. *Polymer* **2004,** *45* (5), 1569-1575.

(57) Kim, J.; Montero, G.; Habibi, Y.; Hinestroza, J. P.; Genzer, J.; Argyropoulos, D. S.; Rojas, O. J., Dispersion of Cellulose Crystallites by Nonionic Surfactants in a

Hydrophobic Polymer Matrix. *Polymer Engineering and Science* **2009,** *49* (10), 2054-2061.

(58) Siqueira, G.; Bras, J.; Dufresne, A., New Process of Chemical Grafting of Cellulose Nanoparticles with a Long Chain Isocyanate. *Langmuir* **2010,** *26* (1), 402-411.

(59) Ljungberg, N.; Bonini, C.; Bortolussi, F.; Boisson, C.; Heux, L.; Cavaille, J. Y., New nanocomposite materials reinforced with cellulose whiskers in atactic polypropylene: Effect of surface and dispersion characteristics. *Biomacromolecules* **2005,** *6* (5), 2732-2739.

(60) Wenzel, R. N., Resistance of solid surfaces to wetting by water. *Journal of Industrial and Engineering Chemistry (Washington, D. C.)* **1936,** *28*, 988-94.

(61) Marmur, A.; Bittoun, E., When Wenzel and Cassie Are Right: Reconciling Local and Global Considerations. *Langmuir* **2009,** *25* (3), 1277-1281.

(62) Martin, A. R.; Manolache, S.; Denes, F. S.; Mattoso, L. H. C., Functionalization of sisal fibers and high-density polyethylene by cold plasma treatment. *Journal of Applied Polymer Science* **2002,** *85* (10), 2145-2154.

(63) Wolansky, G.; Marmur, A., Apparent contact angles on rough surfaces: the Wenzel equation revisited. *Colloid Surface A* **1999,** *156* (1-3), 381-388.

(64) Aggarwal, P.; Dollimore, D., The combustion of starch, cellulose and cationically modified products of these compounds investigated using thermal analysis. *Thermochim Acta* **1997,** *291* (1-2), 65-72.

(65) Jain, R. K.; Lal, K.; Bhatnagar, H. L., Thermal Studies on C-6 Substituted Cellulose and Its Subsequent C-2 and C-3 Esterified Products in Air. *European Polymer Journal* **1986,** *22* (12), 993-1000.

(66) Varma, A. J.; Chavan, V. B., Thermal-Properties of Oxidized Cellulose. *Cellulose* **1995,** *2* (1), 41-49.

(67) Fukuzumi, H.; Saito, T.; Okita, Y.; Isogai, A., Thermal stabilization of TEMPO-oxidized cellulose. *Polymer Degradation and Stability* **2010,** *95* (9), 1502-1508.

(68) Kim, U. J.; Kuga, S., Thermal decomposition of dialdehyde cellulose and its nitrogen-containing derivatives. *Thermochim Acta* **2001,** *369* (1-2), 79-85.

(69) Nada, A. M. A.; Hassan, M. L., Thermal behavior of cellulose and some cellulose derivatives. *Polymer Degradation and Stability* **2000,** *67* (1), 111-115.

(70) Vicini, S.; Princi, E.; Luciano, G.; Franceschi, E.; Pedemonte, E.; Oldak, D.; Kaczmarek, H.; Sionkowska, A., Thermal analysis and characterisation of cellulose oxidised with sodium methaperiodate. *Thermochim Acta* **2004,** *418* (1-2), 123-130.

# Chapter 4. Nanocomposites of TEMPO-oxidized Nanocelluloses in Cellulose Acetate Butyrate Matrix

## 4.1. Abstract

TEMPO-oxidized nanocelluloses (TONc) and their hydrophobized derivative were examined as reinforcements in a matrix of cellulose acetate butyrate (CAB). The hydrophobized derivative was the product of amidation between TONc surface carboxyl groups and octadecylamine (ODA) via carbodiimide-mediated coupling. Nanocomposites of the TONc control (Ctrl) and its amidation product (Amd) in CAB matrix were solvent-cast into films and characterized with respect to their optical, dynamic mechanical, and thermal decomposition properties. The TONc-based nanocomposites were compared with conventional microfibrillated cellulose (MFC)-reinforced CAB nanocomposites prepared in a similar manner. At 5 vol % loading, a 22 fold increase in CAB tensile storage modulus in the glass transition region was obtained for the Ctrl-CAB nanocomposite. Amd-CAB and MFC-CAB at similar volume fractions achieved increases of 3.5 and 7.0 fold respectively. Optical transmittance of Ctrl-CAB nanocomposites was practically identical to that of unfilled CAB; Amd-CAB and MFC-CAB nanocomposites on the other hand, transmitted 15 – 25% less light than unfilled CAB. Both light transmittance and dynamic mechanical results indicated uniform nanofibril dispersion in Ctrl-CAB. In contrast, aggregated reinforcements were observed in the Amd and MFC-reinforced CAB nanocomposites. With respect to thermal stability, all the nanocomposites at 5 vol % reinforcement exhibited a nearly identical thermal decomposition behavior as unfilled CAB. However, the magnitude of weight loss preceding the main decomposition event varied directly with the decomposition temperature of the respective nanocellulose reinforcemnts.

## 4.2. Introduction

Polymer nanocomposites are polymer matrix composites in which the fillers measure less than 100 nm in at least one dimension.[1] When the reinforcing materials are nanoscale cellulose (nanocellulose) fibers or rods, the resulting products are cellulose nanocomposites or nanocellulose composites. Research into the composition, preparation, characterization, and applications of cellulose nanocomposites has increased significantly following a 1995 report[2] on

the extraordinary dynamic mechanical performance of tunicin whiskers-reinforced poly(styrene-*co*-butylacrylate) latex. Efficient dispersion of whiskers in the matrix, coupled with mechanical percolation of hydrogen-bonded whiskers, were reported as the main causes of the extraordinary performance. In subsequent years, methods aimed at nanocellulose dispersion and adhesion to matrix such as high intensity mixing of nanocellulose-polymer melts[3-4] and suspensions,[5-6] surfactant coating of nanocelluloses,[7] impregnation of nanocellulose films with concentrated polymer solutions,[8-14] and surface chemical modification of nanocelluloses[6, 15-18] have been reported.

Recently, Saito *et al.*[19-20] reported their preparation of individualized cellulose nanofibrils through mechanical homogenization of TEMPO-oxidized pulp. The resulting TEMPO-oxidized nanocelluloses (TONc) ranged from 3 – 5 nm in width and several hundred nanometers to a few microns in length. Ease of fibril disintegration was attributed to interfibrillar repulsive forces generated by the surface carboxylate groups. With the exceptionally small fibril widths, the oxidized nanocellulose suspensions appeared transparent. Although TONc are relatively new materials, proposed and demonstrated potential applications include additives for paper wet strength improvement,[21] ionic substrates in combination with surfactants for water purification,[22] additives in food,[23] substitutes for cellulose ethers,[24] and coatings for oxygen barrier applications.[25] TONc have also been named as key components or additives in a variety of patented applications including oxygen barrier,[26] gel,[27] thickener,[28] papermaking,[29] inorganic nanoparticle composite,[30] and cosmetic[31] preparations. So far, the potential of TONc as functional additives in cellulosic nanocomposite applications has not yet been explored. Given the multiple surface functionalities,[19-20] high crystallinity,[32-33] and suspension transparency[19-20] of TONc, potential advantages in the utilization of TONc as cellulosic nanocomposite reinforcements were perceived, and served as the motivation for this research.

In this chapter, our goal was to evaluate neat TONc (Ctrl) and a previously described hydrophobized derivative (Amd) as reinforcements in a matrix of cellulose acetate butyrate (CAB). Amd was the product of carbodiimide-mediated coupling of octadecylamine (ODA) to carboxylate groups on TONc surfaces (details of preparation and characterization in Chapter 3). To provide perspective for the performance of TONc-based nanocomposites as they relate to conventional cellulose nanocomposites, films of microfibrillated cellulose (MFC)-reinforced CAB were also prepared and examined for comparison with the primary research materials.

Optical transmittance, dynamic mechanical, and thermal decomposition properties of the nanocomposites were studied as a function of Ctrl volume fraction and reinforcement type (Ctrl, Amd, and MFC) at fixed volume fraction.

## 4.3. Experimental Section

### 4.3.1. Materials

Cellulose acetate butyrate (CAB-381-20, Appendix II) was kindly provided by Eastman Chemical Company, Kingsport, TN. It is a white free-flowing powder with number average molecular weight, $\overline{M}_n$ = 70,000 g mol$^{-1}$; glass transition temperature, $T_g$ =,141 °C, density = 1.2 g mL$^{-1}$, hydroxyl content = 1.8%, and viscosity = 7.6 Pa s (76 poise, ASTM D817 and D1343).[34] The reinforcing nanocelluloses were a TONc control **(Ctrl)**, ODA-modified TONc via carbodiimide-mediated amidation **(Amd)**, and microfibrillated cellulose **(MFC)**. Details of preparation and properties of the various nanocellulose are presented in Chapter 3. Tetrahydrofuran (THF, 99.9%) was purchased from Fisher Scientific and used as the solvent for nanocomposite film-casting.

### 4.3.2. Preparation of Nanocomposite Films

Nanocomposite films were solvent-cast from nanocellulose-CAB blends in THF. Neat CAB samples were prepared the same way from CAB solutions for use as reference. Details for the preparation processes are given next.

#### 4.3.2.1. CAB Solutions and Nanocellulose Suspensions

First, CAB was added to THF in a single-neck flat-bottom flask to obtain a 10 w/v % CAB solution. The flask with its contents was mounted on a rotavapor (BUCHI R-215) and rotated at 100 – 150 rpm in a 60 °C water bath. After the solution became clear, mixing was continued for ~4 h to ensure complete dissolution of CAB. The CAB solution was kept in a fume hood until used.

All nanocellulose suspensions were prepared at a concentration of 1 w/v %. Aqueous Ctrl and MFC suspensions were solvent exchanged into THF via ethanol. The suspensions were first exchanged into ethanol by repeated centrifugation and decanting of the supernatant. Ethanol suspensions were subsequently exchanged into THF in a similar manner. Amd was dispersed

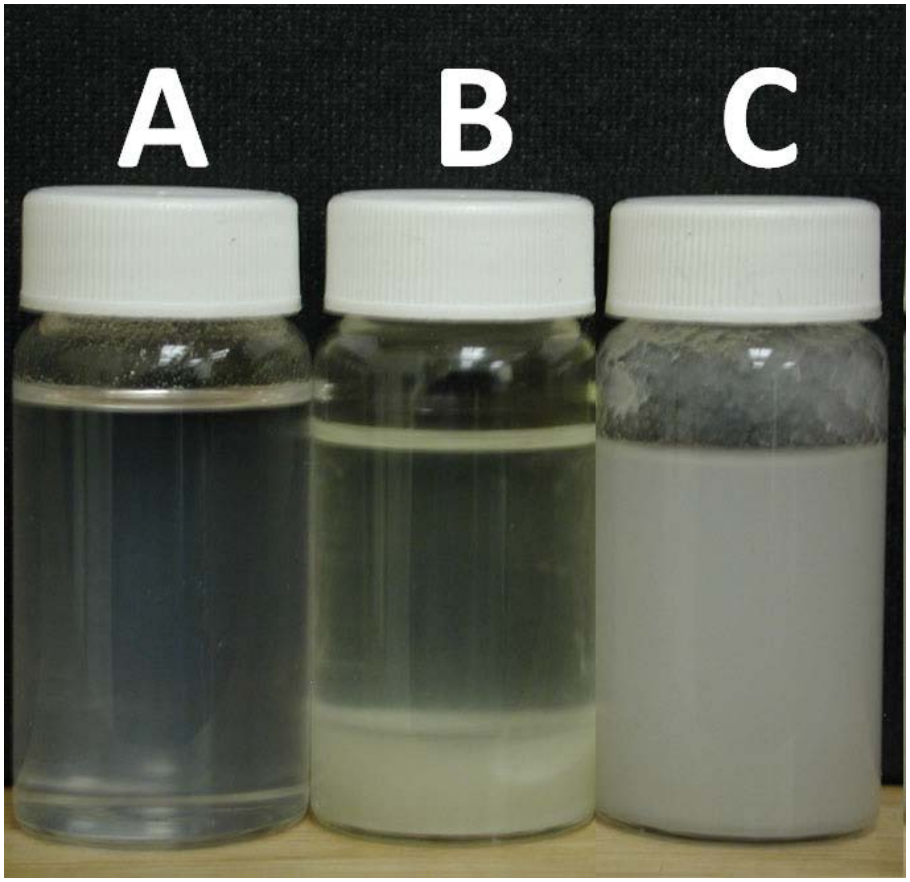


**Figure 4.1** One week-old nanocellulose suspensions (1 vol %) in THF: (A) Ctrl, (B) Amd, and (C) MFC.

directly into THF from the freeze-dried state as previously demonstrated in Chapter 3. Each suspension was sonicated (Sonics model GE 505) for five minutes to fully disperse the nanocelluloses. Figure 4.1 shows the sonicated THF-based suspensions after one week of storage. Ctrl and MFC suspensions appear stable whereas Amd flocculates (as already discussed in Chapter 3, section 3.4.5). Discussions of optical transmittance and dynamic mechanical properties (in later sections) make further references to Figure 4.1.

#### 4.3.2.2. Solvent–casting

Suspensions containing various nanocellulose-to-CAB volume ratios (Table 4.1) were thoroughly mixed for ~10 min using the rotavapor setup described under the previous section. The nanocomposite suspensions were immediately transferred into polytetrafluoroethylene

**Table 4.1** Nanocomposite Film Identities and Compositions

| Sample ID | Fibril content, vol % | CAB content, vol % |
|---|---|---|
| CAB | 0.0 | 100 |
| Ctrl-CAB | 0.5 | 99.5 |
| | 1.0 | 99.0 |
| | 2.5 | 97.5 |
| | 5.0 | 95.0 |
| Amd-CAB[a] | 0.5 | 99.5 |
| | 5.0 | 95.0 |
| MFC-CAB | 5.0 | 95.0 |

[a]To maintain a constant cellulose volume fraction for all samples, ODA was excluded from the calculation of solids content in Amd. Therefore the listed fibril content for Amd-CAB represents only the cellulose portion of Amd.

(PTFE) dishes and set in a fume hood until solvent evaporation was complete. Initially, the solvent-cast films became severely distorted as a result of rapid solvent evaporation. Covering the dishes with paper towels held in place with rubber bands slowed the rate of THF evaporation and overcame the film distortion problem. The films (~0.5 mm thick) were further dried under vacuum (1.33 mbar, 50 °C, 2 h), allowed to cool in a desiccator over phosphorus pentoxide ($P_2O_5$), and then heat-treated as described next.

#### 4.3.2.3. Heat Treatment of Cast Films

Due to drying stresses associated with solvent evaporation, inhomogeneities with respect to nanocellulose distribution in film samples were expected. To minimize or eliminate this effect, heat-treatment was used to relax the matrix to a state of thermal equilibrium followed by rapid cooling to minimize loss of the equilibrium state. Films were placed between aluminum sheets and hot-pressed (140 MPa[a], Carver Bench Top Press, 3 min) followed by cooling (~12 °C/min) to room temperature. The treatment temperature (144 ± 2 °C) was selected to be slightly above the manufacturer-supplied $T_g$ (141 °C) of the CAB matrix. The originally opaque films could be

[a] Obtained from dividing the applied load by the cross-sectional area of punched out films of uniform diameter.

seen through after heat treatment and they ranged in thickness from 0.11 to 0.15 mm. The heat-treated films were vacuum-dried (1.3 mbar, 60 °C, 4 h) and stored in a desiccator over $P_2O_5$.

### 4.3.3. Characterization of Nanocomposite Films

#### 4.3.3.1. Optical Properties: UV-visible Spectroscopy (UV-vis) and Polarized Light Microscopy (PLM)

Optical transmittance was used as a measure of transparency for nanocomposites and CAB films. Optical transmittances of film samples were measured with a Thermo Electron UV-vis Evolution 300 spectrophotometer equipped with a xenon lamp. Transmittance spectra were acquired over the 200 to 1000 nm range using a spectral bandwidth of 2 nm. Samples were prepared in the form of discs (7.5 mm diameter) from nanocomposites reinforced with 5 vol % fibrils. A background spectrum was acquired from the empty sample holder, and was automatically subtracted from each sample spectrum.

A polarized light microscope (Zeiss Axioscope) was used to detect nanocellulose aggregation (if present) in nanocomposite films. Specimens similar to those used in UV-vis examinations were imaged in transmission (magnification 100×) with a Nikon digital camera (DS-Qi1Mc) and processed with a Nikon image processing software (NIS Elements BR).

#### 4.3.3.2. Differential Scanning Calorimetry (DSC)

Heat-treated film samples were subjected to DSC scans in a TA Instrument DSC Q100. The goal of DSC experiments was to detect and measure the amount of matrix crystallinity, if present. Single heating and cooling scans were performed at 10 and 5 °C $min^{-1}$ respectively from 50 to 250 °C.

#### 4.3.3.3. Dynamic Mechanical Analysis (DMA)

DMA experiments were performed in tension on neat CAB and nanocomposites using a TA Instrument DMA Q800. To obtain sample sizes with the correct geometry factor[a], strips (5-6 mm wide) were cut out from the heat-treated films and mounted in the DMA tension clamp to lengths of 15-18 mm. Specimen widths and thicknesses were obtained by averaging

[a] Ratio of specimen length to cross-sectional area. Chosen specimen dimensions followed recommendations of TA Instruments DMA User Manual.

measurements taken at three points on each specimen. Thermal scans were performed in air and consisted of a single temperature ramp (30 to 160 °C) at 3 °C $min^{-1}$ and 10 Hz. A static force of 0.005 N was chosen to maintain specimen tension during oscillation. A linear viscoelastic region (LVR), defined to be the limit of strain for which the specimen's tensile storage modulus changes by up to 5% was determined for each film composition at both the lower and upper experimental temperatures. Based on strain sweep results for the determination of LVR, a strain of 0.06 (10 µm amplitude) was used for all experiments.

#### 4.3.3.4. Thermogravimetric Analysis (TGA)

TGA was performed under similar conditions as described in Chapter 3, section 3.3.3.5. In summary, samples (10 – 12 mg) were scanned in dry air from room temperature to 600 °C at 10 °C $min^{-1}$ using a dynamic rate experiment (resolution = 4). Only thermal decomposition studies on heat-treated nanocomposite and neat CAB films were performed.

## 4.4. Results and Discussion

### 4.4.1. Film Optical Transmittances and Nanocellulose Dispersion States

Transparency is one of the material properties desired when nanoscale reinforcements are used with transparent matrices. Due to the size scale of nanoscale reinforcements (much lower than the wavelength range of visible light), transmittance properties of nanocomposites that are identical to that of the unfilled matrix can be expected when the nanoreinforcements are well-dispersed. With homogeneous nanofibril dispersion, mechanical reinforcement can be expected with little to no impairment to matrix transparency.[13] Percent transmittance ($\%T = I/I_0$ where I is intensity of emergent radiation and $I_0$ is intensity of incident radiation) data derived from UV-vis measurements define the clarity or transparency of a measured sample. In transmittance versus wavelength (λ) plots (Figure 4.2), transmittance increases sharply up to 400 nm, which is approximately the lower limit of the visible region. Over the visible region (λ = 400 – 1000 nm), the slopes of transmittance curves decrease significantly. On the effects of the different nanocelluloses on matrix transmittance properties, optical transmittance values are compared at 590 nm (approximately the midpoint of the

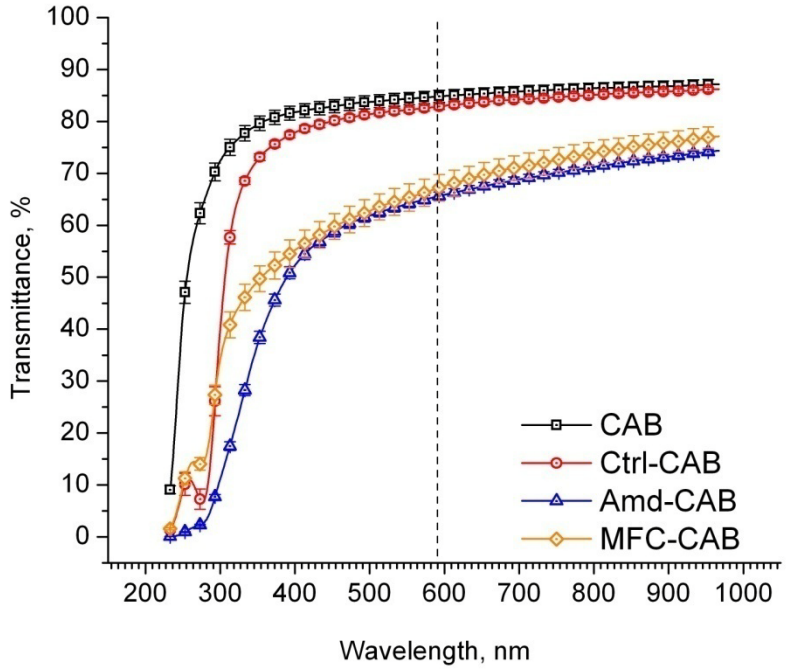


**Figure 4.2** Optical transmittance characteristics of CAB and nanocomposites reinforced with 5 vol % nanocelluloses.

visible spectrum (Table 4.2). At the nanocellulose loading of 5 vol %, Ctrl deteriorates the transparency of CAB by only 2%. Amd and MFC on the other hand, deteriorate CAB transparency by approximately 20%. Differences in dispersion quality were already apparent in the THF suspensions of the nanocelluloses as displayed in Figure 4.1. Over time, both Ctrl and MFC suspensions remained stable (Figure 4.1 A and C) but the former appeared significantly more transparent. This effect is due to both the sizes (3 – 5 nm in width) of Ctrl nanofibrils, which are too small to scatter light, and the likelihood of stronger interactions between Ctrl and THF. The situation was much different with respect to the Amd suspension (Figure 4.1 B), in which the solids flocculate over time, as discussed in section 3.4.5 of Chapter 3. It is assumed that these characteristics of the nanocellulose suspensions were carried over into their blends with the CAB solutions, and led to the observed differences in film transparencies.

To evaluate the state of nanocellulose aggregation, nanocomposites films were examined in transmission under polarized light microscopy. It was expected that the presence of any

**Table 4.2** UV-vis transmittance values (T%) at λ = 590 nm and thicknesses (t) of CAB and 5 vol % nanocomposite films.

| Sample ID | t, mm | T% |
|---|---|---|
| CAB | 0.10 (0.01) | 84.8 (1.2) |
| Ctrl-CAB | 0.10 (0.02) | 82.8 (0.6) |
| Amd-CAB | 0.12 (0.01) | 65.5 (0.8) |
| MFC-CAB | 0.12 (0.02) | 67.1 (2.6) |

Standard deviations are shown in parentheses for three replications

aggregates with sizes on the order of or in excess of the wavelength of visible light will be detected. According to Figure 4.3, neat CAB and Ctrl-CAB nanocomposites are characterized by completely dark fields, which imply that the dispersion of Ctrl in CAB does not generate nanofibril aggregates of detectable sizes. The small fibril widths (3-5 nm) of TONc that failed to scatter light when dispersed in an aqueous medium[19-20] is likely a major contributing factor to the high transparency recorded for Ctrl-CAB nanocomposites. On the other hand, bright regions with sizes on the order of microns are evident in the Amd and MFC-reinforced CAB films (Figure 4.3 C and D). The size scale of aggregates appears significantly smaller in the Amd-based nanocomposites than the MFC-based ones, which is very likely related to the much smaller widths of the parent TONc. These results clearly complement the observations made in the UV-vis studies and confirm the existence of a better-quality dispersion of Ctrl compared to Amd and MFC. In a previous report by Ayuk *et al.*,[35] the UV-vis transmittance of CAB at ~550 nm decreased by 22 and 48% respectively when reinforced with 5 and 10 wt % (3.3 and 6.7 vol %)[a] of wood-derived CNCs. Their findings reflect a greater light scattering effect from CNCs compared to TONc (Ctrl), and is more consistent with the behavior of MFC-reinforced CAB from this study. With respect to Amd-CAB nanocomposites, it appears that the low polarity surfaces of Amd nanofibrils failed to achieve adequate fibril-matrix interaction and resulted in nanofibril aggregation.

[a] Weight to volume fraction conversions assume a density of 1.5 g $mL^{-1}$ for cellulose.

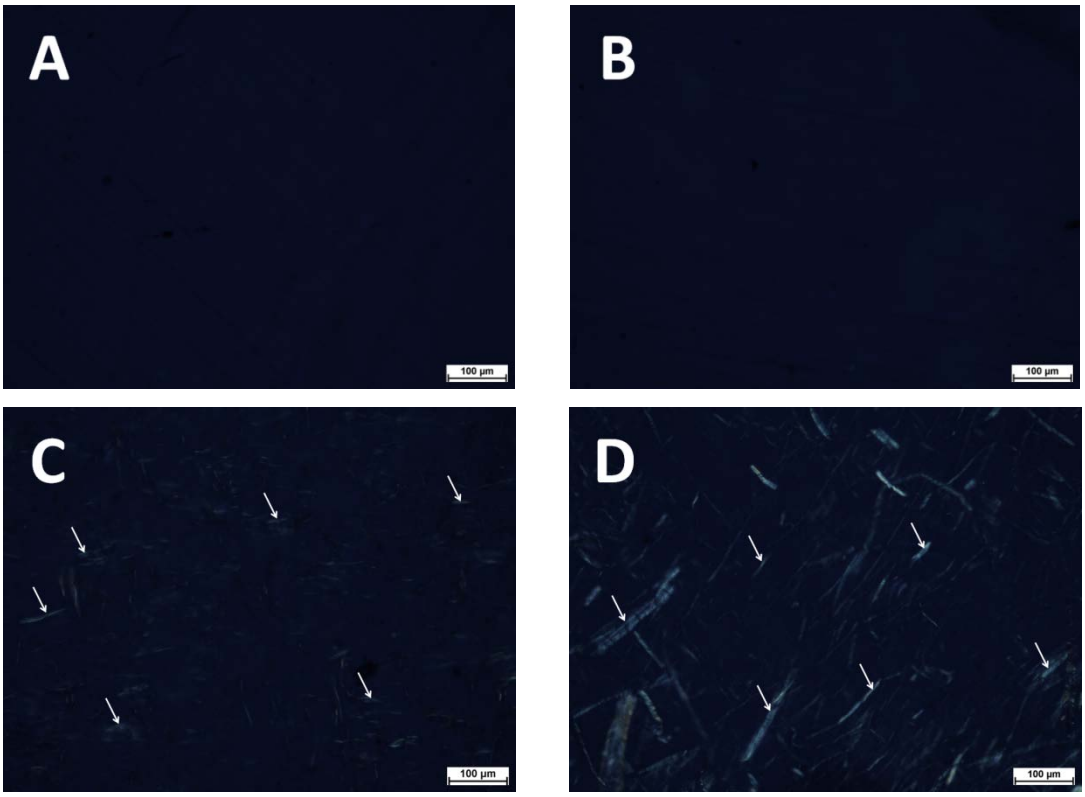


**Figure 4.3** Polarized light microscopy images of (A) unfilled CAB, (B) Ctrl-CAB, (C) Amd-CAB, and (D) MFC-CAB nanocomposite films reinforced with 5 vol % nanocelluloses. Micron scale nanofibril aggregates and bundles (arrowed) can be seen in (C) and (D) but not in (B).

### 4.4.2. DSC

DSC thermograms of heat-treated CAB and nanocomposites films in the range of 50 to 250 °C are displayed in Figure 4.4. Also shown, for reference, is a thermogram of the original CAB-381-20 powder. The first heating scan of the reference CAB is characterized by a strong melting endotherm with a peak located at 165.7 °C. No melting endotherm in observed in the thermograms of film samples, which indicates that the heat treatment process excluded the crystallization of CAB. Moreover, following the removal of sample thermal histories in the first heating scan, no CAB crystallization occurred in the subsequent cooling run, as evidenced by the absence of exothermic peaks during the cooling process (Figure 4.4 B). Glass transition events associated with the heating and cooling scans are bordered with vertical lines in Figure 4.4.

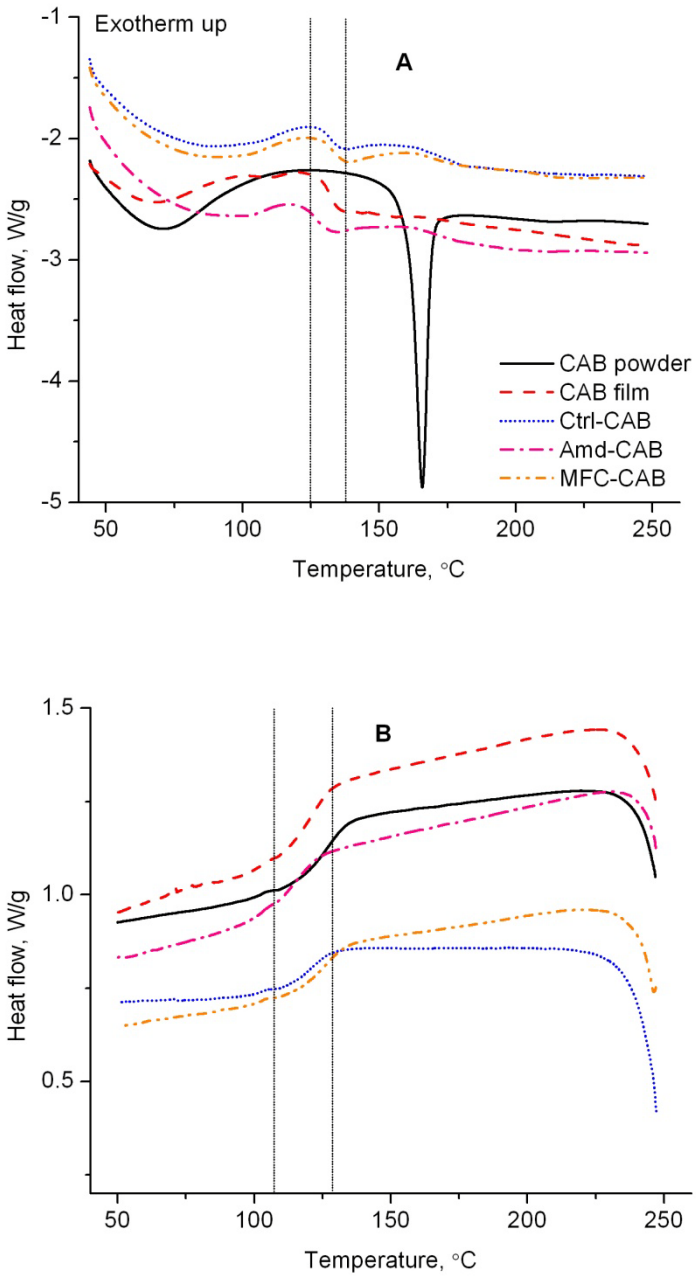


**Figure 4.4** DSC thermograms for (A) heating and (B) cooling scans of neat CAB and nanocomposites. A sample of the original CAB powder is included as a reference. Glass transition events are bordered with vertical lines.

### 4.4.3. Viscoelastic Properties of Nanocomposite Films

Dynamic mechanical properties of the various nanocellulose-CAB nanocomposites were studied in tension. Tensile storage moduli (E´) and tan δ data were chosen as representative viscoelastic properties for analyzing and discussing the effects of film composition and nanocellulose volume fraction on nanocomposite properties.

#### 4.4.3.1. Effect of Ctrl Volume Fraction

Dynamic mechanical properties of Ctrl-CAB nanocomposites were studied at four levels of nanofibril loading (Figure 4.5). In the glassy region (upper limits ranging from 108 to 115 °C for 5 vol % and neat CAB respectively), E´ curves of nanocomposites are only slightly displaced, vertically, relative to neat CAB (Figure 4.5 A). In the glassy region, matrix chains are immobilized and the nanofibril inclusions have practically no effect on nanocomposite stiffness, as has been reported in other studies.[36-37] At the onset of glass transition, E´ of CAB undergoes a rapid decline because of cooperative relaxation of CAB chain segments. A decline is also observed in the nanocomposite plots; however, data in this region are shifted to significantly higher values, which increase with increasing Ctrl volume fraction. Tan δ is the ratio of loss to storage modulus and its magnitude relates directly with the capacity of a material to dampen or dissipate energy. In Figure 4.5 B, heights of tan δ peaks decrease as the volume fraction of Ctrl increases. In addition, the tan δ peaks appear to broaden with increasing Ctrl volume fraction. Dependencies of dynamic mechanical properties on Ctrl volume fraction at $T_g$ (peaks of the tan δ transitions) are graphically depicted in Figure 4.6. Figure 4.6 A shows that E´ increases almost linearly up to 2.5 vol % and then exponentially between 2.5 and 5 vol %. Thus at 5 vol %, E´ of Ctrl-CAB nanocomposite is nearly 22 times that of neat CAB compared to a mere 3.4 times increase at 2.5 vol %. A linear dependence of $T_g$, tan δ peak height, and tan δ peak width on volume fraction of Ctrl is also observed from, at least, 1 to 5 vol % reinforcement (Figure 4.6 B to D). A slight depression in $T_g$ (relative to neat CAB) is associated with an increase in Ctrl volume fraction (Figure 4.6 B). Lower temperature shifts in $T_g$ as a function of reinforcement volume fraction have been reported in a number of nanocomposite systems such as magnetite-filled polyurethane[38] and carbon nanotube-reinforced polypropylene.[39] Kotsilkova *et al.*[39] cited possible reasons for $T_g$ suppression in nanocomposite systems as confinement of polymer molecules in nanoscale spaces in the immediate vicinities of nanoparticles, strong polymer-

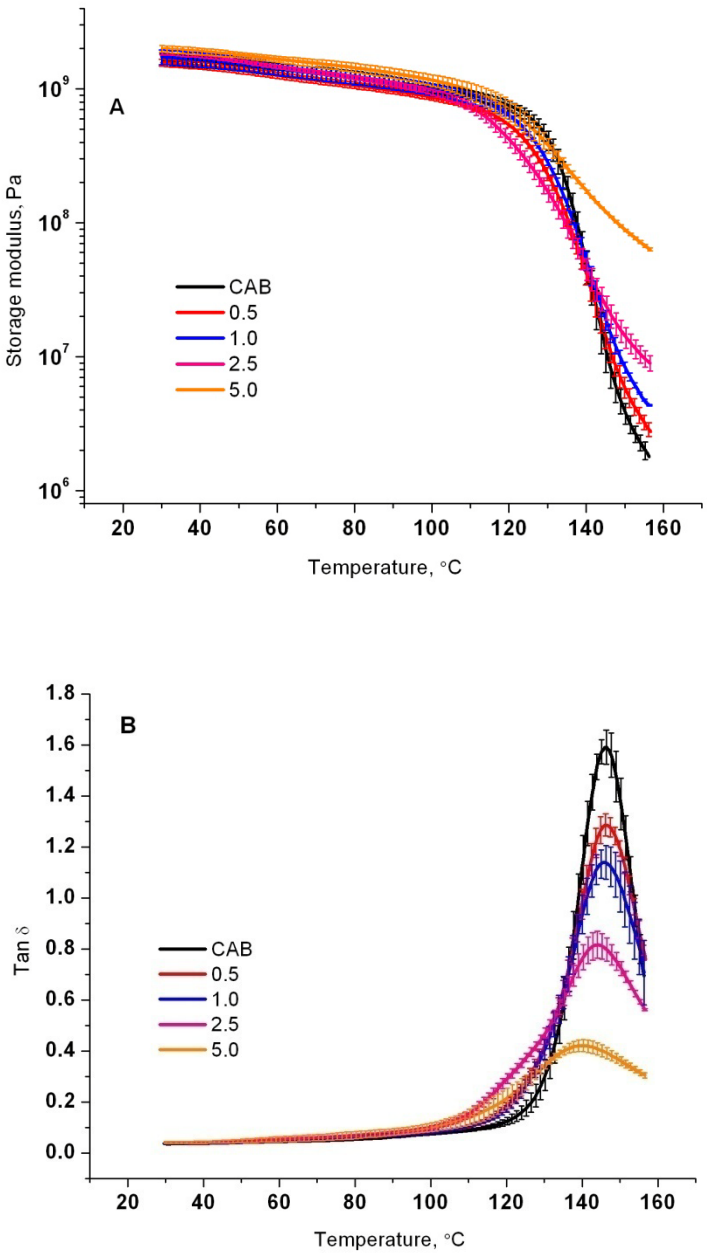


**Figure 4.5** DMA thermal scans of neat CAB and Ctrl-CAB nanocomposites performed at 3 °C/min. (A) tensile storage moduli and (B) tan δ plots. Numbers in legend represent volume fractions (%) of Ctrl. Error bars represent ±1 standard deviations from three replications.

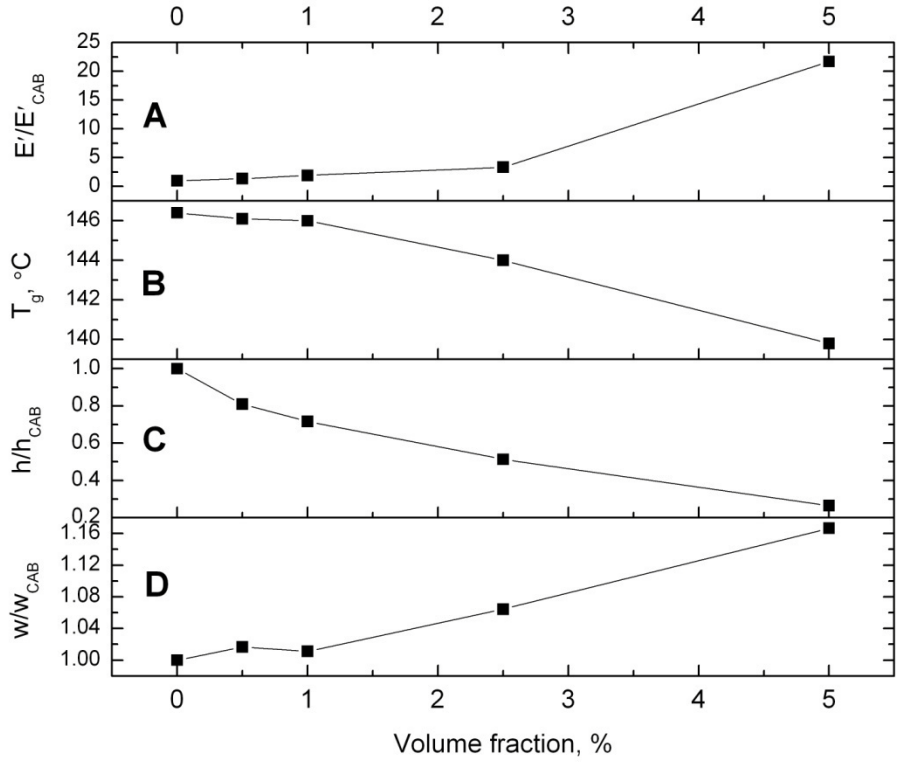


**Figure 4.6** Dependencies of dynamic mechanical properties of Ctrl-CAB nanocomposites on volume fraction of Ctrl at $T_g$ (peaks of tan δ, (B)). (A) E′, (C) tan δ heights, h and (D) widths, w normalized with respect to CAB (0 vol. %).

particle interactions leading to reduced molecular packing of polymer chains, and free volume increases. Numerous studies have reported decreases in heights of tan δ peaks in dependence of filler or reinforcement volume fraction.[17, 38, 40-41] Broadening of tan δ peaks with the inclusion of filler particles is also encountered frequently, and is generally attributed to changes in the matrix relaxation behavior induced by its interactions with the included particles.[41-42] At 5 vol % reinforcement, Ctrl-CAB nanocomposites portray a nearly 80% reduction in height (Figure 4.6 C) and a 16% increase in width (Figure 4.6 D) relative to CAB tan δ peak.

Related studies on CAB-based nanocomposites reinforced with bacterial cellulose (BC)[15] and microcrystalline cellulose (MCC)-derived nanocrystals[35] (Figure 4.7) revealed similar trends as that shown in Figure 4.6 A. The dispersion state of BC was not discussed while some level of aggregation was reported for the MCC-derived nanocrystals. With respect to Ctrl-CAB

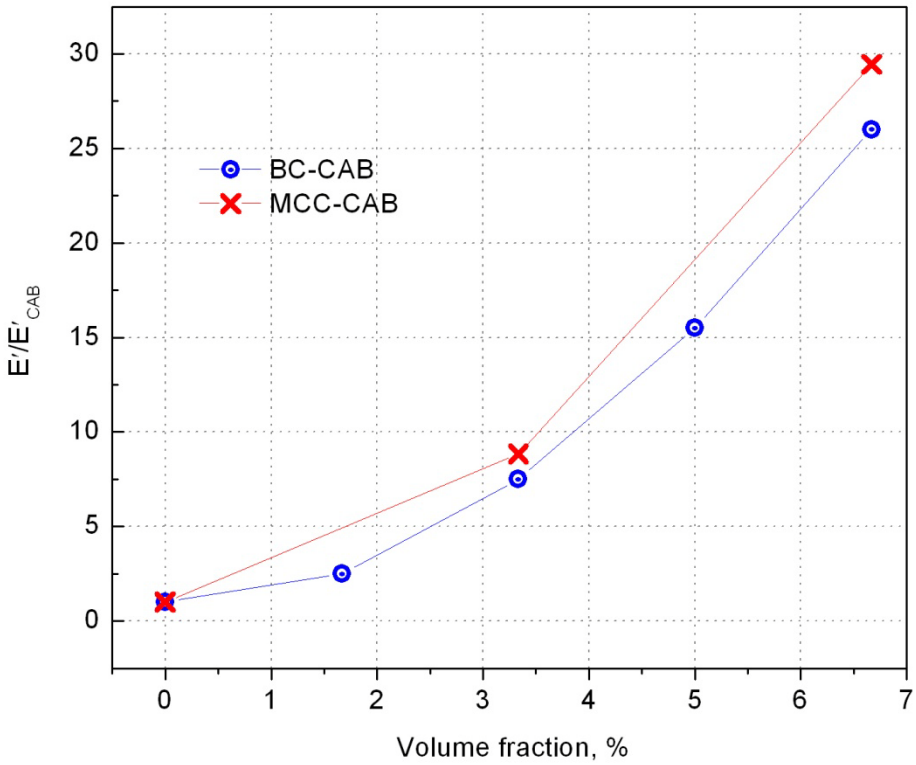


**Figure 4.7** Normalized tensile storage moduli (at $T_g$) of CAB-based nanocomposites reinforced with bacterial cellulose (BC) and microcrystalline cellulose (MCC) nanocrystals as a function of nanofibril volume fraction. Zero volume fraction corresponds to neat CAB

nanocomposites, the combination of high optical transparency with a relatively high storage modulus in the post-glass transition region could have significant implications for the performance of CAB in its films, coatings, and adhesives applications.

#### 4.4.3.2. Comparison of Ctrl, Amd, and MFC Nanocomposites

Comparison of viscoelastic characteristics was used as an additional criterion to evaluate the effects of modifying TONc surfaces with ODA. E´ and tanδ properties of Amd and Ctrl-CAB nanocomposites at 0.5 vol % reinforcement are first presented (Figure 4.8). Over the experimental temperature range, E´ of Amd-CAB is exactly superimposed on that of CAB (Figure 4.8 A). Ctrl-CAB follows a similar path but deviates slightly to lower E´ values at the inflection zone of the glass transition. Beyond the point of inflection (glass transition region),

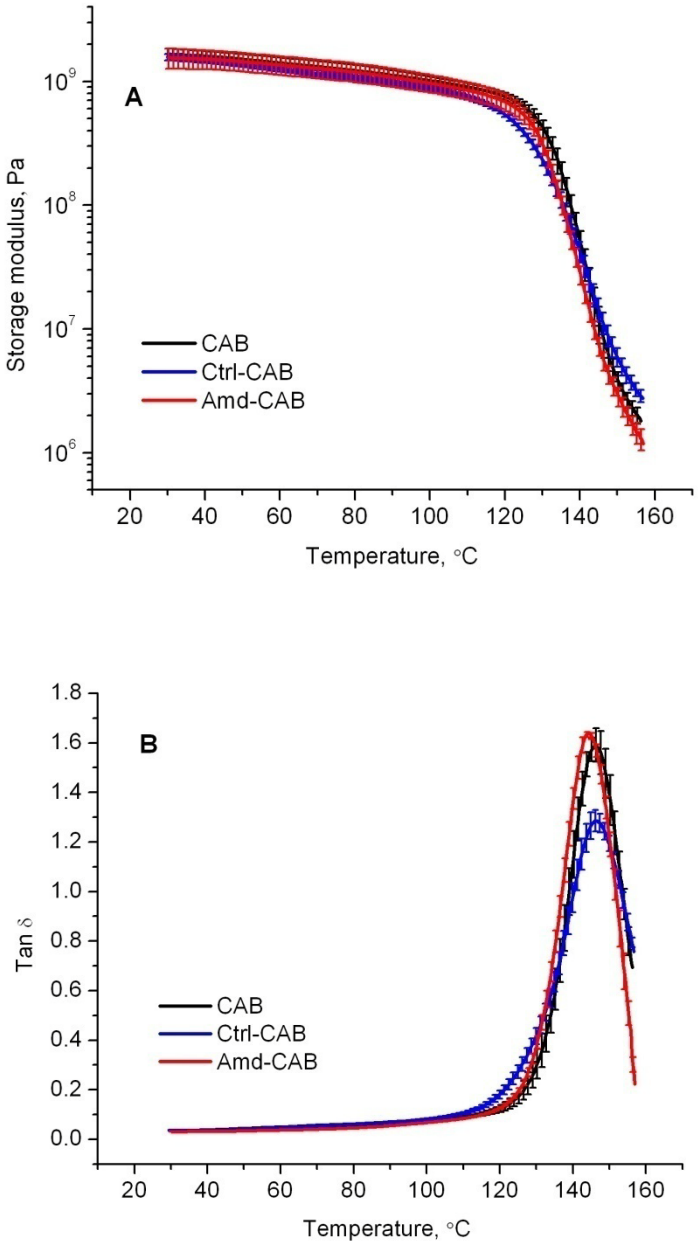


**Figure 4.8** Comparison of viscoelastic properties of Ctrl-CAB and Amd-CAB nanocomposites at 0.5 vol % reinforcement.

however, E´ of Amd-CAB declines at a higher rate than that of Ctrl-CAB resulting in ultimate E´ values of the respective nanocomposites residing below and above that of CAB. Tan δ peak heights (Figure 4.8 B) indicate that the energy damping behavior of CAB was unaffected by Amd but significantly reduced by reinforcement with Ctrl.

More significant differences are observed among the nanocomposites reinforced at 5 vol % (Figure 4.9). At this loading, MFC-CAB is included as a conventional nanocellulose reference. In the glassy region (Figure 4.9 A), shifts in E´ with respect to neat CAB are negligible for both MFC-CAB and Ctrl-CAB. Amd-CAB on the other hand, undergoes a significant shift to lower E´ values in the upper glassy region. In the glass transition region, a distinct separation among E´ performances is observed. Differences in viscoelastic properties at $T_g$ were quantified and the results illustrated in Figure 4.10. Compared to the dramatic 22-fold increase in E´ of CAB when reinforced with Ctrl, Amd and MFC reinforcements result in only 3.5 and 7-fold increases at the same volume fraction (Figure 4.10 A) The magnitudes of E´ are complemented by their corresponding normalized tan δ peak heights , which decrease in the order Amd > MFC > Ctrl (Figure 4.10 C)

The observed nanocomposite performances are clearly related to the dispersion quality of their respective reinforcements in suspension (Figure 4.1) and in film formulations (Figure 4.2 and Figure 4.3). With respect to Ctrl-CAB, the extraordinary E´ performance in the glass transition region is believed to originate, in addition to efficient nanofibril dispersion, from the existence of a fibril-fibril network. Favier *et al.* demonstrated the existence of such a network in highly individualized tunicin whisker-reinforced poly(styrene-*co*-butylacrylate) latex.[2, 43-44] They concluded that a threshold of 1 vol % tunicin whiskers was sufficient to achieve an interfibrillar hydrogen bonding network in the matrix based on a mechanical percolation model.[45] An interfibrillar hydrogen-bonded network of Ctrl nanofibrils, if present in Ctrl-CAB, will involve both –COOH and –OH groups on Ctrl surfaces compared to only –OH groups on the surfaces of conventional nanocelluloses. The substitution of surface –COOH groups by ODA molecules during the synthesis of Amd resulted in nanofibril flocculation in THF and, subsequently, in CAB. Grunert *et al.*[15] reported that E´ improvement in the transition region was less when CAB was reinforced, at identical volume fractions, with trimethylsilylated BC than with plain BC nanocrystals. They cited the reduced net cellulose content in trimethylsilylated nanocrystals as a possible source of E´ disparity. Composites of plasticized CAB matrix reinforced with wood fibers resulted in fiber dispersion qualities that depended on fiber surface treatment.[46] Among water-washed, alkaline-extracted, and acetylated fibers, the highest quality dispersion, and consequently composite strength and modulus performances, resulted from fiber acetylation. The authors cited strong adhesion between acetylated fibers and CAB matrix

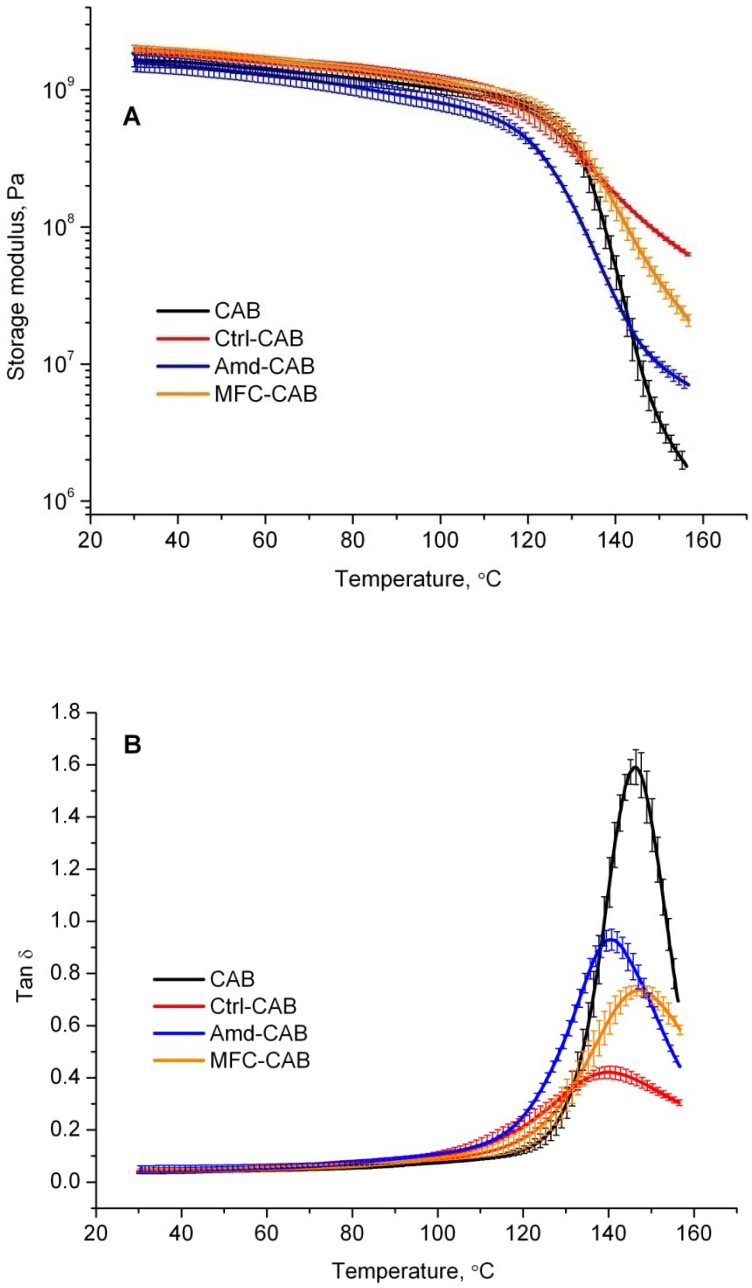


**Figure 4.9** Comparison of viscoelastic properties of CAB and nanocomposites at 5 vol % reinforcement.

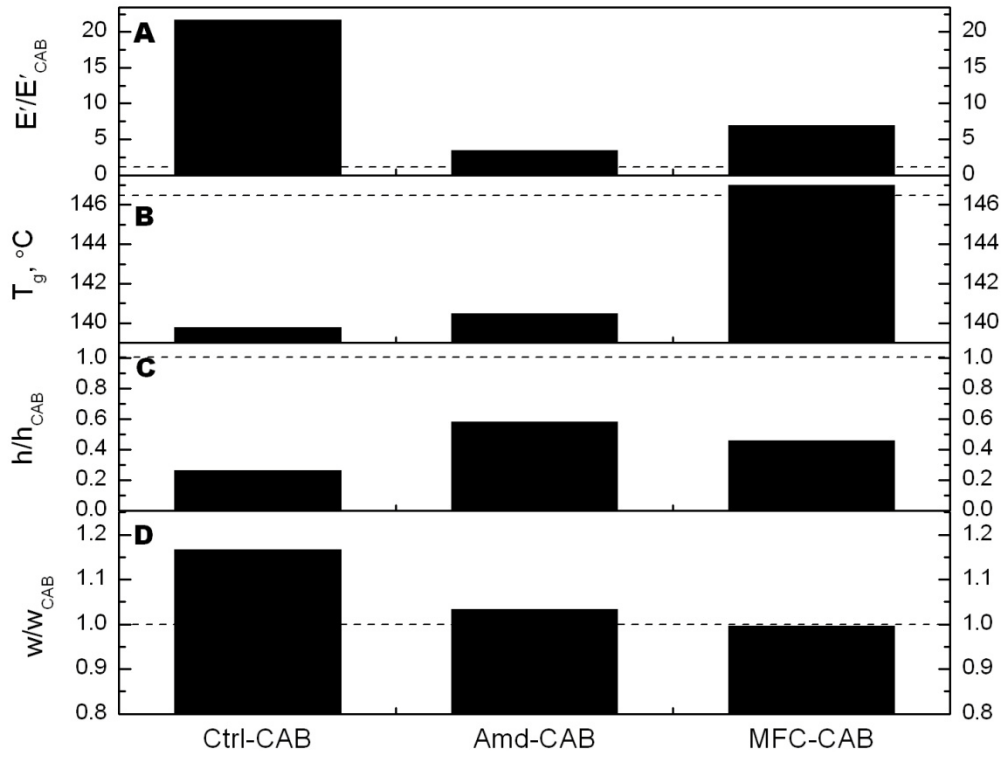


**Figure 4.10** Comparison of (A) normalized storage moduli, tan δ peak (C) heights and widths (D) at (B) $T_g$ of 5 vol % reinforced nanocomposites. Dashed lines mark the positions of the CAB reference.

to explain the observed dispersion quality and mechanical performance improvement. The importance of both nanofibril sizes and individualization to nanocomposite viscoelastic properties can also be deduced from the observed differences between Ctrl and MFC reinforcing capacities. Although stable suspensions are achieved for both Ctrl and MFC in THF (Figure 4.1), significant light scattering is evident in the latter implying the existence of larger sizes of fibril units and/or networks.

In Figure 4.10 B, the $T_g$ of CAB decreases by a similar magnitude with the inclusion of both Amd and Ctrl. However, due to the relatively weak reinforcement of CAB by Amd, the lower $T_g$ of Amd-CAB is more likely due to plasticizing of CAB matrix by the ODA molecules present on Amd surfaces. MFC, though it imparts moderately high reinforcement to CAB with a corresponding decrease in damping, appears to have negligible effect on the $T_g$ and relaxation

behavior of CAB (Figure 4.10 B and D). No shifts in $T_g$ or broadening of tan δ peaks accompanied the glass transition of MFC-CAB nanocomposites, which indicates that inclusion of MFC does not significantly alter the relaxation behavior of CAB. This observation contrasts significantly with the effect of Ctrl on CAB relaxation as observed from tan δ transition behavior. A side-by-side comparison of viscoelastic properties at selected temperatures in the glassy and glass transition regions is made in Table 4.3 for all the evaluated nanocomposites.

### 4.4.4. Thermal Decomposition Properties of Nanocomposite Films

Decomposition thermograms – WL and DWL – of the nanocomposites reinforced with 5 vol % nanocelluloses are displayed, along with those of neat CAB and the respective nanocelluloses (Figure 4.11, Figure 4.12, and Figure 4.13). The nanocellulose thermograms have previously been discussed in Chapter 3, and are only shown here for comparison with their corresponding nanocomposites.

As a result of the low (5%) nanocellulose volume fraction, the thermal decomposition patterns of the nanocomposites are nearly identical to that of neat CAB. However, the lower decomposition temperatures of the nanocellulose reinforcements, compared to CAB, lead to decreases in onset of thermal decomposition in the nanocomposites (insets in weight loss plots). Percentages of weight loss in the region preceding the main decomposition event are compared at an arbitrary reference temperature of 300 °C (points labeled on insets). The data show that at 300 °C, the magnitudes of weight loss in the nanocomposites increase in the order MFC-CAB < Amd-CAB < Ctrl-CAB. This pattern of weight loss is consistent with the direction of increase (Ctrl < Amd < MFC) in intrinsic decomposition temperatures of the corresponding nanocelluloses (labeled peaks on DWL plots). Retention or improvements in matrix thermal stability of cellulosic nanocomposites have been reported in several studies.[35, 47-50] For example, Ayuk *et al.*[35] reported shifts in the onset of thermal decomposition to higher temperatures when a CAB matrix was reinforced with 5 and 10 wt % cellulose whiskers. The authors indicated delays in diffusion of degradation products from the nanocomposites due to the presence of cellulose whiskers. Also in nanocomposites of cellulose whisker-grafted polyurethanes, Cao *et al.*[50] reported nanocomposite peak thermal decomposition temperatures that exceeded those of the reinforcement and unfilled polymer by 67 °C and above. They attributed the superior nanocomposite thermal stability to complete coverage of the cellulose whiskers by the grafted

**Table 4.3** Dynamic mechanical properties of CAB and all nanocomposites selected from glassy (40 °C) and relaxed (150 °C) regions of the spectra. $T_g$ is taken from the peak of tan δ plots. ± 1 standard deviations are shown in parentheses.

| Sample ID | Fibril content, vol % | E´, MPa | | E´/ E´$_{(CAB)}$[a] | | $T_g$, °C |
|---|---|---|---|---|---|---|
| | | 40 °C | 150 °C | 40 °C | 150 °C | |
| CAB | 0.0 | 1600 (158) | 3.80 (0.66) | 1.00 | 1.00 | 146.4 (1.2) |
| Ctrl | 0.5 | 1492 (87.5) | 5.74 (0.98) | 0.93 | 1.51 | 146.1 (0.1) |
| | 1.0 | 1658 (196) | 8.37 (0.79) | 1.04 | 2.20 | 146.0 (0.1) |
| | 2.5 | 1742 (36.4) | 14.4 (2.58) | 1.09 | 3.77 | 144.0 (0.1) |
| | 5.0 | 1911 (107) | 89.3 (2.04) | 1.19 | 23.5 | 139.8 (0.1) |
| Amd | 0.5 | 1517 (263) | 2.96 (0.49) | 0.95 | 0.78 | 144.4 (0.3) |
| | 5.0 | 1904 (89.5) | 9.85 (0.87) | 1.19 | 2.59 | 140.5 (0.1) |
| MFC | 5.0 | 1877 (141) | 40.5 (5.72) | 1.17 | 10.6 | 147.0 (1.7) |

[a]Normalized storage modulus with respect to unfilled CAB

polyurethane chains which resulted in confined structures in the nanocomposites. In the present work, peak decomposition temperatures and corresponding maximum WL rates (Table 4.4) of the nanocomposites are clearly identical to those of neat CAB.

## 4.5. Conclusions

TONc (Ctrl) forms non-flocculating, stable, and transparent suspensions in THF, probably due to strong solvent-fibril interactions and individualization of the nanosized fibrils. Consequently, the transparency of CAB is preserved when reinforced with Ctrl. Hydrophobization of TONc surfaces (Amd), on the other hand, results in flocculated suspensions that ultimately leads to nanofibril aggregation in CAB matrix. With respect to MFC (conventional nanocellulose reference), insufficient individualization of the nanocellulose results in formation of opaque THF suspensions and subsequent aggregation in CAB. As a result of aggregation, both Amd and MFC reinforcements deteriorate the transparency of CAB matrix by 20%. The quality of nanocellulose dispersion also accounts for the differences in dynamic mechanical performances among the nanocomposites. Tensile storage moduli in the glass transition region of Ctrl-CAB nanocomposites increases linearly between 0 and 2.5 vol %, and

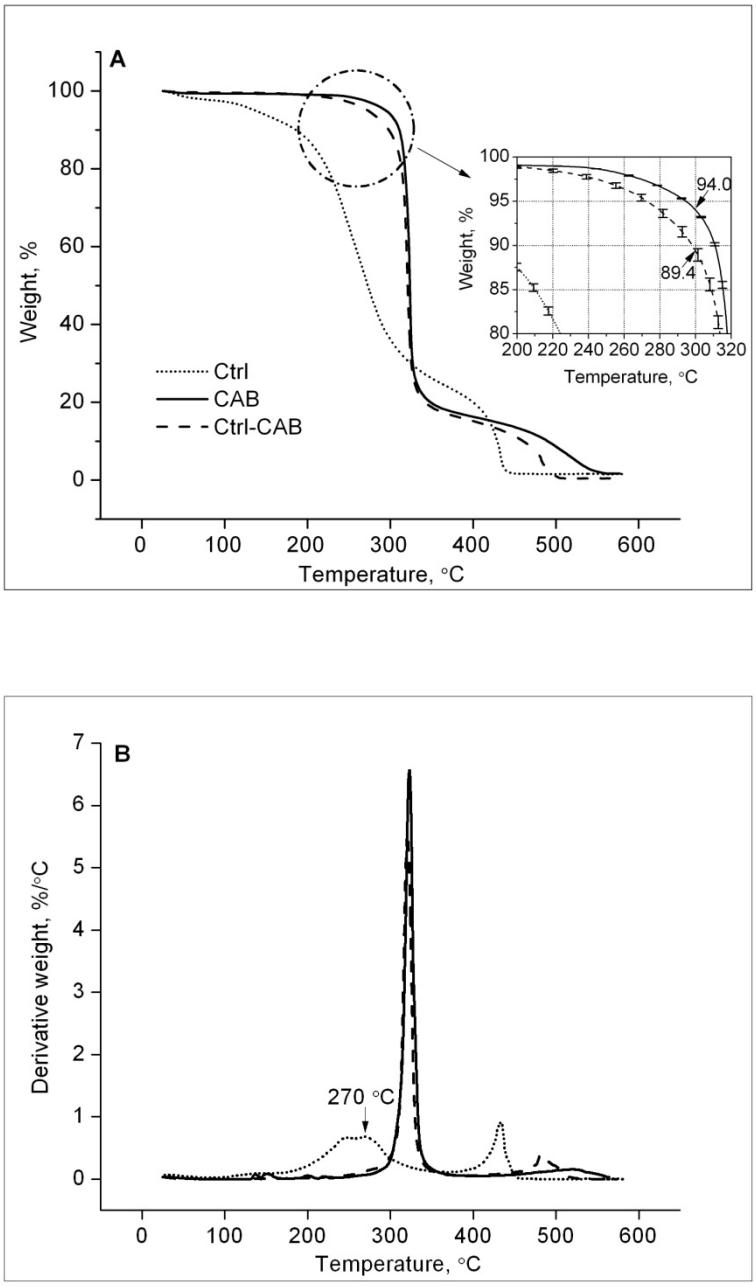


**Figure 4.11** (A) WL and (B) DWL as a function of temperature for Ctrl, CAB and 5 vol % Ctrl-CAB. Inset in (A) shows sample weights remaining at 300 °C of neat CAB and Ctrl-CAB nanocomposite. Error bars in inset represent ±1 standard deviation.

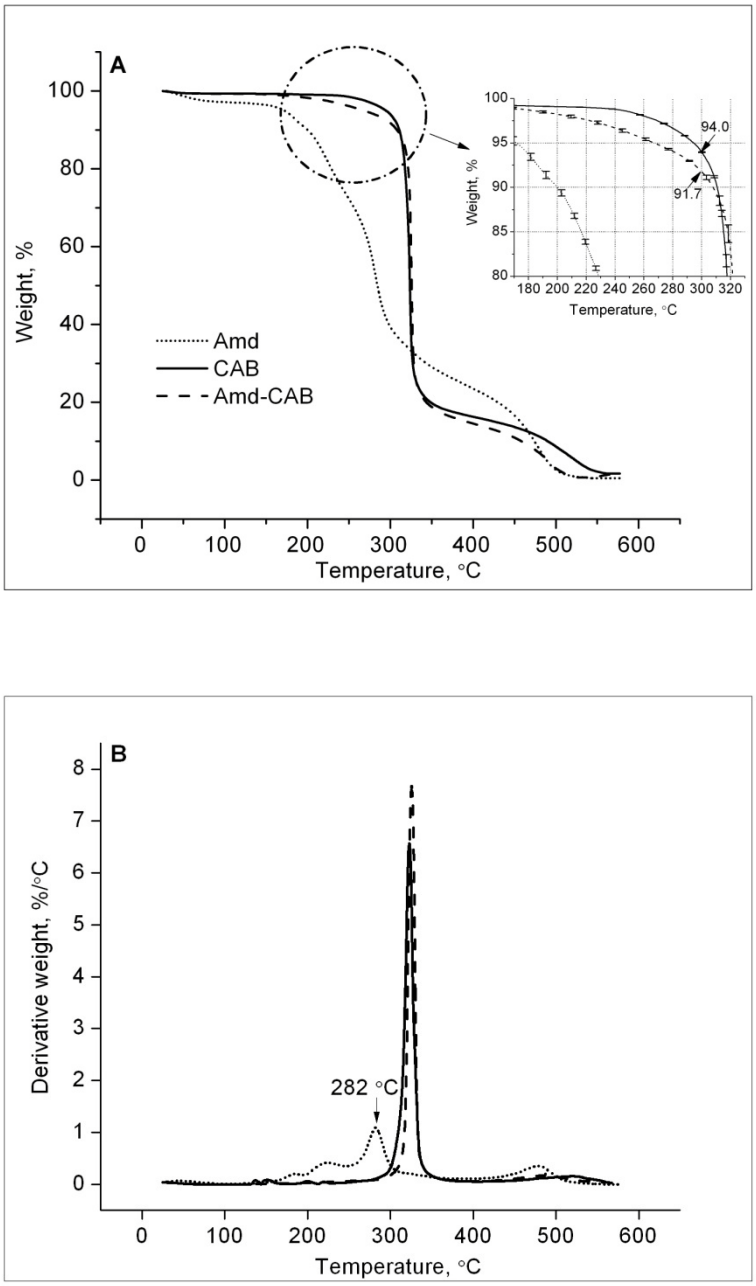


**Figure 4.12** (A) WL and (B) DWL as a function of temperature for Amd, CAB and 5 vol % Amd-CAB. Inset in (A) shows sample weights remaining at 300 °C of neat Amd and Amd-CAB nanocomposite. Error bars in inset represent ±1 standard deviation.

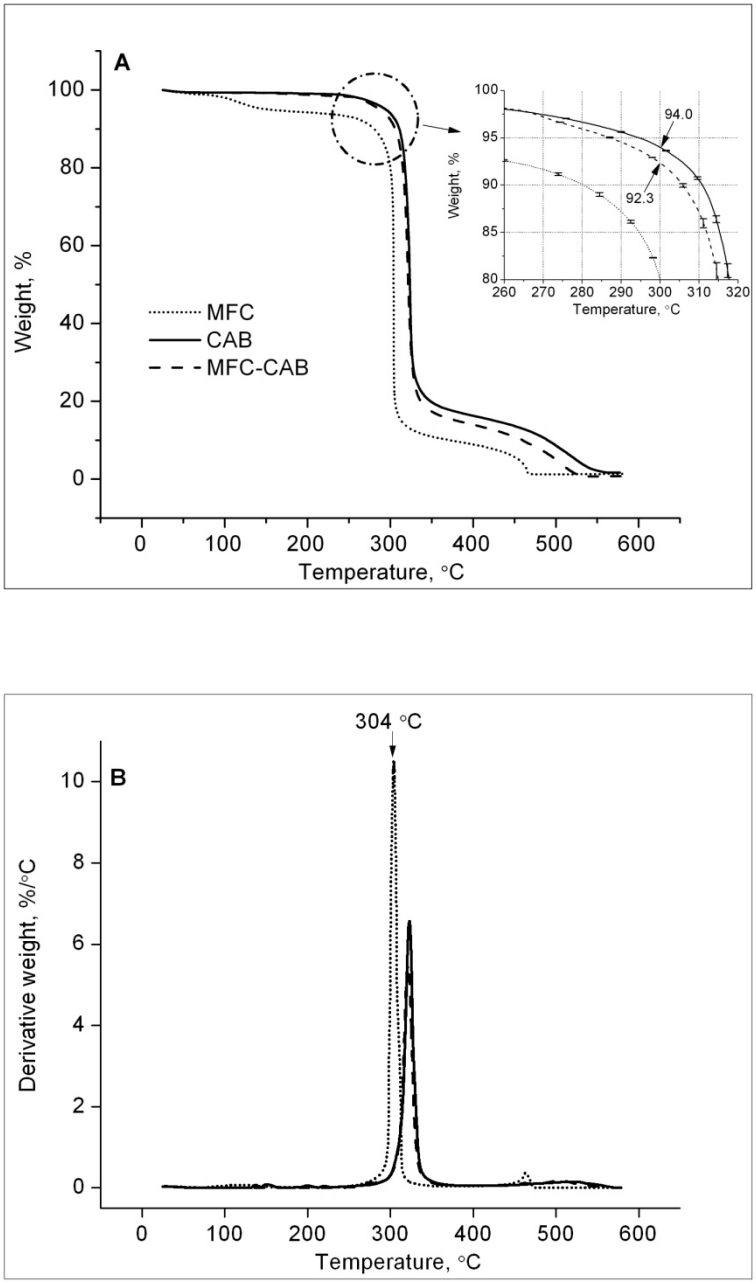


**Figure 4.13** (A) WL and (B) DWL as a function of temperature for MFC, CAB and 5 vol % MFC-CAB. Inset in (A) shows sample weights remaining at 300 °C of neat CAB and MFC-CAB nanocomposite. Error bars in inset represent ±1 standard deviation.

**Table 4.4** TGA maximum decomposition rate temperatures and corresponding DWL of CAB and 5 vol % nanocomposites.

| Sample ID | Temperature, °C | DWL, %/°C |
|---|---|---|
| CAB | 323 | 6.57 |
| Ctrl-CAB | 321 | 5.51 |
| Amd-CAB | 326 | 7.68 |
| MFC-CAB | 321 | 5.45 |

then exponentially from 2.5 to 5 vol % Ctrl. It is proposed, based on these observations that besides the existence of a high fibril-matrix interfacial region created by the homogeneous dispersion of Ctrl, a continuous nanofibril network may be present at the volume fraction associated with the non-linear modulus increase. At 5 vol % reinforcement, the tensile storage modulus of CAB in the glass transition region increases by 22, 7.0, and 3.5 fold when reinforced with Ctrl, MFC, and Amd respectively. The relative reinforcing capacities of the nanocelluloses result directly from the differences in dispersion quality. The findings from this study indicate that without the need for surface modification, TONc represents a suitable reinforcement for the preparation of transparent CAB nanocomposites.

The main decomposition temperature of CAB is unaltered by the presence of nanocelluloses. However, relative to neat CAB, nanocomposite thermal stabilities in the region preceding the main CAB decomposition are slightly decreased due to the presence of the less thermally stable nanocelluloses. The fraction of nanocomposite weight loss in this region is observed to increase as the peak decomposition temperature of the corresponding nanocellulose decreases.

## 4.6. References


(1) Schandler, L. S.; Brinson, L. C.; Sawyer, W. G., Polymer nanocomposites: A small part of the story. *Jom-Us* **2007,** *59* (3), 53-60.

(2) Favier, V.; Chanzy, H.; Cavaille, J. Y., Polymer Nanocomposites Reinforced by Cellulose Whiskers. *Macromolecules* **1995,** *28* (18), 6365-6367.

(3) Oksman, K.; Mathew, A. P.; Bondeson, D.; Kvien, I., Manufacturing process of cellulose whiskers/polylactic acid nanocomposites. *Composites Science and Technology* **2006,** *66* (15), 2776-2784.

(4) Bondeson, D.; Oksman, K., Polylactic acid/cellulose whisker nanocomposites modified by polyvinyl alcohol. *Compos. Pt. A-Appl. Sci. Manuf.* **2007,** *38* (12), 2486-2492.

(5) Liu, H. Y.; Liu, D. G.; Yao, F.; Wu, Q. L., Fabrication and properties of transparent polymethylmethacrylate/cellulose nanocrystals composites. *Bioresource Technol* **2010,** *101* (14), 5685-5692.

(6) Lopez-Suevos, F.; Eyholzer, C.; Bordeanu, N.; Richter, K., DMA analysis and wood bonding of PVAc latex reinforced with cellulose nanofibrils. *Cellulose* **2010,** *17* (2), 387-398.

(7) Heux, L.; Chauve, G.; Bonini, C., Nonflocculating and chiral-nematic self-ordering of cellulose microcrystals suspensions in nonpolar solvents. *Langmuir* **2000,** *16* (21), 8210-8212.

(8) Nakagaito, A. N.; Iwamoto, S.; Yano, H., Bacterial cellulose: the ultimate nano-scalar cellulose morphology for the production of high-strength composites. *Applied Physics a-Materials Science & Processing* **2005,** *80* (1), 93-97.

(9) Nakagaito, A. N.; Yano, H., The effect of morphological changes from pulp fiber towards nano-scale fibrillated cellulose on the mechanical properties of high-strength plant fiber based composites. *Applied Physics a-Materials Science & Processing* **2004,** *78* (4), 547-552.

(10) Nakagaito, A. N.; Yano, H., Novel high-strength biocomposites based on microfibrillated cellulose having nano-order-unit web-like network structure. *Applied Physics a-Materials Science & Processing* **2005,** *80* (1), 155-159.

(11) Nakagaito, A. N.; Yano, H., Nanocomposites based on cellulose microfibril. *Cellulose Nanocomposites: Processing, Characterization, and Properties* **2006,** *938,* 151-168.

(12) Shimazaki, Y.; Miyazaki, Y.; Takezawa, Y.; Nogi, M.; Abe, K.; Ifuku, S.; Yano, H., Excellent thermal conductivity of transparent cellulose nanofiber/epoxy resin nanocomposites. *Biomacromolecules* **2007,** *8* (9), 2976-2978.

(13) Yano, H.; Sugiyama, J.; Nakagaito, A. N.; Nogi, M.; Matsuura, T.; Hikita, M.; Handa, K., Optically transparent composites reinforced with networks of bacterial nanofibers. *Adv. Mater.* **2005,** *17* (2), 153-+.

(14) Gindl, W.; Keckes, J., Tensile properties of cellulose acetate butyrate composites reinforced with bacterial cellulose. *Composites Science and Technology* **2004,** *64* (15), 2407-2413.

(15) Grunert, M.; Winter, W. T., Nanocomposites of cellulose acetate butyrate reinforced with cellulose nanocrystals. *Journal of Polymers and the Environment* **2002,** *10* (1-2), 27-30.

(16) Habibi, Y.; Goffin, A. L.; Schiltz, N.; Duquesne, E.; Dubois, P.; Dufresne, A., Bionanocomposites based on poly(epsilon-caprolactone)-grafted cellulose nanocrystals by ring-opening polymerization. *J. Mater. Chem.* **2008,** *18* (41), 5002-5010.

(17) Lu, J.; Askeland, P.; Drzal, L. T., Surface modification of microfibrillated cellulose for epoxy composite applications. *Polymer* **2008,** *49* (5), 1285-1296.

(18) Tingaut, P.; Zimmermann, T.; Lopez-Suevos, F., Synthesis and Characterization of Bionanocomposites with Tunable Properties from Poly(lactic acid) and Acetylated Microfibrillated Cellulose. *Biomacromolecules* **2010,** *11* (2), 454-464.

(19) Saito, T.; Nishiyama, Y.; Putaux, J. L.; Vignon, M.; Isogai, A., Homogeneous suspensions of individualized microfibrils from TEMPO-catalyzed oxidation of native cellulose. *Biomacromolecules* **2006,** *7* (6), 1687-1691.

(20) Saito, T.; Kimura, S.; Nishiyama, Y.; Isogai, A., Cellulose nanofibers prepared by TEMPO-mediated oxidation of native cellulose. *Biomacromolecules* **2007,** *8* (8), 2485-2491.

(21) Saito, T.; Isogai, A., Wet strength improvement of TEMPO-oxidized cellulose sheets prepared with cationic polymers. *Ind Eng Chem Res* **2007,** *46* (3), 773-780.

(22) Alila, S.; Aloulou, F.; Beneventi, D.; Boufi, S., Self-aggregation of cationic surfactants onto oxidized cellulose fibers and coadsorption of organic compounds. *Langmuir* **2007,** *23* (7), 3723-3731.

(23) Suh, D. S.; Lee, K. S.; Chang, P. S.; Kim, K. O., Physicochemical properties of cellulose selectively oxidized with the 2.2,6,6-tetramethyl-1-piperidinyl oxoammonium ion. *Journal of Food Science* **2007,** *72* (5), C235-C242.

(24) Bragd, P. L.; van Bekkum, H.; Besemer, A. C., TEMPO-mediated oxidation of polysaccharides: survey of methods and applications. *Topics in Catalysis* **2004,** *27* (1-4), 49-66.

(25) Fukuzumi, H.; Saito, T.; Wata, T.; Kumamoto, Y.; Isogai, A., Transparent and High Gas Barrier Films of Cellulose Nanofibers Prepared by TEMPO-Mediated Oxidation. *Biomacromolecules* **2009,** *10* (1), 162-165.

(26) Mukai, K.; Kumamoto, Y.; Isogai, A.; Meiwa, Z.; Maezawa, T.; Ugajin, T. Gas-barrier material, gas-barrier molded article, and method for producing the gas-barrier molded article. 2009-JP71889 2010074340, 20091225., 2010.

(27) Isogai, A.; Kado, H.; Goi, Y. Gel compositions containing oxidized cellulose fibers with good resistance to salts and ionic surfactants. 2008-197847 2010037348, 20080731., 2010.

(28) Isogai, A.; Kado, H.; Goi, Y. Spray compositions containing oxidized cellulose fibers as thickeners, and sprayers therefor. 2008-197849 2010037200, 20080731., 2010.

(29) Suzuki, A.; Miyawaki, S.; Katsukawa, S.; Abe, H.; Iijima, Y.; Isogai, A. Cellulose nanofiber-containing base paper for processing paper. 2008-93496 2009243010, 20080331., 2009.

(30) Kato, T.; Isogai, A.; Saito, T.; Oaki, Y.; Nishimura, T. Composite material, functional material, process for producing composite material, and process for producing composite-material thin film. 2008-206488 2010043144, 20080810., 2010.

(31) Isogai, A.; Kado, H.; Goi, Y. Cosmetics compositions containing oxidized cellulose fibers and functional components. 2008-197848 2010037199, 20080731., 2010.

(32) Araki, J.; Wada, M.; Kuga, S., Steric stabilization of a cellulose microcrystal suspension by poly(ethylene glycol) grafting. *Langmuir* **2001,** *17* (1), 21-27.

(33) Habibi, Y.; Chanzy, H.; Vignon, M. R., TEMPO-mediated surface oxidation of cellulose whiskers. *Cellulose* **2006,** *13* (6), 679-687.

(34) Cellulose-Based Specialty Polymers. Eastman Chemical Company Publication E-325G EASTMAN Cellulose-Based Specialty Polymers http://www.eastman.com/Literature_Center/E/E325.pdf: 2009.

(35) Ayuk, J. E.; Mathew, A. P.; Oksman, K., The Effect of Plasticizer and Cellulose Nanowhisker Content on the Dispersion and Properties of Cellulose Acetate Butyrate Nanocomposites. *Journal of Applied Polymer Science* **2009,** *114* (5), 2723-2730.

(36) Ljungberg, N.; Bonini, C.; Bortolussi, F.; Boisson, C.; Heux, L.; Cavaille, J. Y., New nanocomposite materials reinforced with cellulose whiskers in atactic polypropylene: Effect of surface and dispersion characteristics. *Biomacromolecules* **2005,** *6* (5), 2732-2739.

(37) Kim, J.; Montero, G.; Habibi, Y.; Hinestroza, J. P.; Genzer, J.; Argyropoulos, D. S.; Rojas, O. J., Dispersion of Cellulose Crystallites by Nonionic Surfactants in a Hydrophobic Polymer Matrix. *Polymer Engineering and Science* **2009,** *49* (10), 2054-2061.

(38) Razzaq, M. Y.; Anhalt, M.; Frormann, L.; Weidenfeller, B., Mechanical spectroscopy of magnetite filled polyurethane shape memory polymers. *Mat Sci Eng a-Struct* **2007,** *471* (1-2), 57-62.

(39) Kotsilkova, R.; Ivanov, E.; Krusteva, E.; Silvestre, C.; Cimmino, S.; Duraccio, D., Isotactic Polypropylene Composites Reinforced with Multiwall Carbon Nanotubes, Part 2: Thermal and Mechanical Properties Related to the Structure. *Journal of Applied Polymer Science* **2010,** *115* (6), 3576-3585.

(40) Leyva, M. E.; Barra, G. M. O.; Moreira, A. C. F.; Soares, B. G.; Khastgir, D., Electric, dielectric, and dynamic mechanical behavior of carbon black/styrene-butadiene-styrene composites. *Journal of Polymer Science Part B-Polymer Physics* **2003,** *41* (23), 2983-2997.

(41) Ogata, N.; Kawakage, S.; Ogihara, T., Structure and thermal/mechanical properties of poly(ethylene oxide) clay mineral blends. *Polymer* **1997,** *38* (20), 5115-5118.

(42) Alexandre, M.; Dubois, P., Polymer-layered silicate nanocomposites: preparation, properties and uses of a new class of materials. *Materials Science & Engineering R-Reports* **2000,** *28* (1-2), 1-63.

(43) Favier, V.; Canova, G. R.; Cavaille, J. Y.; Chanzy, H.; Dufresne, A.; Gauthier, C., Nanocomposite Materials from Latex and Cellulose Whiskers. *Polymers for Advanced Technologies* **1995,** *6* (5), 351-355.

(44) Favier, V.; Canova, G. R.; Shrivastava, S. C.; Cavaille, J. Y., Mechanical percolation in cellulose whisker nanocomposites. *Polymer Engineering and Science* **1997,** *37* (10), 1732-1739.

(45) Ouali, N.; Cavaille, J. Y.; Perez, J., Elastic, Viscoelastic and Plastic Behavior of Multiphase Polymer Blends. *Plast Rub Compos Pro* **1991,** *16* (1), 55-60.

(46) Glasser, W. G.; Taib, R.; Jain, R. K.; Kander, R., Fiber-reinforced cellulosic thermoplastic composites. *Journal of Applied Polymer Science* **1999,** *73* (7), 1329-1340.

(47) Kumar, A. P.; Singh, R. P., Novel hybrid of clay, cellulose, and thermoplastics. I. Preparation and characterization of composites of ethylene-propylene copolymer. *Journal of Applied Polymer Science* **2007,** *104* (4), 2672-2682.

(48) Paralikara, S. A.; Simonsen, J.; Lombardi, J., Poly(vinyl alcohol)/cellulose nanocrystal barrier membranes. *J Membrane Sci* **2008,** *320* (1-2), 248-258.

(49) Samir, M. A. S. A.; Alloin, F.; Sanchez, J. Y.; Dufresne, A., Cellulose nanocrystals reinforced poly(oxyethylene). *Polymer* **2004,** *45* (12), 4149-4157.

(50) Cao, X. D.; Habibi, Y.; Lucia, L. A., One-pot polymerization, surface grafting, and processing of waterborne polyurethane-cellulose nanocrystal nanocomposites. *J. Mater. Chem.* **2009,** *19* (38), 7137-7145.

# Chapter 5. A New Bio-based Nanocomposite: Fibrillated TEMPO-oxidized Celluloses in Hydroxypropylcellulose Matrix

Paper originally published in *Cellulose* under the following reference information: A new bio-based nanocomposite: fibrillated TEMPO-oxidized celluloses in hydroxypropylcellulose matrix, *Cellulose* **2009**, *16*, 227, **Johnson, R. K.**; Zink-Sharp, A.; Renneckar, S. H.; Glasser, W. G.;

## 5.1. Abstract

Utilization of TEMPO-oxidized nanocelluloses in bio-based nanocomposites is reported for the first time. TEMPO-oxidized wood pulps (net carboxylate content 1.1 mmol/g cellulose) were fibrillated to varying degrees using a high intensity ultrasonic processor. The degree of fibrillation was controlled by varying sonication time from 1 to 20 min. The sonication products were then characterized independently and used as fillers (5 wt % loading) in hydroxypropylcellulose nanocomposite films. Nanofibril yields ranging from 11 to 98 wt % (on fiber weight basis) were obtained over the range of sonication times used. Suspension viscosities increased initially with sonication time, peaked with gel-like behavior at 10 min of sonication and then decreased with further sonication. The thermal degradation temperature of unfibrillated oxidized pulps was only minimally affected (6°C decrease) by the fibrillation process. Dynamic mechanical analysis of the nanocomposites revealed strong fibril-matrix interactions as evidenced by remarkable storage modulus retention at high temperatures and a suppression of matrix glass transition at "high" (~5 wt %) nanofibril loadings. Creep properties likewise exhibited significant (order of magnitude) suppression of matrix flow at high temperatures. It was also believed, based on morphologies of freeze-fracture surfaces that the nanocomposites may be characterized by high fracture toughness.

## 5.2. Introduction

When composite materials are fully derived from bio-based components, desirable benefits such as biodegradability and biocompatibility are emphasized. Proceeding from such interests is the development of nanocomposites derived from nanoscale cellulosic elements in bio-based polymer matrices.[1-4] So far, the most commonly used nanocelluloses are microfibrillated

celluloses (MFCs)[5,6] and cellulose nanocrystals (CNCs).[3,7,8] Microfibrillated celluloses are produced by a two-step process: mechanical refining of wood and natural fiber pulps followed by several passes through a high intensity homogenizer.[9-11] The product is a dense network of highly fibrillated celluloses ranging from 10 to 100 nm in width. CNCs on the other hand, are generated from acid hydrolysis of pulp fibers. The hydrolysis process dissolves amorphous regions in the fiber leaving intact the crystalline fraction.[12] The nanocrystalline suspensions are washed and further homogenized by ultrasonic treatment.

Recently, Saito *et al.*[13] reported their discovery of individualized cellulose nanofibrils following homogenization of oxidized cellulose fibers. Cellulose fibers were oxidized via the 2,2,6,6-tetramethylpiperidine-1-oxyl (TEMPO)-mediated oxidation process, which converts primary alcohols to aldehydes and carboxylate groups. When polysaccharides such as cellulose are oxidized in an aqueous medium, a primary oxidant, commonly sodium hypochlorite (NaOCl) is needed for in situ activation of the TEMPO radical.[14] NaOCl concentrations in the range of 2.5 to 3.8 mmol / g cellulose allowed for nanofibrillation of more than 90 % of wood and cotton fibers.[13] The nanofibrils from wood pulp ranged from 3 – 5 nm in width and several hundred nanometers to a few microns in length. Ease of fibril disintegration was attributed to interfibrillar repulsive forces generated by surface carboxylate groups. With the exceptionally small fibril widths, the homogenized oxidized cellulose suspensions appeared transparent. It has also been reported that TEMPO-mediated oxidation produces no change in crystallinity of cellulose even at a high oxidation level of 10 mmol NaOCl / g cellulose.[15] Unlike conventional microfibrillation and acid hydrolysis processes, which yield microfibril networks and short crystallite bundles respectively, fibrillated celluloses from TEMPO-mediated oxidation generate long individualized nanofibrils with diverse surface functionalities (carboxyl, aldehyde, and hydroxyl). We perceive that the unique physical and chemical characteristics of these fibrillated oxidized celluloses could offer significant potential in the fields of coatings, composites reinforcement, packaging, and drug delivery.

Utilization of TEMPO-oxidized celluloses as nanofillers in a bio-based polymer matrix was the subject of this study. Properties of fiber-reinforced composites depend on a variety of factors which include fiber dimensions, fiber volume fraction, and fiber-matrix interfacial adhesion. Since TEMPO-mediated oxidation of pulp produces easily fibrillated products, regulating exposure time to a homogenizer can be used to control the nanofibril fraction within a fixed

volume of oxidized pulp. This approach to controlling nanofibril volume fraction can be used for controlling properties of nanocellulose-filled biopolymer composites. (Nakagaito and Yano 2004) have previously investigated the influence of fibrillation degree on cellulose nanocomposite properties using phenol formaldehyde-bonded MFC mats. They controlled the degree of MFC fibrillation by varying the number of passes through (1) a refiner only and (2) a refiner followed by a homogenizer. A significant increase in bending strength was found when MFCs underwent 30 passes through the refiner and subsequent passes through the homogenizer. Young's modulus on the other hand was only marginally influenced. Morphological studies on the MFCs revealed that fibrillation of the starting pulp fibers was only superficial when the number of refiner passes was fewer than 16. By 30 passes, the bulk of the pulp fibers had fibrillated into fine nanofibril networks, which provided the needed surface area for the observed strength enhancement. In the present paper, ultrasonication was employed to fibrillate TEMPO-oxidized cellulose fibers of a softwood pulp. Nanofibril volume fraction was controlled by varying sonication time. The fibrillated products were utilized as reinforcing fillers in solvent-cast hydroxypropylcellulose (HPC) films, which were then evaluated by dynamic mechanical and creep compliance testing.

## 5.3. Experimental

### 5.3.1. Materials

Never-dried kraft pulp (Douglas-fir) served as starting cellulose fiber. The pulp of 85 % brightness was kindly provided by Weyerhaeuser Company, Washington, USA. Further bleaching of the pulp was achieved in acidified sodium chlorite solution using the method of.[16] The samples were preserved in a refrigerator below 8 °C until used. Sulfite pulp (Tembec Inc Temalfa 95A) was used for preparation of CNCs. HPC (average $M_w$ = 100,000 g / mol, molar substitution 3.4 to 4.4 propylene oxide groups per anhydroglucose unit), TEMPO, NaOCl, NaBr, HCl, NaOH, and ethanol were purchased from Sigma-Aldrich and used as received.

### 5.3.2. TEMPO-mediated Oxidation

Never-dried pulp (20 g fiber weight, 123 mmol primary alcohol) was suspended in 800 mL of high purity water (resistivity at 25°C = 18.2 M Ω.cm) and agitated with an overhead stirrer operating at 500 rpm. A 10 mL aqueous solution of TEMPO (0.25 g, 1.60 mmol) and NaBr (2.5

g, 24.3 mmol) was prepared, added to the pulp suspension, and the mixture was stirred continuously for about 5 minutes. A 12.4 % NaOCl solution (39.8 mL, 4.00 mmol) was added drop-wise to the mixture while maintaining a pH of 10 ± 0.2 with addition of 0.5 M NaOH solution. After about 50 min, no further change in pH was observed, indicating the end of the reaction. Ethanol (30 ml) was then added to fully quench the reaction and the pH was adjusted to 7.0 with a 0.5 M HCl solution. The suspension was vacuum-filtered, washed several times with deionized water and stored at <8 °C until used. Appearance and morphology of oxidized product were similar to those of the starting pulp fibers.

### 5.3.3. Fibrillation of Oxidized Fibers

Oxidized fibers were first milled to 60 mesh (250 µm) sizes using a Wiley® mini-mill. Fiber suspensions (0.3 wt % solids) were prepared by dispersing 0.5 g milled fibers in 150 mL of deionized water. The suspensions were sonicated with a Sonics® ultrasonic processor (Model GE 505) for varying amounts of time (details in Table 5.1). A double-walled glass beaker connected to a circulating ice water bath was used to prevent overheating of suspension during sonication (schematic of setup shown in Figure 5.1). Sonicated suspensions were stored at <8 °C in plastic bottles until used.

### 5.3.4. Preparation of CNCs and MFCs

CNC preparation followed a previously reported method.[17] MFCs were prepared from the original pulp stock used for TEMPO-mediated oxidation. Pulp suspensions (0.25 wt %) were dispersed in deionized water and fibrillated by 20 passes through a high intensity homogenizer (Microfluidics M-110 EH) operated at 30,000 psi i.e. ~207 MPa.

### 5.3.5. Characterization of Fibrillated Fibers

#### 5.3.5.1. Yield

Sonicated suspensions were centrifuged at 4550*g* rcf for 20 min to separate the nanofibrils (in supernatant fraction) from unfibrillated and partially fibrillated fibers (referred to as UPFs henceforth) in the sediment fraction. The separated fractions were dried at 50 °C in a forced air oven and yields (i.e. solids content after drying) were calculated according to equation 1.

**Table 5.1** Yields from sonication and weight fractions in nanocomposites of nanofibrils and UPFs

| Sonication time, min | Nanofibrils | | UPFs[a] | |
|---|---|---|---|---|
| | Yield, %[b] | Weight fraction, %[c] | Yield, %[b] | Weight fraction, %[c] |
| 1 | 10.5 (1.2) | 0.52 | 88.8 (0.7) | 4.44 |
| 5 | 41.7 (3.2) | 2.08 | 57.1 (3.3) | 2.85 |
| 10 | 86.5 (2.0) | 4.33 | 12.9 (2.6) | 0.64 |
| 15 | 96.8 (0.7) | 4.84 | 3.0 (0.7) | 0.15 |
| 20 | 97.5 (1.0) | 4.88 | 2.5 (1.4) | 0.12 |

[a]Unfibrillated and partially fibrillated fibers

[b] From sonicated suspensions (using equation 1)

[c] In nanocomposites reinforced with 5 wt % fiber (determined independently for nanofibrils and UPFs).

$$\text{Yield},\% = \frac{\text{weight of dried solids}}{\text{initial fiber weight}} \times 100 \qquad (1)$$

Yield results represent averages of three replications.

#### 5.3.5.2. Transparency

Light transmittance through sonicated suspensions was measured in a UV-VIS spectrophotometer (Thermo Scientific Corporation Evolution 300). The instrument was operated in transmission mode using a Xenon light source. Data were collected in the visible region (400 to 800 nm).

#### 5.3.5.3. Morphology

Nanofibrils and UPFs were imaged by transmission electron microscopy (TEM) and scanning electron microscopy (SEM) respectively. Ten microliter drops of supernatant suspensions

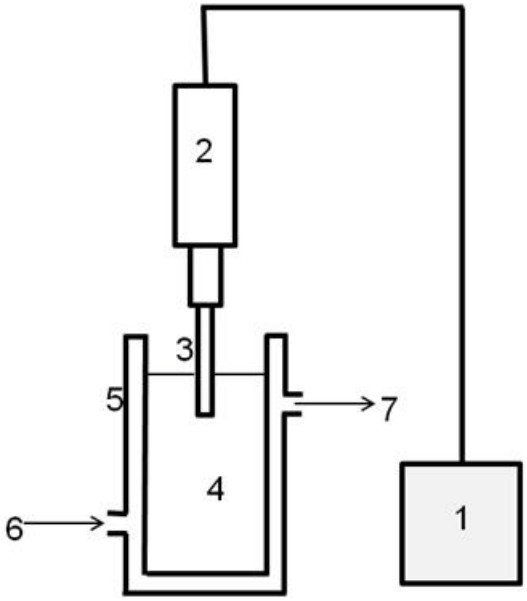


**Figure 5.1** Schematic of ultrasonication setup for cellulose fibrillation. (1) power control; (2) piezoelectric converter; (3) ultrasonic probe; (4) cellulose suspension; (5) double-walled glass beaker; (6) ice water inlet and (7) outlet

(0.01 wt %) were placed on formvar-coated copper grids (300 mesh). Prior to complete drying, the specimens were stained with uranyl acetate negative stain (2 %). The samples were imaged in a Philips EM 420 transmission electron microscope operating at 100 kV. Images were acquired electronically with an installed CCD camera. SEM samples were prepared by dropping 50 µL sediment suspensions (0.01 wt %) onto clean silicon wafers followed by air-drying for 24 hours. Samples were pre-coated with 3 nm gold-palladium sputter prior to imaging in a LEO Zeiss1550 field emission scanning electron microscope.

#### 5.3.5.4. Thermal Stability

A thermogravimetric analyzer (TA Instruments Q 500) was used to monitor the thermal degradation behavior of the sonicated celluloses. Freeze-dried samples *ca.* 10 – 12 mg from each treatment level were used. Thermogravimetric analysis (TGA) tests were performed in air at a heating rate of 20 °C / min. Accuracy of thermal degradation temperature was enhanced by selecting the high resolution-dynamic mode which automatically adjusts the heating rate when the instrument senses a weight loss.

#### 5.3.5.5. Flow

Flow properties of sonicated suspensions were measured with a Brookfield Viscometer (model DV-II + Pro). The small sample adapter accessory was used to achieve rapid and precise temperature control and to improve accuracy of viscosity measurements. The experiments were conducted on 10 mL samples at shear rates of 6.8 – 68 $sec^{-1}$. An external temperature control unit was used to maintain the experimental temperature of 25 ± 0.1 °C.

### 5.3.6. Composite Film Preparation

An HPC solution (7 wt %) was prepared by dissolving 70 g HPC in 1 L deionized water. The solution was stirred overnight to ensure complete dissolution of the polymer. Fibrillated fiber suspensions were mixed with appropriate amounts of HPC solution to yield 5 wt % fiber loadings. The blends were transferred into polystyrene dishes (150 cm diameter) and dried at 35 °C in a forced air oven. Dried films (~0.5 mm thick), were recovered after 6 to 7 days and further conditioned at 50 % relative humidity for 24 hours.

### 5.3.7. Film Characterization

#### 5.3.7.1. Viscoelastic Properties

Dynamic mechanical and creep properties were measured in tension using a TA Instruments 2980 Dynamic Mechanical Analyzer. Specimen widths and lengths of 5.0 ± 0.1 mm and 18 ± 0.5 mm respectively were used. Dynamic measurements were made from 0 to 150 °C at a 5 °C / min heating rate and 1 Hz. Ten minute-creep data were collected at multiple temperatures under a 0.60 MPa stress.

#### 5.3.7.2. Morphological Properties

Some of the creep and dynamic mechanical specimens were embrittled in liquid nitrogen and fractured in cross-section for SEM observations. Samples were adhered onto silicon wafers and sputter coated as previously described.

## 5.4. Results and Discussion

Fibrillated celluloses from TEMPO-oxidized wood pulp were mechanically derived using ultrasonication. By means of conductometric titration,[18] the carboxylate concentration of the

oxidized pulp was calculated as 1.1 mmol / g cellulose. This is well within the oxidation range (0.99 – 1.23 mmol / g) earlier reported for effective disintegration.[13] Nanofibril fraction in the pulp suspensions were controlled by varying sonication time. Biopolymer-based nanocomposites films using HPC as a matrix and the fibrillated oxidized celluloses as fillers were fabricated. Characteristics of the ultrasonication products as well as dynamic mechanical and creep properties of the nanocomposite films are presented. Oxidized cellulose nanocomposites are also compared with those containing CNCs and MFCs as fillers.

### 5.4.1. Fibrillated Oxidized Cellulose Properties

Nanofibril yields of 10.5 to 97.5 wt % were obtained compared with 88.8 to 2.5 wt % UPFs from the sonication process (Table 1). Yield calculations from equation 1 reveal a linear dependence of yield on sonication time in the range of 1 to 10 min sonication (Figure 5.2). Increasing the sonication time beyond 10 min results in a nearly 100 % conversion to nanofibrils, as evidenced by the 96.7 and 97.5 wt % yields at 15 and 20 min sonication times respectively. It appears ten minutes of sonication is sufficient to convert the bulk of the oxidized pulp fibers into nanofibrils. It is important to note that changing probe size and volume of material to be processed may result in different yield responses to sonication time.

Appearances of sonicated suspensions after standing for 24 hr are depicted in Figure 5.3 A. Corresponding light transmittance data collected in the visible range of a UV-VIS spectrophotometer are also displayed in Figure 5.3 B. A substantial increase (*ca.* 65 %) in transparency is observed when sonication time is increased from 5 to 10 min. This is equivalent to a >50 % increase in nanofibril content (Table 1). In the previous report of [13], transparencies of TEMPO-oxidized suspensions were also found to increase with increasing degree of oxidation.

Electron micrographs of nanofibrils and UPFs were acquired with TEM and SEM respectively. Individualized nanofibrils with shapes and sizes similar to those from previous reports[13,19] are observed (Figure 5.4 A). Using an image processing software, nanofibril widths of between 2.5 and 4 nm were measured. However no solitary nanofibrils suitable for length measurements could be identified. UPFs on the other hand vary widely in morphology as would be expected of fibers undergoing fibrillation under intense mechanical stresses. Partially fibrillated fibers having an appearance similar to the example shown in Figure 5.4 B were encountered frequently in the sediment fractions. Similar broom-like structures were also

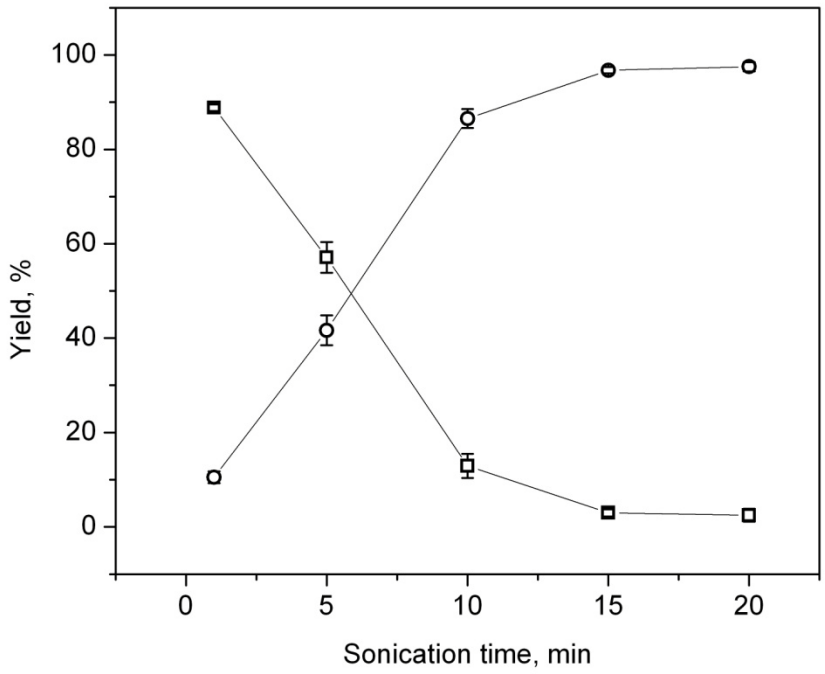


**Figure 5.2** Yields of nanofibrils (circles) in supernatant fractions and of UPFs (squares) in sediment fractions as a function of sonication time (calculated from equation 1). using weight of starting material as basis.

observed from light microscopy images (not shown). This pattern of disintegration suggests that a simultaneous fibrillation-axial splitting of the fiber walls precedes a complete conversion of the fiber wall into nanofibrils. Images c, d, and e of Figure 5.4 depict sediment fractions of 1, 10, and 20 min sonication times respectively. Both unfibrillated and partially fibrillated fibers were seen at every level of sonication. However, the proportion of unfibrillated fibers decreased drastically when sonication times reached 15 and 20 min. A crude estimation of unfibrillated fiber dimensions from SEM imaging was made using the SEM image acquisition software. Average lengths and widths of 262 ± 156 μm and 24.2 ± 7 μm respectively were determined for the ~80 fibers measured. These length averages are representative of the 60 mesh sizes of the starting fibers.

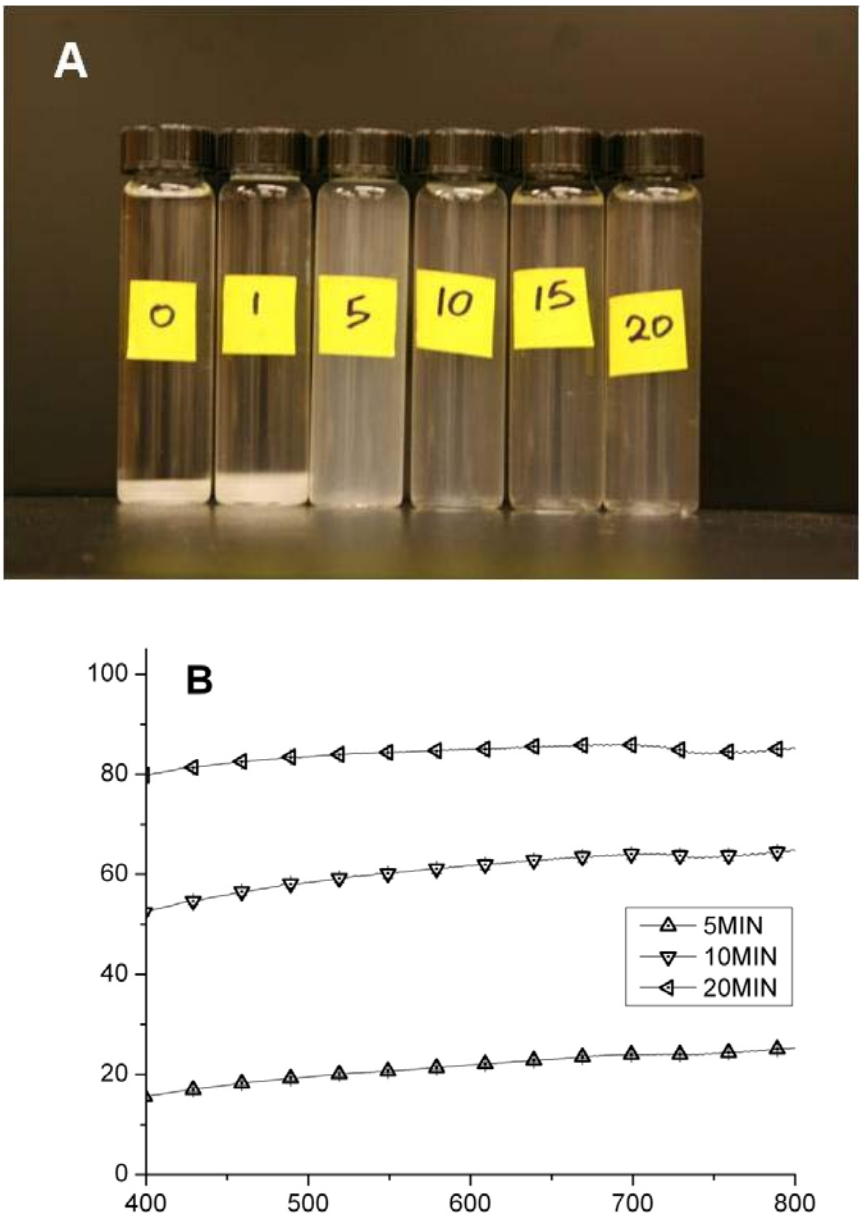


**Figure 5.3** (A) Fibrillated cellulose suspensions (0.3 wt % solids) 24h after sonication. Labels represent sonication times in minutes. (B) Transmittance spectra for 5, 10, and 20 min sonicated suspensions in (A) recorded in the visible region with a UV-vis spectrophotometer.

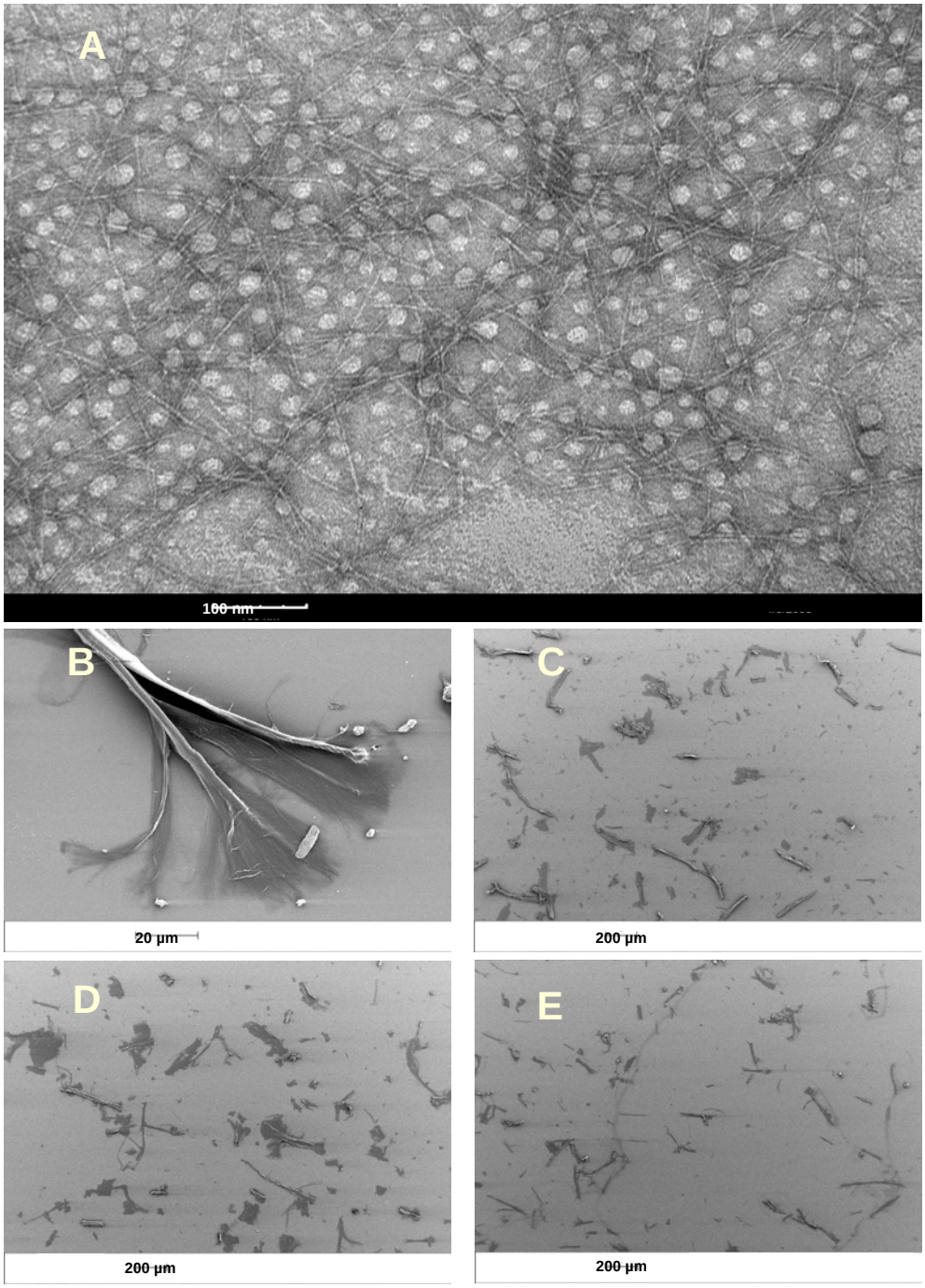


**Figure 5.4** Electron micrographs of fibrillated celluloses. (A) TEM of supernatant fractions showing nanofibrils of widths 2.5 – 4 nm (indicated with arrows); SEM of (B) single fiber from sediment fraction undergoing disintegration and C – E 0.01 wt % sediment fractions for 1, 10, and 20 min sonication times respectively.

TEMPO-oxidized celluloses undergo multiple degradation events as revealed by linear (Figure 5.5 A) and differential (Figure 5.5 B) weight loss versus temperature TGA plots. Reports describing similar degradation patterns have been made for oxidized celluloses prepared from other methods[20-22] and for sulfuric acid-hydrolyzed CNCs.[23] El-Sakhawy[20] attributed these multiple degradation events to early dehydration, fragmentation, and ultimately to decomposition of carbohydrate residues. The main degradation temperatures of TEMPO-oxidized celluloses occur in the range of 225 – 231 °C (Figure 5.5 B) and represent a drastic decline from the degradation temperature (318 °C) of the unoxidized wood pulp (plot not shown). The narrow difference (6 °C) in peak degradation temperatures implies a rather weak dependence of thermal degradation temperature on nanofibril weight fraction. On the other hand, the degradation rate (weight loss per unit rise in temperature, shown as peak heights in Figure 5.5 B) increases with increasing sonication time or nanofibril fraction. This can be attributed to the high surface area accompanying the nanofibrillation process, which increases the effective mass of cellulose consumed per unit rise in temperature.

Viscosity measurements revealed that suspension viscosities increased (to a maximum) with increasing sonication time and then started to decline with further sonication (Figure 5.6). At the maximum viscosity (10 min sonication), the sonicated suspensions exhibited a gel-like character that could be readily distinguished (visually) from suspensions treated at other sonication times. The initial rise to a maximum viscosity can be attributed to the increasing proportion of high surface area nanofibrils that strongly interact with the aqueous medium. Additional energy input from longer sonication times disperses the nanofibrils which may have existed in the suspension as networks (having gel-like behavior) at the peak viscosity. In the earlier report of Saito *et al.*[19], 0.1 w/v % TEMPO-oxidized pulp suspensions were magnetically stirred over periods ranging from a few hours to several days. Viscosity rose sharply from 0 – 12 hr, achieved a maximum in 3 days, and declined steadily with continuous stirring to 10 days. It was recently reported that the high viscosities of TEMPO-oxidized nanocellulose suspensions could be restored by storing the suspensions at a low temperature (5 °C) for an extended amount of time (5 weeks).[24]

### 5.4.2. Composite Film Properties

The tensile storage moduli (E') of nanocomposites increase with sonication time up to a limit (Figure 5.7). No increases in E' are observed at sonication times greater than 10 min (notice

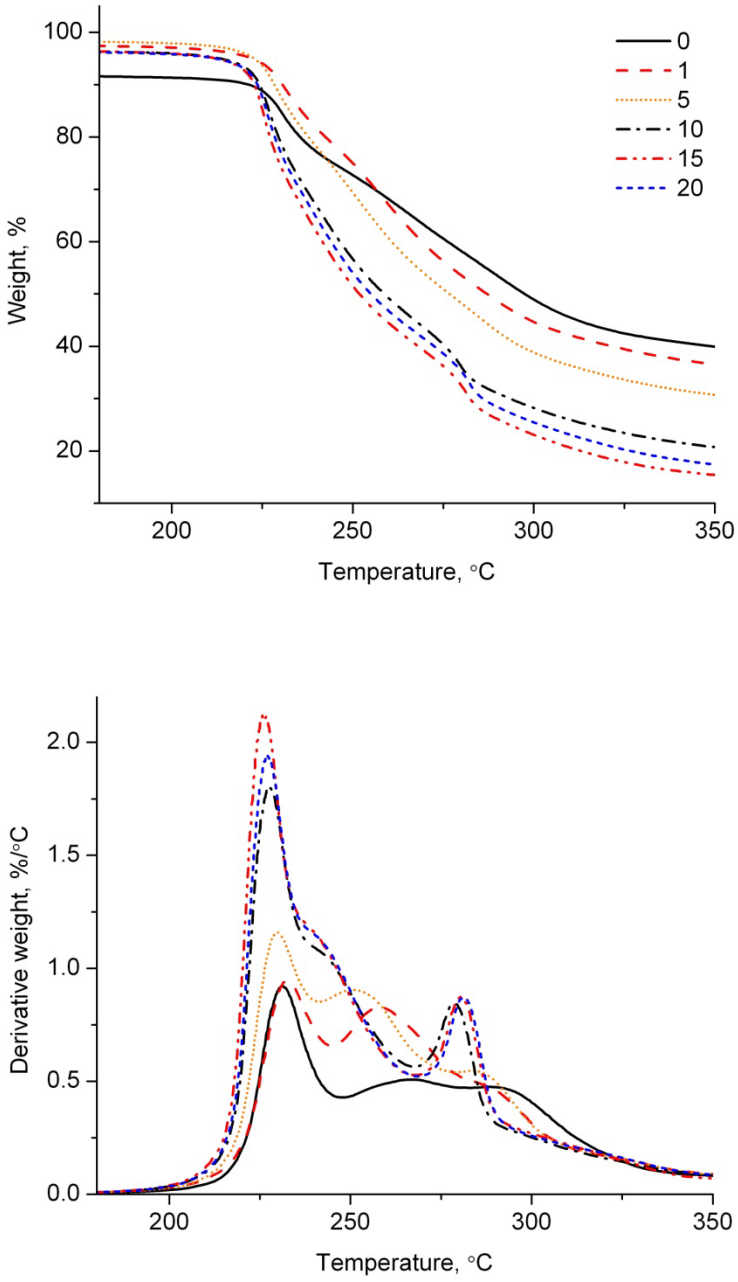


**Figure 5.5** Thermal degradation behavior of freeze-dried TEMPO-oxidized pulp. (A) weight loss and (B) derivative of weight loss as a function of temperature. Scans performed at 20 °C / min in high resolution dynamic rate mode. Legend shows sonication times (in minutes) of starting pulp suspensions.

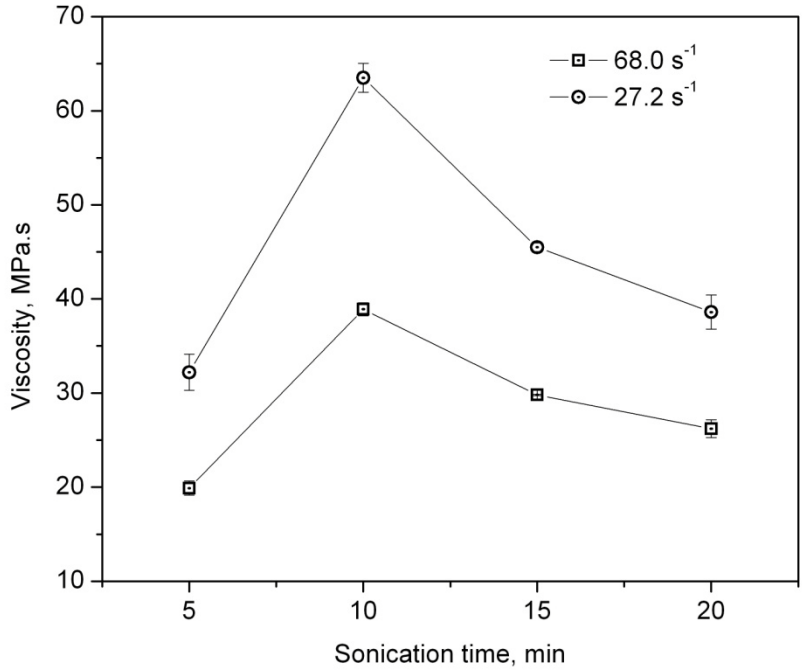


**Figure 5.6** High and low shear rate viscosity dependencies on sonication time of nanofibril suspensions. No data could be obtained for the 1 min sonicated suspension because its viscosity was insufficient for the minimum operating torque of the viscometer.

overlap of the 10 and 20 min E' curves in Figure 5.7). These results indicate that a sonication time of 10 min, at which close to 90 wt % of the starting fibers have been converted to nanofibrils, is sufficient for maximum E' performance. Over the experimental temperature range (0 – 150 °C), the relationship between E' and sonication time is found to be linear in the limits of 1 to 10 min sonication (Figure 5.8). This relationship implies a linear dependence of E' on nanofibril weight fraction by extension of the yield-sonication time relationship in Figure 5.2. The data in Figure 5.8 reveal more effective nanofibril reinforcements at higher temperatures (100 and 150 °C) as shown by the stronger dependence of E' (steeper slopes of regression lines) on sonication time. This is a commonly observed effect in cellulose-based nanocomposite systems found in several cellulose-based nanocomposite reports.[5,25-30]

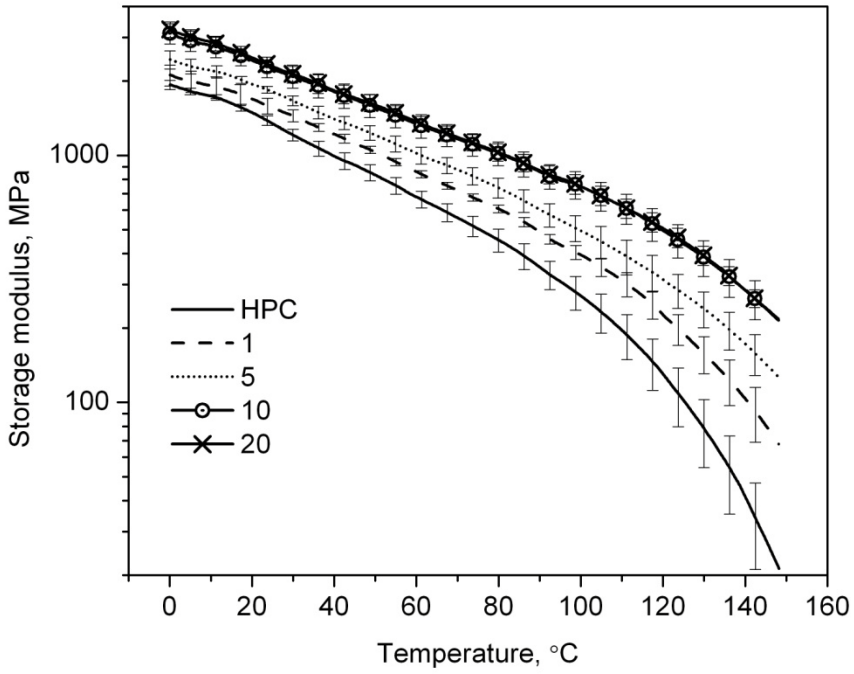


**Figure 5.7** Storage modulus response to temperature of HPC and nanocomposites. Numbers in legend indicate sonication times (in minutes) of starting pulp suspensions. See Table 5.1 for corresponding nanofibril and UPF contents.

High temperature (150 °C) E' comparisons between oxidized cellulose nanocomposites and their CNCs and MFCs counterparts were also made. As shown by the data in Table 1, the nanofibril fraction at all levels of sonication fall short of the maximum 5 wt % in the CNC and MFC-based films. In the latter materials, all of the reinforcing elements are constituted of nanosized fillers whereas in the sonicated suspensions, only a fraction of the reinforcing fillers are of nano-scale dimensions. However, significantly higher E's are obtained in the TEMPO-oxidized systems sonicated for five or more minutes (Figure 5.9). Corresponding tan δ plots (Figure 5.10) show portions of two broad thermal transitions (<25 °C and >100 °C). The lower temperature transition is limited to neat HPC and the nanocomposites sonicated for 1 and 5 min. This event corresponds to the glass transition temperature ($T_g$) of HPC which has been reported as ranging from 10 to 20 °C depending on the characterization method used.[31] Similar $T_g$s are observed for CNCs and MFCs nanocomposites (inset in Figure 5.10). This transition is, however, clearly absent from the nanocomposites reinforced with 10 and 20 min sonicated

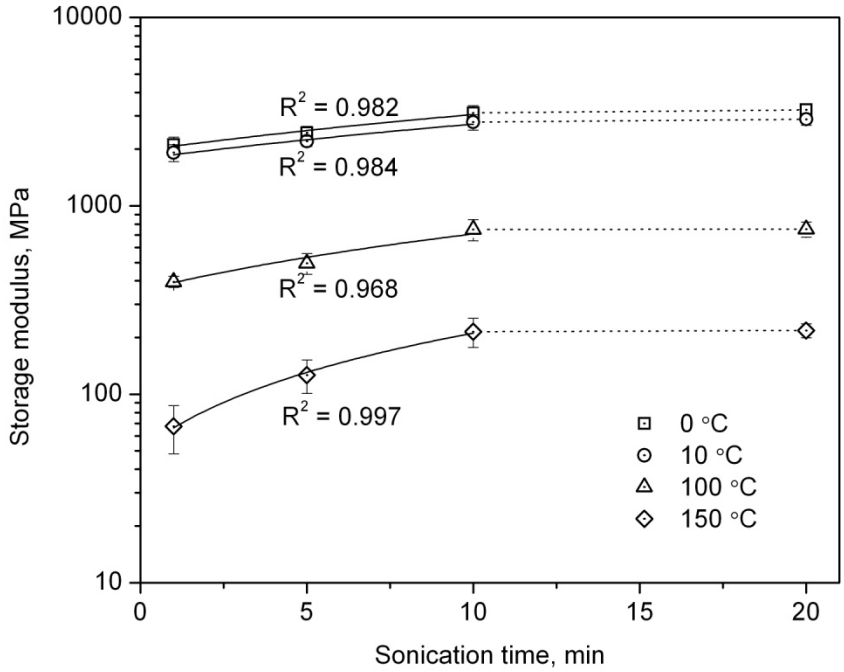


**Figure 5.8** Dependence of storage moduli on sonication times at low (0 and 10 °C) and high (100 and 150 °C) temperature regimes. Solid regression lines show regions of linear dependencies and their corresponding $R^2$ values.

nanofibrils. $T_g$ suppression at high sonication times (i.e. higher nanofibril volume fraction) suggests that HPC interactions with TEMPO-oxidized cellulose nanofibrils may be influenced by the nanofibril volume fraction. The superior performance of TEMPO-oxidized cellulose nanocomposites may be strongly dependent on the unique combination of oxidized cellulose nanofibril characteristics. These include (1) the presence of diverse surface functional groups (OH, CHO, and $COO^-$) resulting from TEMPO-mediated oxidation, (2) the exceptionally high surface area to volume ratio expected from nanofibril individualization, and (3) the high aspect (length / diameter) ratios evident from TEM imaging (see Figure 5.4 and Saito *et al.*[19]). All of these conditions can significantly restrict HPC chain mobility at $T_g$ leading to the observed effects on E' and tan δ. Future work on TEMPO-oxidized cellulose nanocomposites will look into the role of surface chemical properties on nanocomposite properties.

Time-dependent strain response under static stress conditions is the primary outcome of creep compliance experiments. Tensile creep compliance D(t) is the ratio of the time dependent

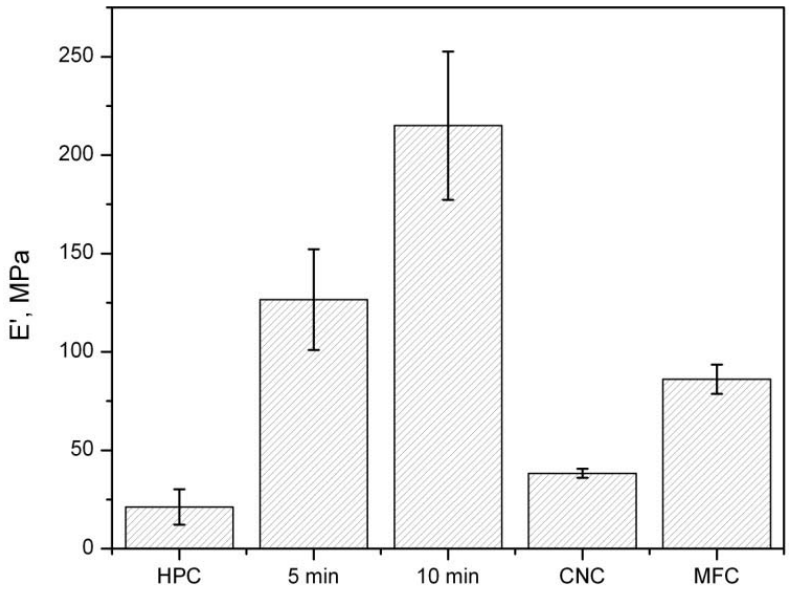


**Figure 5.9** Storage moduli comparisons at 150 °C for neat HPC and nanocomposites. 5 and 10 min represent sonication times of oxidized pulp suspensions. CNC and MFC represent cellulose nanocrystals and microfibrillated celluloses respectively.

tensile strain ε(t) to the applied tensile stress $\sigma_{E,0}$. Ten minute-D(t) results of neat and reinforced HPCs at sub-$T_g$ (0 °C) and above $T_g$ (100 °C) regions are shown in Figure 5.11. The inset shows a typical set of creep curves collected at 100 °C. Low D(t) values with no uniform time-dependence are recorded in the sub-$T_g$ region where HPC chains are essentially frozen. However, at 100 °C, D(t) of neat HPC and the nanocomposites increase by approximately two and one order(s) of magnitude, respectively. The nanofibril volume fraction effect is evident from the linear ($R^2$ = 0.985) decrease in D(t) as a function of sonication time. Again, compared to CNC and MFC counterparts, the oxidized cellulose nanocomposites exhibit lower D(t) at high temperatures (Figure 5.12). These observations are consistent with the DMA results discussed previously.

Freeze-fractured cross-sections of HPC and nanocomposite (5 and 20 min sonication) films are displayed in Figure 5.13. Nanofibrils were not visible on the fracture surfaces even at very high magnifications. The limits of the SEM resolution were probably reached taking into consideration the combination of exceptionally small nanofibril dimensions (3 – 4 nm) and the

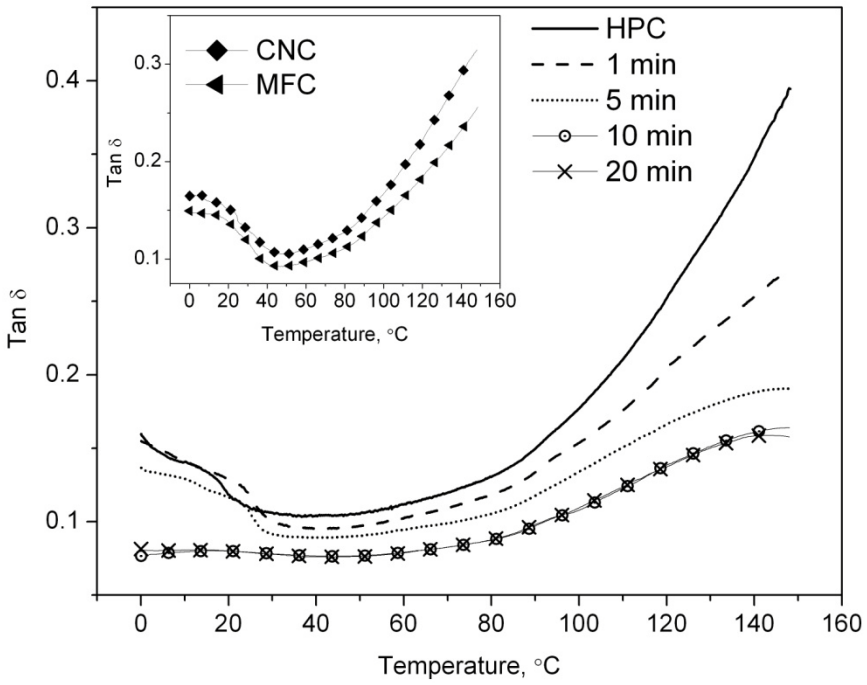


**Figure 5.10** Tan δ versus temperature of neat HPC and nanocomposites. Numbers in legend indicate sonication times (in minutes) of starting pulp suspensions. Inset shows corresponding plots for CNCs and MFCs.

thin barrier created by sputter coating. An interesting observation however, is the differences in grain sizes of the surface roughness. Surface roughness grain sizes are significantly reduced on the nanocomposite fracture surfaces compared to neat HPC. Except for the nanocomposites loaded with fibrillated oxidized celluloses sonicated for 1 min (image not shown) where roughness grain sizes were only slightly reduced, all remaining nanocomposite fracture surfaces showed grain sizes similar to those in Figure 5.13 B and C. Observations similar to this were reported for fracture-toughened intercalated clay-epoxy nanocomposites.[32] Crack propagation followed a torturous path arising from the very short interparticle distances between clay nanoparticles. It is reported that such toughening mechanisms are not normally observed with fully exfoliated clay.[33] However, with intercalated clay, the lateral micron-sized lengths of the clay nanoplatelets are believed to offer crack bridging mechanisms which are responsible for the tortuous crack propagation behavior. In the present nanocomposites, the surface roughness is observed to be uniform across the sample surface. This may imply, in addition to the

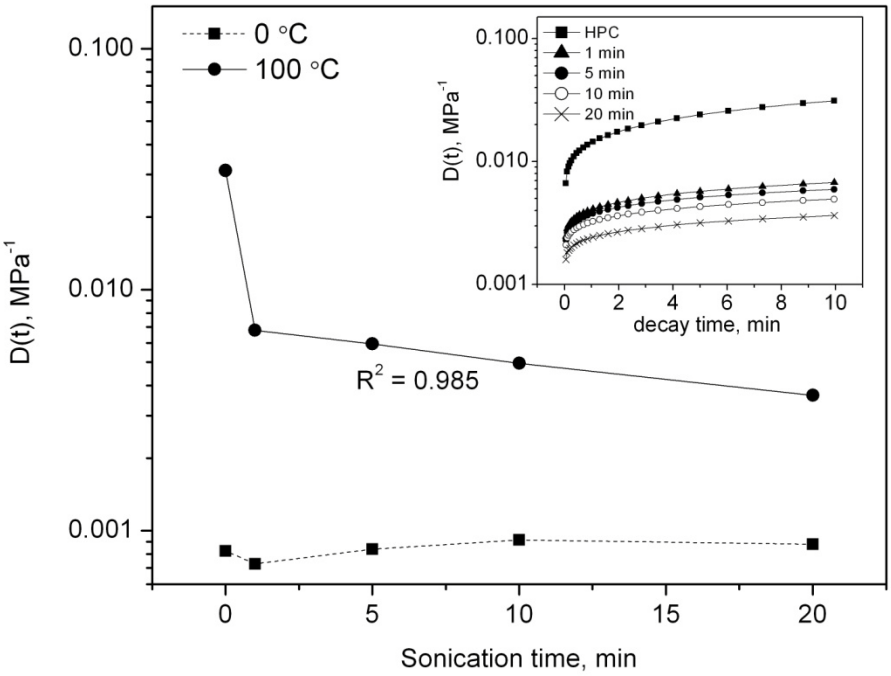


**Figure 5.11** Dependence of tensile creep compliance on sonication time at sub-Tg (0 °C) and above Tg (100 °C) conditions. Data represents 10 min creep under 0.6 MPa static stress. 0 min on sonication time axis corresponds to neat HPC. Inset shows typical creep curves at 100 °C.

interfibrillar distance factor, strong nanofibril-matrix interfaces and uniform nanofibril dispersion. These propositions however require verification with actual fracture toughness measurements.

## 5.5. Conclusions

Cellulosic nanofibrils from the mechanical disintegration of TEMPO-oxidized celluloses were recently discovered. High intensity sonication was used in this study to control fibrillation of TEMPO-oxidized wood pulp by varying sonication time. Nanocomposite films based on HPC matrix and fibrillated oxidized celluloses were synthesized, characterized, and compared with those from conventional CNCs and MFCs. The conclusions reached are as follows:

1. Based on our selected treatment conditions, 10 min is found sufficient to convert the bulk (*ca* 90 wt %) of the pulp fibers into nanofibrils.

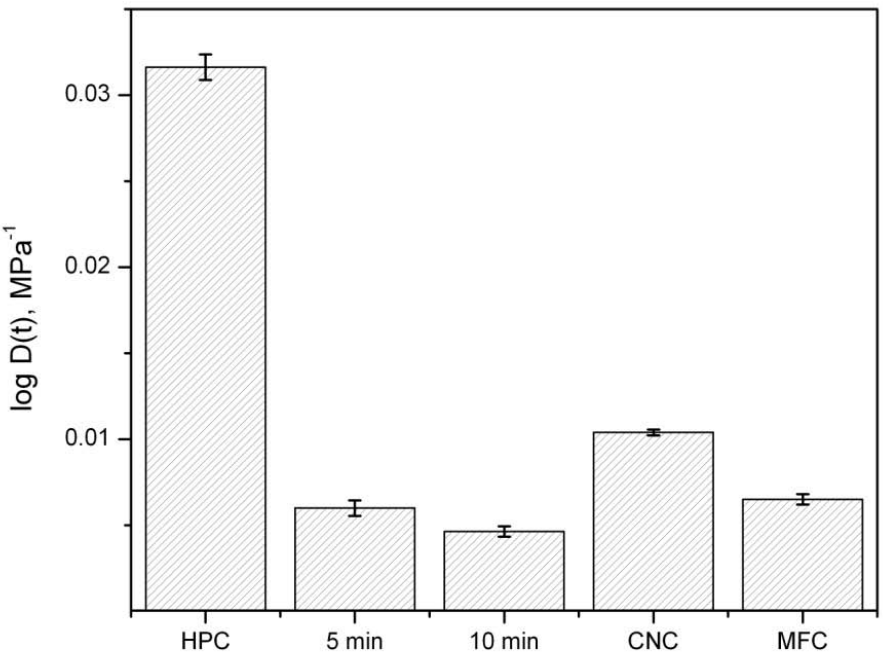


**Figure 5.12** Comparison of creep compliance at 100 °C of HPC and nanocomposite films. 5 and 10 min represent the sonication times of oxidized pulp suspensions. CNC and MFC represent cellulose nanocrystals and microfibrillated celluloses respectively.

2. Storage modulus and creep compliance performances of oxidized cellulose nanocomposites exhibit a direct dependence on nanofibril weight fractions, particularly at elevated temperatures.
3. Tan δ data indicate weight fraction-dependent interactions between oxidized cellulose nanofibrils and HPC matrix.
4. Comparison of high temperature E' performances suggest stronger fibril-matrix interactions in the oxidized nanofibrils- than conventional (CNCs and MFCs)-filled nanocomposites. Roughness grain sizes of oxidized cellulose-HPC nanocomposite fracture surfaces suggest
5. strong fibril-matrix interactions, good fibril dispersion, and probability of crack bridging mechanisms operating at the nanofibril length scales.

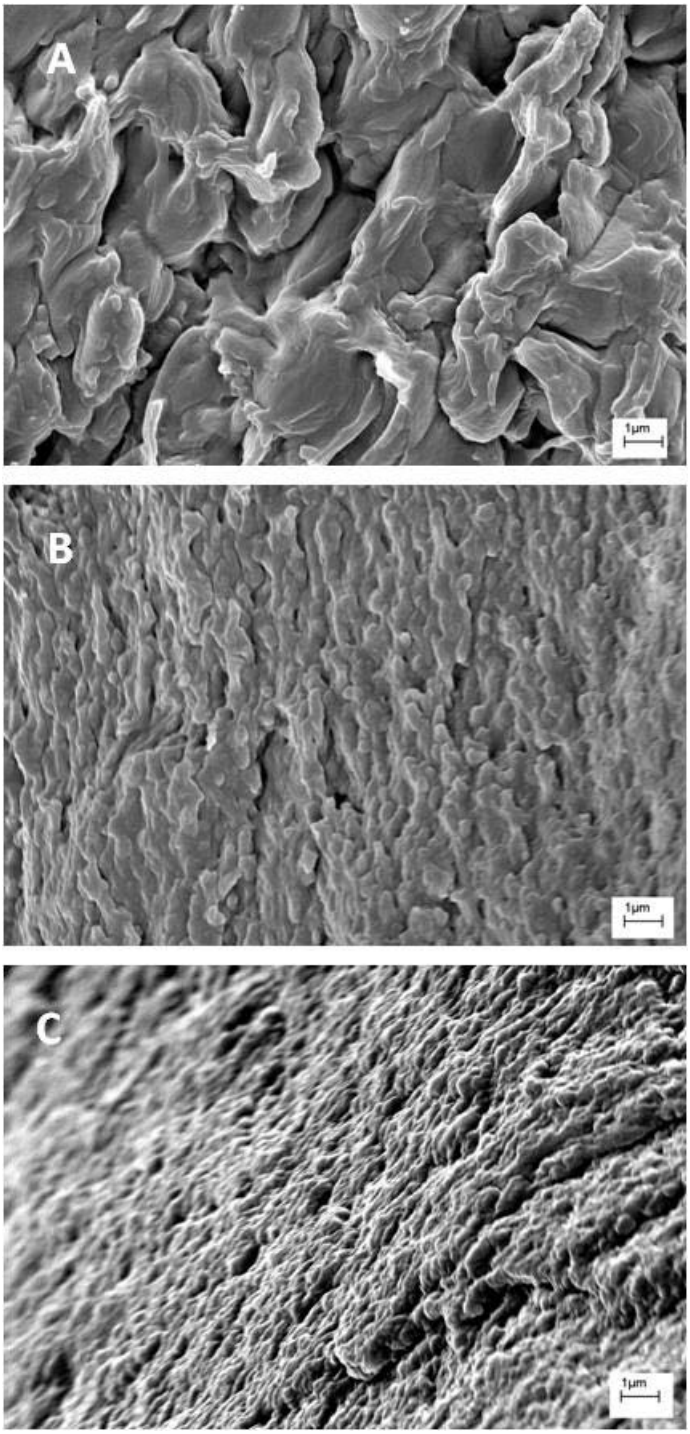


**Figure 5.13** SEM fracture surfaces of (A) HPC and (B and C) nanocomposite films. (B) and (C) were fabricated from suspensions sonicated for 5 and (C) 20 min respectively.

## 5.6. References


(1) Gindl, W.; Keckes, J. *Polymer* **2005**, *46*, 10221.

(2) Matsumura, H.; Sugiyama, J.; Glasser, W. G. *Journal of Applied Polymer Science* **2000**, *78*, 2242.

(3) Petersson, L.; Oksman, K. *Cellulose Nanocomposites: Processing, Characterization, and Properties* **2006**, *938*, 132.

(4) Wibowo, A. C.; Misra, M.; Park, H. M.; Drzal, L. T.; Schalek, R.; Mohanty, A. K. *Compos. Pt. A-Appl. Sci. Manuf.* **2006**, *37*, 1428.

(5) Svagan, A. J.; Samir, M. A. S. A.; Berglund, L. A. *Biomacromolecules* **2007**, *8*, 2556.

(6) Zimmermann, T.; Pohler, E.; Geiger, T. *Advanced Engineering Materials* **2004**, *6*, 754.

(7) Grunert, M.; Winter, W. T. *Journal of Polymers and the Environment* **2002**, *10*, 27.

(8) Petersson, L.; Kvien, I.; Oksman, K. *Composites Science and Technology* **2007**, *67*, 2535.

(9) Herrick, F. W.; Casebier, R. L.; Hamilton, J. K.; Sandberg, K. R. *Microfibrillated Cellulose: Morphology and Accessibility*, 1983; Vol. 37.

(10) Turbak, A. F.; Snyder, F. W.; Sandberg, K. R. *Journal of Applied Polymer Science: Applied Polymer Symposium* **1983**, *37*, 815.

(11) Nakagaito, A. N.; Yano, H. *Applied Physics a-Materials Science & Processing* **2005**, *80*, 155.

(12) Edgar, C. D.; Gray, D. G. *Cellulose* **2003**, *10*, 299.

(13) Saito, T.; Nishiyama, Y.; Putaux, J. L.; Vignon, M.; Isogai, A. *Biomacromolecules* **2006**, *7*, 1687.

(14) Bragd, P. L.; van Bekkum, H.; Besemer, A. C. *Topics in Catalysis* **2004**, *27*, 49.

(15) Saito, T.; Isogai, A. *Biomacromolecules* **2004**, *5*, 1983.

(16) Wise, L. E.; Murphy, M.; D'Addieco, A. A. *Paper Trade Journal* **1946**, *122*, 11.

(17) Beck-Candanedo, S.; Roman, M.; Gray, D. G. *Biomacromolecules* **2005**, *6*, 1048.

(18) Katz, S.; Beatson, R. P.; Scallan, A. M. *Svensk Papperstidning* **1984**, *87*, R48

(19) Saito, T.; Kimura, S.; Nishiyama, Y.; Isogai, A. *Biomacromolecules* **2007**, *8*, 2485.

(20) El-Sakhawy, M. *Journal of Thermal Analysis and Calorimetry* **2000**, *63*, 549.

(21) Kumar, V.; Yang, T. R. *Carbohydr. Polym.* **2002**, *48*, 403.

(22) Varma, A. J.; Chavan, V. B. *Polymer Degradation and Stability* **1995**, *49*, 245.

(23) Wang, N.; Ding, E. Y.; Cheng, R. S. *Polymer* **2007**, *48*, 3486.

(24) Lasseuguette, E.; Roux, D.; Nishiyama, Y. *Cellulose* **2008**, *15*, 425.

(25) Ljungberg, N.; Bonini, C.; Bortolussi, F.; Boisson, C.; Heux, L.; Cavaille, J. Y. *Biomacromolecules* **2005**, *6*, 2732.

(26) Favier, V.; Chanzy, H.; Cavaille, J. Y. *Macromolecules* **1995**, *28*, 6365.

(27) Samir, M. A. S. A.; Alloin, F.; Sanchez, J. Y.; El Kissi, N.; Dufresne, A. *Macromolecules* **2004**, *37*, 1386.

(28) Helbert, W.; Cavaille, J. Y.; Dufresne, A. *Polymer Composites* **1996**, *17*, 604.

(29) Dalmas, F.; Cavaille, J. Y.; Gauthier, C.; Chazeau, L.; Dendievel, R. *Composites Science and Technology* **2007**, *67*, 829.

(30) Chazeau, L.; Cavaille, J. Y.; Canova, G.; Dendievel, R.; Boutherin, B. *Journal of Applied Polymer Science* **1999**, *71*, 1797.

(31) Rials, T. G.; Glasser, W. G. *Journal of Applied Polymer Science* **1988**, *36*, 749.

(32) Zerda, A. S.; Lesser, A. J. *Journal of Polymer Science Part B-Polymer Physics* **2001**, *39*, 1137.

(33) Zilg, C.; Mulhaupt, R.; Finter, J. *Macromolecular Chemistry and Physics* **1999**, *200*, 661.

# Chapter 6. Conclusions

With a water-DMF co-solvent system, conversion of TONc surface carboxyl groups to hydrophobic ODA groups is complete irrespective of treatment method. However, contrary to desired expectations, organic solvent suspensions of hydrophobized TONc are unstable and their use as reinforcements in CAB matrix results in fibril aggregation. In the preparation of solvent-cast nanocomposites, surprisingly stable suspensions of as-prepared TONc are formed in THF and the nanocomposites fabricated thereof preserve the optical clarity and generate up to a 22-fold increase in the rubbery-state tensile storage modulus of the CAB. The extraordinary reinforcing effect is attributed to both homogenous nanocellulose dispersion and the possible existence of a nanofibril network above some threshold volume fraction. The optical and dynamic mechanical performances of TONc are also not matched by those of similarly prepared CAB nanocomposites reinforced with microfibrillated cellulose (MFC), a conventional nanocellulose reference. Thermal decomposition behavior of CAB is only minimally altered (in the region preceding the main CAB decomposition) by the inclusion of nanocellulose reinforcements. The amount of weight loss in this region relates to the thermal decomposition temperatures of the corresponding nanocelluloses in a direct way.

The explanations underlying the performance of CAB matrix nanocomposites can be extended to account for the superior dynamic mechanical and creep performance properties of TONc-reinforced HPC compared to their MFC and CNC-reinforced counterparts (Chapter 5).

The collective evidence from this study indicates that TONc (without the need for surface hydrophobization) can be expected to outperform conventional nanocelluloses when both are used as reinforcements in cellulose-based matrices. Evidently, the advantages gained from the use of TONc can be attributed to their high surface area-to-volume ratio, their capacity for individualization in suspension, and their multiple surface functionality.

# Appendix A

## GLI Method Summary
## Determination of Nitrogen by the Kjeldahl Method

**Governing SOP:** E7-1 Rev 12 **Analyte:** N **Range:** 0.3–3 mg N*

**Upper limit of range can be extended by dilution.*

**Summary**

The general principle of the Kjeldahl method depends upon the conversion of nitrogen to ammonium acid sulfate by the digestion of the organic material with concentrated sulfuric acid, sodium sulfate and copper sulfate catalyst.

| | | |
|---|---|---|
| **Scope** | This method is applicable to amines, amides, amino acids and their derivatives but generally fails to give quantitative results with heterocyclic nitrogen, N=N linkages and N–O linkages. This method fails to account for nitrogen in the form of azide, azine, azo, hydrazone, nitrate, nitrite, nitrile, nitro, nitroso, oxime, and semi-carbazone. | |
| **Decomposition** | The sample is digested in a mixture of concentrated sulfuric acid, sodium sulfate, and copper sulfate. The organic material is oxidized and the nitrogen converted to ammonium sulfate. Excess sodium hydroxide is added, and the ammonia is distilled and absorbed in a boric acid solution. | |
| **Determination** | 1. Titration with 0.01 N or 0.1 N $H_2SO_4$ to a methyl red/methylene blue indicator endpoint.<br>*OR*<br>2. For low level titrations, ion-selective electrode (GLI Analytical Procedure E7-6) | |
| **Quantitation Limit** | 0.3 mg N (titration) | |
| **Precision & Accuracy**<br>**k-0703**<br>**k-0704** | RSD<br>1.71<br>3.51 | RE<br>–0.48<br>–0.74 |
| **Interferences** | Excess $NO_3$, very large quantity of salt or inorganic solids | |
| **Calculations** | $$\%Nitrogen = \frac{(mL\ titration - mL\ blank)\ (N)\ (14.01)\ (100)}{(mg\ of\ sample)}$$<br>N = normality of titrant | |

**References**


Bradstrut, R.B. *The Kjeldahl Method for Organic Nitrogen*, Academic Press, New York, 1965.

Steyermark, Al. *Quantitative Organic Microanalysis*, Academic Press, New York, 1961.

ASTM E-778-81. *Nitrogen in the Analysis Samples of Refuse-Derived Fuel.*

USP 23/NF18. *Nitrogen Determination* <461>. Method I, II.

*Standard Methods for the Examination of Water and Waste Water* (19thEd.) American Public Health Association, American Water Works Association, Water Environment Federation, Washington, DC 1995.

# Appendix B

**Calculation of Degree of Substitution, DS, from Nitrogen Content Data**

**Using the Method of Vaca-Garcia et al.**

**Amd**

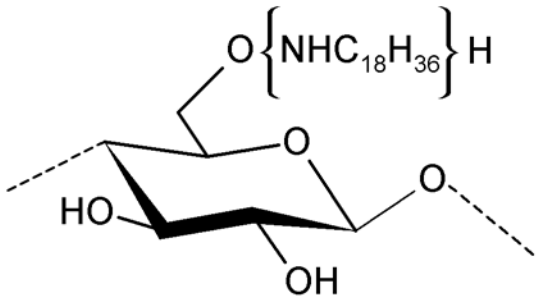


Structure of unit

Molecular formula: $C_{6+18\,DS}\,H_{10+37\,DS}\,O_5\,N_{0+DS}$

$$\text{Nitrogen content, } N = \frac{14.0067\,(0+DS)}{12.011(6+18\,DS)+1.008\,(10+37\,DS)+15.999\,(5)+14.0067\,(0+DS)}$$

N from Kjeldahl analysis (three replications) = 0.0158, 0.0168, 0.0161

**ICmplx**

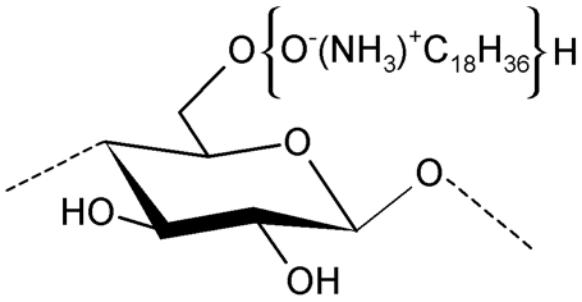


Structure of unit

Molecular formula: $C_{6+18\,DS}\,H_{10+39\,DS}\,O_{5+DS}\,N_{0+DS}$

$$\text{Nitrogen content, } N = \frac{14.0067\,(0+DS)}{12.011(6+18\,DS)+1.008\,(10+39\,DS)+15.999\,(5+DS)+14.0067\,(0+DS)}$$